Estimation of Satellite Derived Flood Area and Volumes to Monitor Environmental Watering Events

Saba Zehra

Faculty of Science

The University of Sydney

2023

A thesis submitted in fulfilment of the requirements for the degree of Master of Philosophy

Statement of Originality

This is to certify that to the best of my knowledge; the content of this thesis is my own work. This thesis has not been submitted for any degree or other purposes.

I certify that the intellectual content of this thesis is the product of my own work and that all the assistance received in preparing this thesis and sources have been acknowledged.

Saba Zehra

Summary

Wetlands are significant repositories of biological diversity and play an essential role in maintaining ecosystem services. The Macquarie Marshes in northern New South Wales is one of those significant wetlands recognised for its rich biodiversity and ecology. In 1986, the Macquarie Marshes Ramsar site was designated under the Ramsar Convention on the List of Wetlands of International Importance (Capon SJ, 2018). In 2009, Macquarie Marshes were reported to be declining primarily due to the flow alteration from river regulations. In addition, numerous environmental stressors, including increased temperatures attributed to climate change, reduced water flows due to drought, and over-extraction of water for agriculture has contributed to the deterioration of the internationally significant Marshes. Complicating the understanding is the fact that Australia is considered as a land of "drought and flooding rains" referring to the climate of Australia, which is highly variable and unpredictable. The Macquarie Marshes experienced extensive flooding events, especially in 2016-17 due to an increase in the water flow in Macquarie River related to a strong La Niña climate cycle. The area has also experienced drought conditions when there is insufficient water flowing in the river or due to the diversion of water to irrigated lands. This variability makes it challenging to predict water availability for the marshes and can have a substantial effect on the wetland's health and the ecosystem dependent on the Marshes. Mapping the inundation patterns of the Macquarie Marshes is essential for understanding the impacts of climate variability and human interventions on these important ecosystems and for effective management and conservation.

The Sentinel satellite constellation, part of the European Union's Copernicus program was launched in 2013. These satellites have enhanced surface water extents' estimation capabilities due to their higher revisit rates and fine resolution. The Sentinel 1 and 2 data set were used to identify, map, and monitor water bodies and their features. To capture sufficient time variability, the study analysed 28 Sentinel-1 and 47 Sentinel-2 images covering the La Niña year 2022. The Sentinel-1 images were pre-processed and co-registered to delineate water. For mapping water bodies using Sentinel-2, multiple water detection algorithms Water Index (WI), Automated Water Extraction Index with shadow ($AWEI_{shadow}$), Automated Water Extraction Index with no shadow ($AWEI_{no\ shadow}$) and Modified Normalized Difference Water Index (MNDWI) were used to quantify flooded areas based on the Sentinel 2 satellite data. The integration of Sentinel-1 and Sentinel-2 serves to not only minimise the temporal lag between satellite acquisitions but also addresses the constraints inherent in Sentinel 2 data. Sentinel 1 can tackle limitations from Sentinel 2, such as cloud coverage and time intervals under different weather conditions. Flooded areas obtained using different water indices were compared with the river discharge at several gauge stations located at different reaches of the Macquarie River. Overall, the Water Index (WI) gave the best results relative to PlanetScope verification data, but all Sentinel 2 methods indicated some underestimation of overall water areas. Sentinel 1 appeared to strongly overestimate the flooded area. Therefore, the final step fuses the Sentinel-1 and Sentinel-2 data, using a layer-stacking technique; the random forest (RF) classifier was then applied to predict flooded areas

using the Water Index (WI), other satellite variables and environmental variables related to slope, depressions, land use and rainfall. The Fisher's WI derived from Sentinel-2 data was found to be the most significant predictor. It was though subsequently realised that the inclusion of spectral bands from Sentinel-2 was necessary in the model as that could have helped in the mitigation of the potential biases. Additionally, while the bands of Sentinel-1 were incorporated, and no corresponding index of Sentinel-1 was utilised that could possibly lead to a lack of consistency in the analysis. Finally, floodwater depth of the water inundated using the RF model was calculated using a 5m resolution LiDAR DEM dataset.

To conclude, remote sensing can provide observation of inundated areas and water content; however, challenges remain in terms of data availability for validation, RF model calibration, and potential biases in observations, and also the challenges arise from the lack of continuous data in both spatial and temporal dimensions. Landsat imagery has historically been the main approach in studies focused on hydrological connectivity and surface water monitoring, but one of the challenges of Landsat has been its limited temporal resolution due to its 16-day revisit cycle. This study intends to build on traditional Landsat-based approaches (Mueller et al., 2016) but also extends them in several significant ways. The integration of the data from both active and passive sensors increases the temporal granularity of observations, which enables more frequent monitoring of the Macquarie Marshes, leading to a better understanding of dynamic hydrological processes. Though this study highlights the promising nature of the remote sensing techniques and machine learning models to understand the hydrological connectivity and surface water availability in the Macquarie Marshes; however, there is a need for further validation through global case studies to confirm the applicability of the developed RF model and the accuracy of the results.

Acknowledgements

I would like to express my sincere gratitude to my supervisor, Dr. Willem Vervoort, and my co-supervisor, Dr. Floris Van Ogtrop. I am truly indebted to Willem who provided constructive feedback with an inspiration to continue; without his patient guidance and gentle push, I may never have successfully completed this thesis.

I extend my heartfelt thanks to Ignacio Fuentes and Julieta Rossi for their continuous support during this thesis.

Lastly, I want to thank my family for their encouragement throughout this academic endeavour, with love to Ayaan, Mahrosh, Fizza, Abeer, Zainab & Raveeha.

Content

List of Figures

List of Tables

1 Introduction

Freshwater ecosystems rely on the quality, frequency, timing, and volume of water flow because they regulate hydrological connectivity (Rosenberg et al., 2000). Water flow and inundation are both important aspects of water dynamics. Water flow not only helps in flushing sediment, nutrients, and salt from the river system, but wetlands and floodplains also receive nutrients and sediments through flooding related to high flows. Regular water flow is essential for the maintenance and support of the habitat, health, and resilience of river basins, and allows recovery after drought and dry periods. (Nilsson et al., 2005; Talbot et al., 2018). The flow volume contributes to the depth of water, the rate of rise and fall that can affect ecological and sedimentary processes, and the spatial distribution, which determines the area affected by water coverage (Area, 2018), and the duration of inundation, which has significant implications for the local ecosystem, especially in floodplain and wetland environments. All these factors collectively define the inundation regime of an area and determine its ecological and hydrological impacts. Many different processes, i.e. heavy rainfall, rapid snowmelt, dam failure, and storm surges, can cause inundation. Likewise, flow manipulation, inundation, and fragmentation caused by water resource development impact ecosystems, including sedimentation, anoxia, elimination of turbulent reaches, hindrance of channel development, reduction in the vitality of deltas and floodplain productivity, and massive alteration of aquatic communities (Nilsson et al., 2005; Vorosmarty et al., 2000). Assessing the impact of human intervention on river systems is complicated by high climate variability, which can mask or amplify other effects (Van Dijk et al., 2013).

Australia is no exception, for example, in 2020, continued low and almost nil water flows due to drought conditions severely affected the natural resilience of the Macquarie Marshes and some regions of Macquarie River in the central Murray-Darling Basin (MDB), Australia (Ryan et al., 2021). River flows were cut at the Warren weir to mitigate upstream drought impacts, which resulted in the downstream drying of lakes and wetlands (Davies, Bowers et al. 2018). Generally, the development of dams and weirs provides more secure water for anthropogenic use; however, this disrupts the natural stream seasonal behaviour, and flood and drought cycles are disrupted. This natural cycle is essential for the maintenance of healthy wetlands and waterways (Bond et al., 2008). The climate of Australia is already marked by distinct variability, with seasonal and yearly fluctuations in rainfall and temperature. Substantial regions of the country often experience a shift from hot, dry and arid weather inducing heatwaves and droughts to flooding conditions (Puszka, 2021). The long dry periods are interspersed with periods of high flow that can restore and reinvigorate the wetlands. Likewise, the river environment in the Murray-Darling Basin (MDB) can be invigorated by floods (Pittock, 2019); however, the development of water resources in the Murray-Darling Basin means that the majority of floods are now released in a controlled manner for irrigation purposes and flood management (Chen et al., 2020). This has caused salinisation, a decline in health of wetlands and rivers and spread of blue-green algal blooms (Casanova, 2007). Water auditing would ensure an overall understanding of water availability in the basin, where it is used and to monitor the sensible distribution of water in the basin (Sturman et al., 2004). As result, there is a need for the development of a water monitoring and accountability mechanism/tool to support effective water management in the MDB.

To accurately account for all water flows and stocks, it is necessary to quantify all water in a river system (Hunink et al., 2019) and the groundwater, as some of the water flowing in rivers originates from groundwater seepage into the streambed (School, 2018). Traditionally, water levels in reservoirs, lakes and rivers are measured through in-situ gauging stations. However, globally, the number of in situ gauging stations has been decreasing (Frappart et al., 2006), and various reservoirs and lakes in developing countries have never been gauged (Zhang et al., 2006). Floods resulting from high flow conditions can provide additional challenges for monitoring, like difficulty in accurately predicting the timing and magnitude of floods, and real-time data availability and quality (Brunner et al., 2021). There are generally three steps to predict flood volumes in space and time in the landscape: 1) the use of a rating curve to derive an annual maximum flow time series using annual maximum water levels at point locations in the landscape, continuous in time; 2) application of a probability distribution function to estimate design peak flows derived from annual maximum flows at point locations; and 3) hydraulic modelling for the simulation of design peak flows across the landscape for specific time periods (Okoli et al., 2019). However, all these three steps are affected by significant uncertainty, i.e., systematic, and random errors associated with direct measurements of river flows (Tomkins, 2014), as well as in the subsequent prediction and forecasting (Krzysztofowicz, 2001). Rating curves use analytical functions to translate water level measurements into river flows. There is uncertainty in developing a rating curve that can result in very high errors, especially in high-flow conditions (Tomkins, 2014), as during flood conditions, there is often no direct observation of river discharge. Both probability and hydraulic models rely on the observed data (derived from uncertain rating curves) to develop further predictions or insights. Calibration of hydraulic models can introduce additional parameter uncertainty (Huang & Liang, 2006). Finally, if hydraulic models are used for conditions (such as extreme flood conditions) for which they are not calibrated, they can also be affected by significant uncertainties (Gu et al., 2018).

Satellite radar or satellite laser altimetry is an alternative technique for estimating continuous water levels in space in open water bodies (especially in areas with limited gauging stations or difficult accessibility), flood monitoring (Schumann et al., 2007), hydraulic modelling, and river discharge estimation. Satellite radar/laser altimeters are profiling tools that can be effectively used to estimate the water levels in rivers, lakes, and wetlands (Ebaid & Aziz, 2017). Altimetry data, in conjunction with bathymetric and topographic data, can be valuable source of water surface elevation, and can also be used to infer the inundation extent. They provide an understanding of both the vertical dynamics (water levels) and horizontal spread (inundation extent) of water bodies (Shen et al., 2019). The advantages of using satellite data are their global coverage and availability at relatively short temporal scales, and by now, having relatively long time series. As a result, there has been an exponential growth in the volume of available satellite data with an enhanced spatial resolution of instruments over time (Dorji & Fearns, 2017). Water mapping, in particular, has gained popularity owing to the growing need to understand floodwater storage and spatiotemporal monitoring of surface water extent and dynamics (Huang et al., 2018). To estimate the extent and volume of floodwater, many studies have implemented different water mapping techniques including machine learning models (Tehrany et al., 2014), remote sensing techniques (Rakwatin et al., 2013), and hydrodynamic models (Liu et al., 2015) providing valuable insights into floodwater storage and dynamics. In line with this trend, the aim of the current study was to develop a methodology for estimating floodwater in the Macquarie Marshes region, utilising Sentinel 1 and 2 images, as well as a high-resolution Digital Elevation Model. This study is an extension of the work of Fuentes et al. (2019a) and Fuentes et al. (2019b), who evaluated the capability of different algorithms to determine flood extent and explored the temporal dynamics of inundated areas and corresponding return periods in the Namoi Catchment. Sentinel 2 images have an edge over other satellite images due to their frequent revisit capabilities, finer spatial resolution and free access (Du et al., 2016), and Sentinel 1 images have been reported to enable the detection of flood water beneath the vegetation (Tsyganskaya et al., 2018). This is essential for the Area of Interest (AOI) of this study as the Macquarie Marshes consists of swamps covered by vegetation (*Restoring and protecting the Macquarie River Valley 2017–18 Snapshot*; Service, 1993). Estimation of water storage and flood water volume in the AOI is essential for the assessment of the ecological outcomes of flooding for improved conservation of wetlands and ecology, which is currently lacking in the Macquarie Marshes. Remote sensing can estimate the volume and extent of floodplain water, as they allow for a more comprehensive understanding of the floodplain water extent and volume. Although remote sensing can map the flood extent and estimate water volume, this approach alone may not be sufficient to provide an accurate estimate of the floodplain water volume and extent, and there are no "direct" observations of flooding apart from satellite images, and satellite imagery is not continuous in time.

The structure of the thesis is as follows: Chapter 1 of this study discussed the general introduction of the topic. Chapter 2 provides a literature review, where previous studies related to our research area were reviewed and analysed in order to identify any gaps in the research. Chapter 3 focuses on the assessment of the effectiveness of various indices and algorithms in accurately identifying and mapping water bodies using data from Sentinel 1 and Sentinel 2 satellites. This chapter involves testing different techniques for delineating water and evaluating their performance to determine the most suitable approach for extraction of vegetated water, and also discusses the surface water volume quantification to analyse the water available in wetlands. Chapter 4 presents the conclusion and summary of the research findings, along with their implications. This chapter also provides recommendations for future research based on the results obtained.

2 Literature Review

The objective of this chapter is to provide a comprehensive and critical overview of the existing research on water extent and depth extraction using satellite imagery, with a specific focus on assessing the generalisability of different algorithms for long time series analysis. The review aims to inform and support the development of future research, particularly in the context of complex wetlands with vegetation and shallow water.

2.1 Changing Nature of Flooding in Australia

The geography and variable climate conditions in Australia make it susceptible to frequent flooding (Puszka, 2021). The climate in Australia is predicted to become more variable and extreme in the future, impacting the management of agriculture and natural resources (Howarth, 2022). Over the past few decades, floods caused damage on a large scale in different areas of Australia (Khurshed, 2021; WMO, 2021). In addition, the Intergovernmental Panel on Climate Change (IPCC) has warned about an increase in the frequency of extreme rainfall, droughts, and bushfires for Australia (Toh, 2022). Rising temperatures, induced by climate change, can amplify the maximum precipitation levels and exacerbate extreme flooding (Wasko et al., 2023). According to IPCC 2018 & 2021 reports, Australia is projected to be drier overall, however, it is anticipated that there will be an increase in the frequency and intensity of flooding events due to heavy rainfall. Over the past few years, these trends have become apparent, like the severe drought of 2017-2019 followed by La Niña events in 2020-21 and 2021-22 that resulted in the extreme rainfall events in February-March 2022 in southeast Queensland and New South Wales (https://www.csiro.au/en/research/natural-disasters/floods/causes-and-impacts). According to Australian Government Bureau of Meteorology, despite being the world’s driest inhabited continent, Australia experienced its ninth-wettest year on record in 2022, and the national rainfall was 25% higher than the annual average from 1961 to 1990. The southeastern region received above average rainfall compared to all years since 1900. The persistent rain in eastern Australia caused significant flooding multiple times throughout the year (Falconer, 2023). As examples: in 2022, Queensland received the worst flooding since 2011; and Northern New South Wales (NSW) and Southern Queensland received more than a year of rainfall in less than two months in 2022 (CDP, 2022). In addition, La Niña events have also contributed to an increase in significant flooding periods in Eastern Australia in 2021-22.

As a result, severe floods are a recurring characteristic of the Australian climate. Based on the predicted changes in the rainfall, mentioned above, these events are more likely to continue in the future with increased frequency and severity (Mueller et al., 2016). This has resulted in a pressing need to understand the temporal aspect of these flooding events (Mueller et al., 2016), along with the accurate knowledge of the location, extent, persistence, and recurrence of surface water for water resource assessments and regulation (Pekel et al., 2016). This also raises the question of whether flood monitoring and management strategies can be improved particularly in areas with limited in-situ monitoring systems that experience extreme flood events with large extent and temporal variability (Thomas et al., 2011).

Satellite remote sensing can be a valuable tool for capturing information about surface water in inaccessible and remote areas. Satellite imagery can be used to detect water and understand the hydrological conditions of large rivers, as well as how they interact with highly water-dependent ecosystems like wetlands (Van Dijk & Renzullo, 2011). However, it is quite a challenging task to map the water regime of wetlands, as they are very dynamic and complex ecosystems. Some of the wetlands seasonally inundate while some wetlands are always flooded. They are also said to "act like a sponge", i.e. store water during wet period and release it during dry spells (Acreman & Holden, 2013), and replenishing underground aquifers. One of the most important functions of wetlands is actually groundwater recharge (Kent, 2000; Van der Kamp & Hayashi, 1998). The significant components for operational wetland monitoring, i.e. the public availability of satellite remote sensing data, acquisition of low Earth Orbit satellites every few days (Tayer et al., 2023), and advanced machine learning algorithms (Adeli et al., 2021; Gemechu et al., 2021; Whyte et al., 2018) have created a platform for monitoring of the dynamic behaviour of wetlands.

2.2 Remote sensing using satellites

Mapping water extent in the wetlands using satellite earth observations has been a long practice to delineate and characterise wetlands areas (Hardy et al., 2019). Due to the remote nature and inaccessibility of various semi-arid wetland ecosystems with inadequate gauge data, the remote sensing data provides long-term trend information about the certain changes and overall status of these wetlands. Remote sensing enables quantification of the inundation variability and the associated ecosystem responses. Since 1972, Earth Observation satellite data has been available for Australia, serving as a national archive to observe surface water (Figure 2.1) (Mueller et al., 2016; Tulbure & Broich, 2013). It was early 1970s when Landsat-1 was already used for the flood mapping (Robinove, 1978). Landsat satellites routinely capture images every 16 days. Images acquired during cloudy conditions may obscure visibility, meaning not every flood peak can be observed using Landsat data. However, if these images are captured some time after flood peaks, they can still capture a good proportion of the flood extent. (Mueller et al., 2016). Another huge challenge with mapping wetlands with remote sensing is vegetation cover. Though the techniques for water delineation from optical satellite imagery are well-established and the passive sensors (multispectral, hyperspectral and thermal imagery) have shown great promise, time interval and weather conditions' restrictions sometimes make them less suitable compared to active sensors, such as the Synthetic Aperture Radar (SAR). SAR sensors have increased the availability of high spatio-temporal resolution, and they can capture data in any weather condition.

The multi-spectral and radar sensors measure different types of energy. Multi-spectral sensors measure the reflection of light energy off objects in the environment, while radar sensors measure microwave echo signals. Multi-spectral sensors capture image data within specific wavelength ranges across the electromagnetic spectrum (Figure 2.2). For example, water detection techniques generally take advantage of the absorption of longer wavelengths of light in water, particularly the near and shortwave infra-red parts of the electromagnetic spectrum. This implies that the corresponding infra-red spectral bands in the Sentinel-2 satellites (Band

8, 11 and 12), Landsat-5 and Landsat-7 satellites (Bands 4, 5 and 7), Landsat-8 (Bands 5, 6 and 7) (Flood, 2017) are detecting low to no water reflection with an increase in wavelength, and hence can be used as a spectral indicator for water (Mueller et al., 2016). Table 2.3 includes some of the example indices that exploit the difference in reflectance between two or more selected spectral bands. In contrast, the radar sensors initially transmit microwave signals and then the signals backscattered from the earth's surface are received back. The water detection technique of the radar sensors is based on the assumption that water surfaces are specular reflectors (i.e., very little energy is scattered back to the radar sensor) and are characterised by low SAR backscatter values compared to non-water surfaces. Figure 2.3 shows time series of various multispectral and radar satellites. There are some new satellite constellations, such as Sentinel that have comparatively finer spatial-temporal resolution (Vervoort et al., 2022). Sentinel-1 & Sentinel-2 are among the most recent SAR and optical satellites respectively. Sentinel-1 is a constellation of two radar imaging satellites- Sentinel-1A and Sentinel-1B, that operates in the C-band frequency range. Sentinel-1B is no longer operational now since 23 December 2021 due to some interruptions in the satellite's operations because of an anomaly in its power sub-system (*Mission ends for Copernicus Sentinel-1B satellite*, 2022). While acquiring SAR data, Sentinel-1 records 4 types of signals, i.e., Horizontal Transmit and Horizontal Receive (HH), Horizontal Transmit and Vertical Receive (HV), Vertical Transmit and Vertical Receive (VV) and Vertical Transmit and Horizontal Receive (VH). The backscatter coefficient (sigma naught ($\sigma 0$)) is the main SAR sensor-retrieved parameter. The Vertical transmit-vertical receive (VV) and vertical transmit-horizontal receive (VH) backscatter intensity identify the different land cover classes on the earth's surface, and the variation of these coefficients is on the basis of the surface characteristics like surface shape and roughness, soil moisture content and height above the ground level (Figure 2.4, Figure 2.5). Just like Sentinel-1, the Sentinel-2 mission also consists of a constellation of twin satellites, Sentinel-2A and Sentinel-2B. Sentinel-2 carries a multispectral imaging instrument (MSI) with 13 spectral bands ranging from the visible to the infrared spectrum. The Sentinel-2 mission offers high-resolution optical imagery with spatial resolutions of 10 meters, 20 meters, and 60 meters for different spectral bands. With a spatial resolution of 30 meters for optical bands, and 15 meters for the panchromatic band, Landsat is coarser compared to Sentinel-2 but because of its extensive historical archive dating back several decades, Landsat imagery has been a reliable source for long-term environmental monitoring (Figure 2.1). All of these satellites regularly provide data for a wide range of applications, including mapping and monitoring of land cover, vegetation, water bodies, and other Earth surface features.

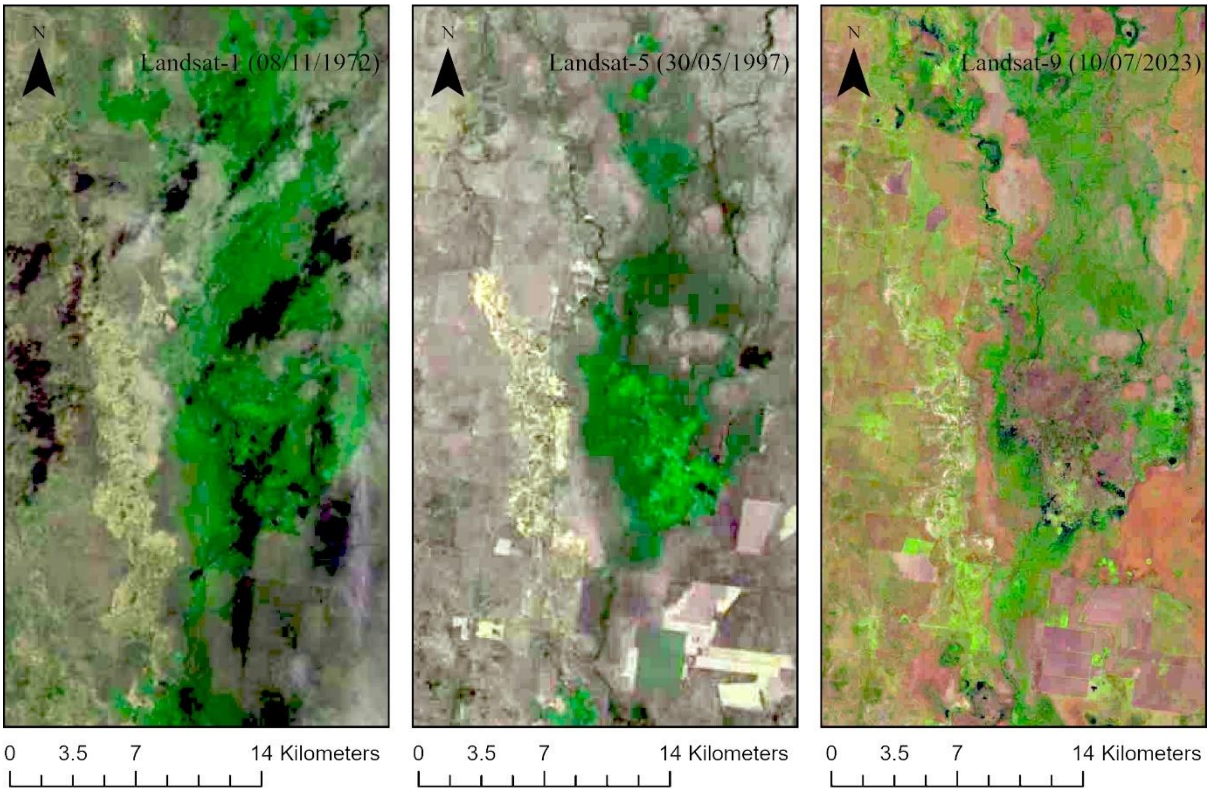

Figure 2.1: Landsat Satellite Images of Macquarie Marshes acquired during different time-periods with Band 1, 2 and 3 (https://earthexplorer.usgs.gov/)

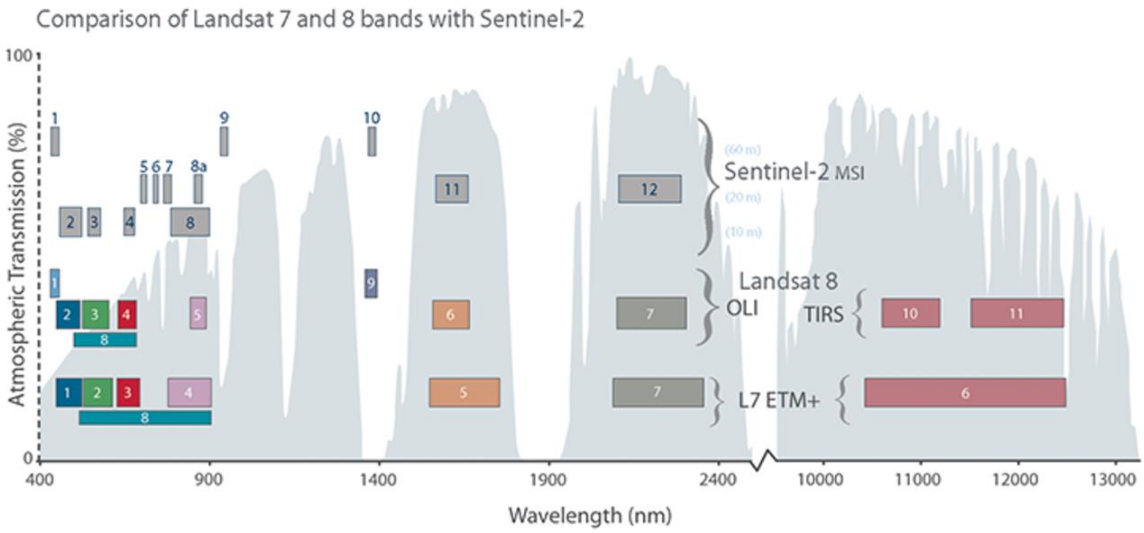

Figure 2.2: Comparison of Sentinel-2 and Landsat (Comparison of Landsat 7 and 8 bands with Sentinel-2, 2015)

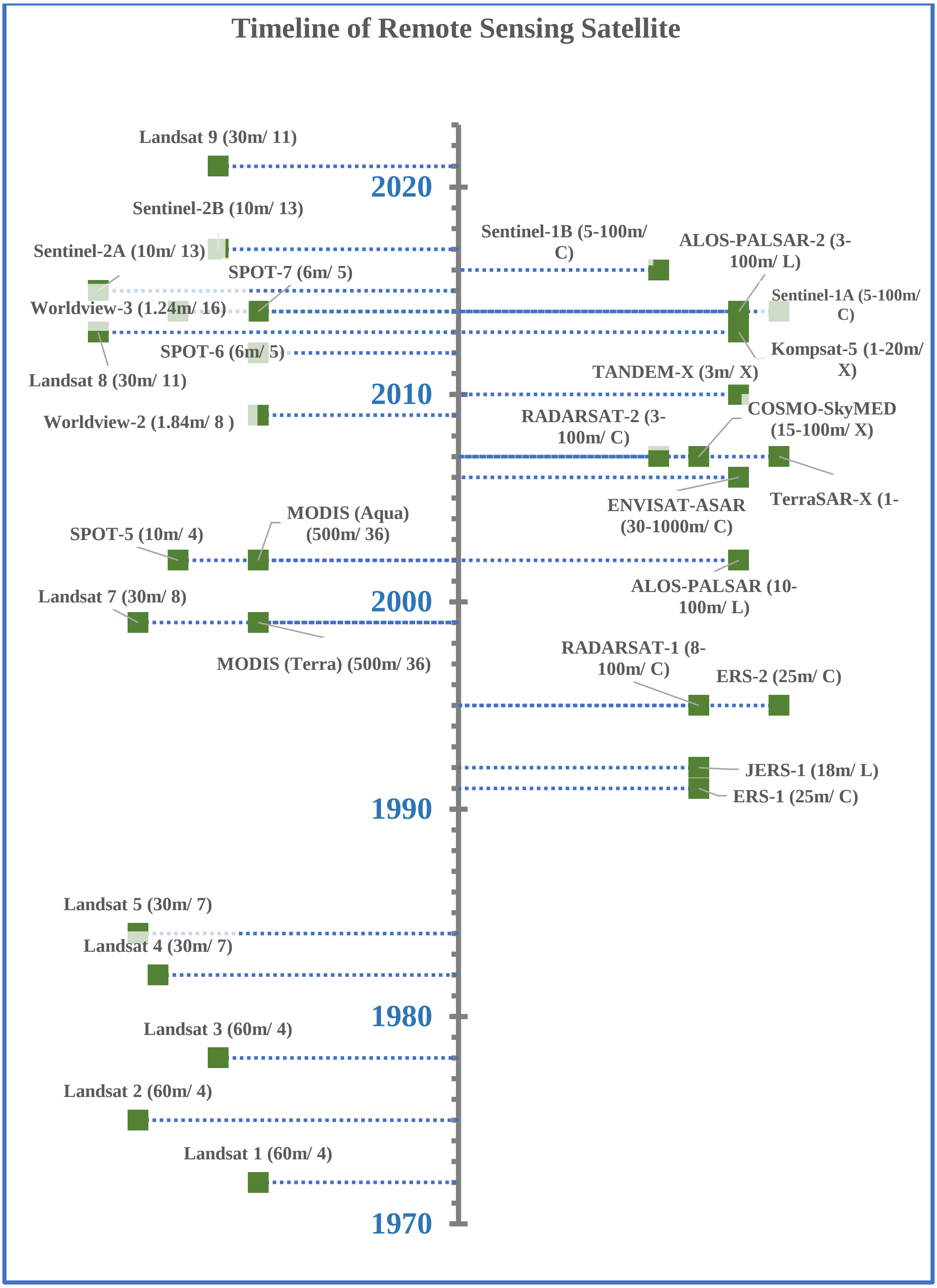

Figure 2.3: Timeline of Remote Sensing Satellites

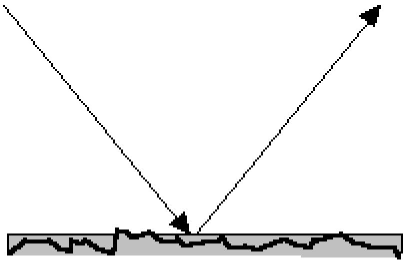

Figure 2.4: Radar is specularly reflected off the water surface, with low backscatter intensity. An example of flooded soil (Liew, 2001)

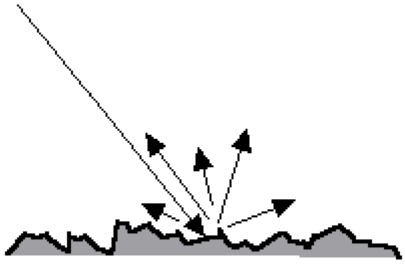

Figure 2.5: Higher backscattered radar intensity in wet soil due to the large difference in electrical properties between water and air (Liew, 2001)

2.3 Role of Satellite Remote Sensing for Floodwater Extent Mapping & Monitoring

As outlined briefly in Chapter 1, satellites are a beneficial tool to map and observe floods (Notti et al., 2018). Satellite remote sensing data has been shown to track surface water extent and map areas affected by flooding (Muszynski et al., 2022). This is particularly valuable for areas where traditional ground-based monitoring methods are not accessible, or where data is limited. The application of satellite remote sensing in flood mapping can help understand factors contributing to flood events, provide a near real-time response to flooding events, and map flood inundation (Revilla-Romero et al., 2015). Several different satellite products have been used for flood mapping. This includes multispectral satellites like Landsat and MODIS, and Sentinel-2 which provide high-resolution images (Halder & Bandyopadhyay, 2022), and can identify flood extent and provide flood damage assessment. Alternatively, radar satellites like Sentinel-1 and Advanced Land Observing Satellite (ALOS) can penetrate clouds and provide images in any weather conditions, which can provide flood mapping possible even during cloud cover or heavy precipitation (Yamaguchi, 2020). Flood mapping can also be done by combining different satellites, which can also make adjustments for sensor bias (Rosenthal et al., 2020). For example, Rosenthal et al. (2020) categorised the near real-time flood event's risk through leveraging the historic observed flood frequency using Landsat, Sentinel-1, and Sentinel-2. Sentinel-1 performed better at detecting more flood-prone areas, while Landsat 8 and Sentinel-2 captured areas that were less susceptible to flooding.

2.4 Approaches to the delineation of Floodwater Extent Using Satellite Images

For this literature review, different keywords and combinations of keywords (Table 2.1) were used in ScienceDirect and Scopus to locate relevant research articles. This specifically focussed on the use of Sentinel satellite imagery and machine learning techniques for the monitoring and detection of water in wetlands. The retrieval of these articles was followed by the evaluation of titles and abstracts of the articles to determine their relevance to the research objectives and questions. The focus is to find answer for the research questions, how well are the Sentinel-1 and Sentinel-2 suited for surface water extent mapping in the complex wetlands with vegetation and shallow water, how "generalisable" the different algorithms are for observing water volumes and extents, with a specific focus on how well the algorithms perform for long time series of images, and finally, how well are threshold segmentation, machine learning classification techniques suited for the estimation of surface water variation. A variety of sensors can be used for water delineation. Figure 2.6 outlined the different applications in water delineation, along with their advantages and disadvantages, synthesising the information gathered from the literature review.

Table 2.1 Keywords used to retrieve articles from Scopus & Elsevier ScienceDirect

Search terms		
Sentinel 1	Sentinel 2	Wetlands
Flooding	Water Delineation	Water Detection
Marshes	Inundation	Algorithms

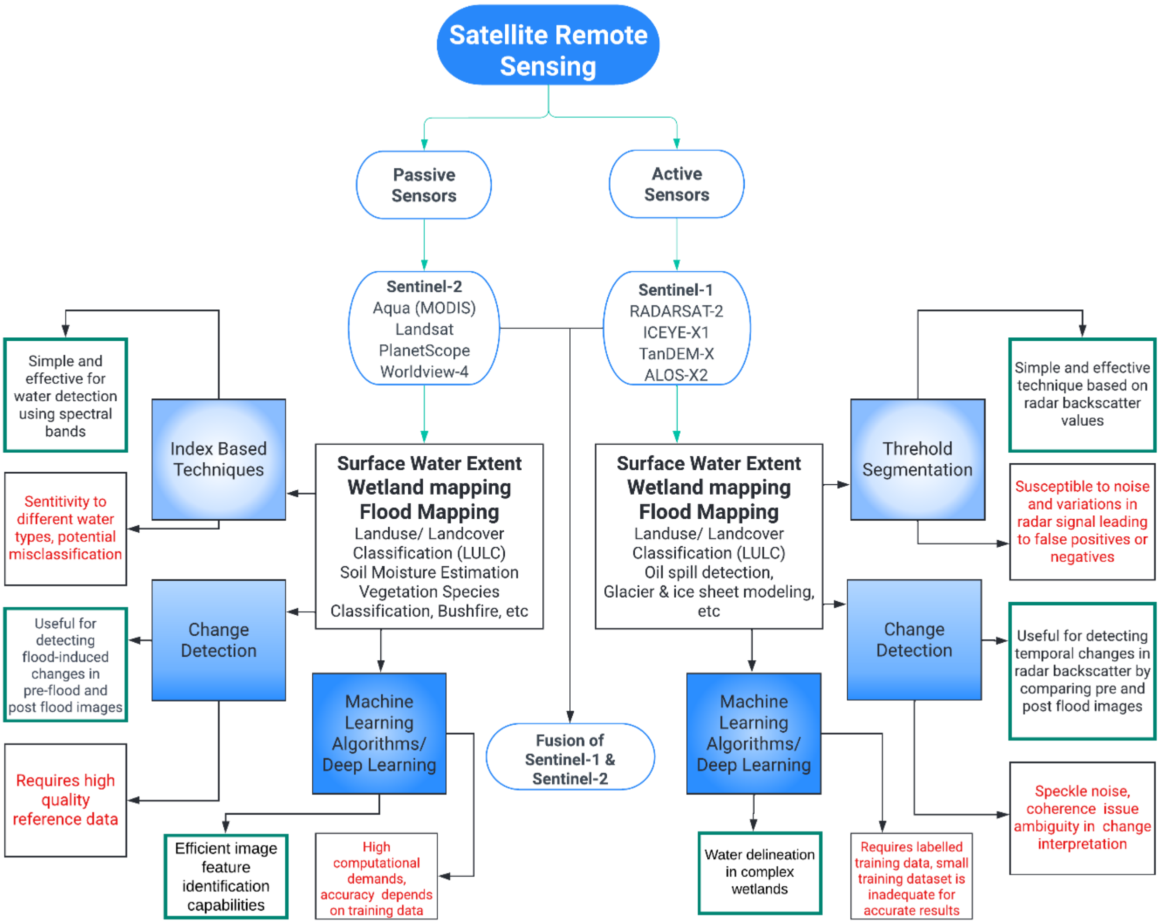

Figure 2.6: Flowchart showing an outline of different sensors with their applications and techniques for water delineation along with their pros and cons, as derived from the literature review

Table 2.2:List of research papers with a focus on wetlands/ flood mapping using Sentinel-1/ Sentinel-2

Sensor	S. No.	Author	Location	Technique Uses	Years covered in the analysis									
					2014	2015	2016	2017	2018	2019	2020	2021	2022	2023
Fusion of Sentinel-1 & Sentinel- 2	1.	**(Vanderhoof et al., 2023)**	Central United States	Two algorithms based on Sentinel-1 and 2 were developed to map open water and vegetated water areas across 12 sites. The data integration for the vegetated water or the mixed pixels was complicated due to the sensor-specific differences (sensitivity to vegetation structure and pixel colour).										
	2.	**(Fichtner et al., 2023)**	Pakistan	Segmentation using a Multi-Spectral Flood Processor based on convolutional neural networks (MS-FP-cnn) for Sentinel-2. Adaptation of the similar CNN for Sentinel-1.										
			Mozambique											
	3.	**(Caballero et al., 2023)**	Bonaerense Valley of Colorado River (BVCR)Argentina	Multi-Output Gaussian Processes Modelling (no need for synchronisation of S1 and S2 acquisitions, long training time was required to reconstruct the VWC maps)										
	4.	**(Bioresita et al., 2019)**	Shannon River Central Ireland	Decision-level fusion using fuzzy logic minimum operator and Bayesian approach (fusion of S1 and S2 using Bayesian sum has an overall accuracy of >99% and >98% for permanent and temporary water surface respectively										
	5.	**(Mohseni et al., 2023)**	Great Lakes, Central East of North America	Wetland mapping using object-based supervised machine learning (ML) classification										
	6.	**(Onojeghuo et al., 2021)**	Southern Alberta	Machine learning classifier algorithms (RF, SVM, and CART)										
	7.	**(Hosseiny et al., 2021)**	Avalon, Newfoundland, Canada	WetNet model for wetland classification										
	8.	**(Manakos et al., 2020)**	Doñana wetlands, Southern Spain	Random Forest										
	9.	**(Li & Niu, 2022)**	China	Automatic classification method based on shape and flooding frequency (AuCoSaFF)										

	10.	**(Mahdianpari et al., 2020)**	Canada	Object-based image analysis (OBIA)/ Random Forest with an overall accuracy of 80%			■	■	■					
	11.	**(Martinis et al., 2022)**	Australia, India, Germany, Sudan, Mozambique	Computation of permanent reference water mask (P-ReWaM) and monthly seasonal reference water masks (S-ReWaM). Sentinel-1 Flood Service (S-1FS) for the derivation of single temporal water masks from Sentinel-1 data and a Multi-Spectral Flood Processor from Sentinel-2 data using convolutional neural networks (MS-FP-cnn)						■	■			
	12.	**(Slagter et al., 2020)**	St. Lucia, wetlands, S Africa	Random Forest			■	■	■					
	13.	**(Kaplan & Avdan, 2018)**	Balikdami, Turkey	Unsupervised/Supervised Deep Learning Classification				●						
Sentinel-1	14.	**(Melkamu et al., 2022)**	Lake Tana, Ethiopia	Histogram-based thresholding method, Hydrodynamic modelling for simulation of flood inundations based on Ribe and the Gumara River time-series discharge data, and the simulated inundation area was similar to SAR-extracted flood inundations							●			
	15.	**(Shahabi et al., 2020)**	Haraz watershed, Mazandaran, Northern Iran	Flood susceptibility was modelled with KKN functions and its ensembles using the Bagging Tree algorithm. Distance to river, and slope were found to be most important factors for flood occurrence. Other flood conditioning factors were elevation, land use/land cover, lithology, curvature, river density, rainfall, topographic wetness index (TWI), stream power index (SPI)			●	●						
	16.	**(Liang & Liu, 2020)**	Ascension Parish, Louisiana	Local thresholding with an overall accuracy of 98.91% (better than Otsu, Gamma fitting, Split based KI)			●							
	17.	**(Yu et al., 2022)**	Lower reaches of Yangtze River, China	Random Forest (RF) algorithm GLCM texture features extraction Angular Second Moment, Contrast, Correlation, Entropy, Inverse Difference Moment, Otsu, KNN & SVM. Gaofen-1 (GF-1 PMS) was used as ground truth data			●				●			
	18.	**(Li & Demir, 2023)**	Central US	Deep learning techniques, ResNet50, U-Net, Flood Inundation Archive, Bmax, Otsu. 30 m NASA MSFC of similar dates as of Sentinel-1 was used for validation.						●				
	19.	**(Foroughnia et al., 2022)**	Sesia River Enza River North Italy	Otsu, Combination thresholding and segmentation, Random Forest- Sentinel-1 (32 parameters), Random Forest- Sentinel-1 & Sentinel-2 (R,G,B,NIR,GLCM derived features, NDWI)				●			●			

	20.	**(Pukanská & Bartoš, 2021)**	Bodrog River, Slovakia	Otsu thresholding and Random Forest				■	■					
	21.	**(Ferrentino et al., 2020)**	Monte Cotugno, Italy	Multi-polarisation analysis for waterline extraction on Single Polarised and Dual Polarised SAR measurements followed by combination of constant false alarm rate (CFAR) and edge detection techniques.			■	■	■					
	22.	**(Pedzisai et al., 2023)**	Mbire District, Northern Zimbabwe	NDFI, NDFVI, the Ensemble of Scenarios Pyramid base (E1) to create six scenarios on the basis of time series built on flood and post-flood images using three pairs of stacks of bi-temporal, penta-temporal & deca-temporal time-series images of similar polarization flood extent maps				●						
	23.	**(Zhao et al., 2020)**	River Severn basin (UK) and the Lake Maggiore (Italy)	Pixel-based time series analyses and object-based spatial analyses			■	■	■					
	24.	**(Muro et al., 2016)**	Lagoon of Fuente de Piedra, in southern Spain, French Camargue, South France	Polarimetric SAR-based time series change detection technique & change detection algorithm (S1-omnibus). Evaluation of performance of S1-omnibus vs. a pairwise comparison of consecutive images.	■	■								
	25.	**(Andrew et al., 2023)**	Ulmarra	Near real-time deployment of a CNN-based transfer learning technique. The accuracy of image classification of three convolutional neural network (CNN)-based encoder–decoders (i.e., U-Net, PSPNet and DeepLapV3) were compared and U-Net marginally outperformed the other models.								●	●	
	26.	**(Mayer et al., 2021)**	Cambodia	Two different data labelling methods of automatic data collection JRC and Edge were used to train a U-Net. Limited ability to perform additional model comparisons due to the high cloud computing cost, and small sample size for validation.						●				
Sentinel-2	27.	**(Pena-Regueiro et al., 2020)**	Prat Cabanes-Torreblanca, Sagunto, Safor, and Pego-Oliva, Spain	NDWI, NDWI, CEDEX, RE-NDWI, AWEIsh, AWEInsh, B_BLUE			●	●	●					
	28.	**(Ludwig et al., 2019)**	El Kala Wetland System, Algeria	Development of an automated method for wetland detection along with NDWI, MNDWI, NDVI, NDMI, NMDI, ABDI1,		■	■	■						

			Sio-Siteko Wetland, Uganda/Kenya Lake Neusiedl, Austria	ABDI2, ND (NIR-SWIR2), ND (GREEN - SWIR2), ND (SWIR1 - SWIR2) There was accurate mapping of open water; however, limitations happened in narrow streams with dense vegetation cover or turbid water (mixed pixels)										
	29.	**(Thapa et al., 2022)**	Thailand	NDWI, NDVI								●		
	30.	**(Tulbure et al., 2022)**	MDB, Australia	Random Forest (surface reflectance in L8/S2 band, NDVI, EVI, NDWI, NDMI, MNDWI, AWEI, Slope and Shaded relief). 500 sample pixel (150 water) and (350 non-water) selected from a stratified random sampling design.										
	31.	**(Laonamsai et al., 2023)**	Ping River in Kamphaeng Phet Province, Northern Thailand	NDWI, MNDWI, SAVI, WRI, and AWEI were used for stream extraction. Threshold of the indices were detemined using the Otsu threshold method. AWEI achieved the highest accuracy and precision at 90% and 99%.		●							●	
	32.	**(Kaplan & Avdan, 2017)**	Sakarbasi wetland, Turkey	Pixel based classification, object based classification, the overall accuracy of proposed index based & object based classification is 99% with a 0.95 kappa			●							

● Single Image

● Multiple Images

2.4.1 Sentinel 1

Numerous methods have been proposed for flood mapping using Sentinel 1 images (Table 2.2). These techniques include histogram based threshold segmentation (Cao et al., 2019; Liang & Liu, 2020), Convolutional Neural Networks (Tavus et al., 2022), advanced approaches based on machine learning (Konapala et al., 2021), clustering algorithms (Landuyt et al., 2020) and change detection (Li et al., 2018; Pedzisai et al., 2023; Tupas et al., 2023).

2.4.1.1 Threshold Segmentation

Threshold segmentation is most commonly used technique for image segmentation. In this technique, a threshold value, either global or local can be applied to the backscatter coefficient to separate water from other land cover types. (Moharrami et al., 2021; Zhang et al., 2020). Global thresholding is a simple technique that selects a single threshold value for the entire image (Twele et al. 2016), considering all pixels above the threshold as one class and all pixels below the threshold as another class. Twele et al (2016) suggested a completely automated process for inundation mapping; the process consisted of geometric correction, automatic thresholding, and a fuzzy logic-based classification refinement. Generally speaking, smooth and non-vegetated flood water surfaces exhibit lower backscatter coefficient values, causing flooded areas to appear darker compared to non-flooded areas (Foroughnia et al., 2022). As a result, a thresholding approach can be used to classify the image into flooded and non-flooded areas. Huang Lin (2021) critiqued the thresholding technique, highlighting that this method works fine in a plain rural area, but this technique is not suitable for complex features as the shadows of buildings and trees can be easily misclassified as water. Gulácsi and Kovács (2020) also put forward that a single σ0 threshold value is not suitable for accurate water cover delineation due to the acquisition changes from scene to scene like wind speed, incidence angle, and wetland ecosystems (Bolanos et al., 2016). The drawback of using global thresholding is that the backscatter variations are not differentiated between different land types and all non-water pixels are treated as a land-class which can lead to misclassification. Liang and Liu (2020) applied a local thresholding approach to a single SAR image acquired on August 19, 2016 that could differentiate between water and non-water pixels with significantly higher accuracy compared to the conventional global-thresholding methods. Local thresholding techniques use different thresholds for varying regions of an image. Local thresholding involves separating the image into different land and water clusters, then using different thresholds for each cluster which has the potential to identify flood areas more accurately (Liang & Liu, 2020).

Otsu thresholding (Otsu, 1979), also known as maximum between-class variance method (Chen & Zhao, 2022), is a global thresholding technique that can be useful for mapping surface water bodies when they have a distinct backscattering coefficient compared to the surrounding land (Kavats et al., 2022). The Otsu method hypothesises that the bimodality exists in the frequency histogram between the object and background distributions, and the image segmentation produces more accurate results if the ratio between the object and the background is closer to 1:1 (Chen & Zhao, 2022). However, the results may be misleading in case of water bodies having similar backscattering coefficients. Also, in water bodies mainly covered with vegetation, the frequency histogram could be closer to a single peak rather than bimodal because the vegetation does not necessarily have low backscatter intensity values like water or higher backscatter values like artificial surfaces, bare rock (Chen & Zhao, 2022). Scattering within one scene can also have a different strength in different polarisations (for instance, vegetation canopies cause volume scatters and VH is more sensitive to volume scatters) (Liang & Liu, 2020). VV polarised data sets are more reliable as compared to VH polarized sets for flood water extraction due to their better contrast among water and non-water features (Melkamu et al., 2022).

Melkamu, Bagyaraj et al. (2022) applied a global histogram-based thresholding method to extract flooded and non-flooded areas using a VV-polarised data set (Figure 2.7). However, many studies have shown that using a combination of VV-VH data can yield better results for surface water mapping (Xing et al., 2018). The earlier mentioned paper by Liang and Liu (2020) proposed a novel technique of local thresholding which showed improved accuracy compared to traditional methods. They applied an intersection operation to combine water maps derived from two different polarizations (VV and VH) of an image. The intersection operation helps reduce commission errors (incorrect identification of features in an image) but may result in a slight increase of omission errors (non-identification or missing out of a feature in an image). Using accurate elevation data can yield more accurate implementation of hydrological constraints for the mapping in a machine learning model (Liang & Liu, 2020). Li and Demir (2023) also demonstrated an enhancement of the result with a 30m input data with the addition of a slope layer as compared to a machine learning model trained only on VV and VH bands. In their case, the performance of deep learning models trained on 10m datasets was enhanced with the addition of DEM and Height Above Nearest Drainage (HAND) (Li & Demir, 2023).

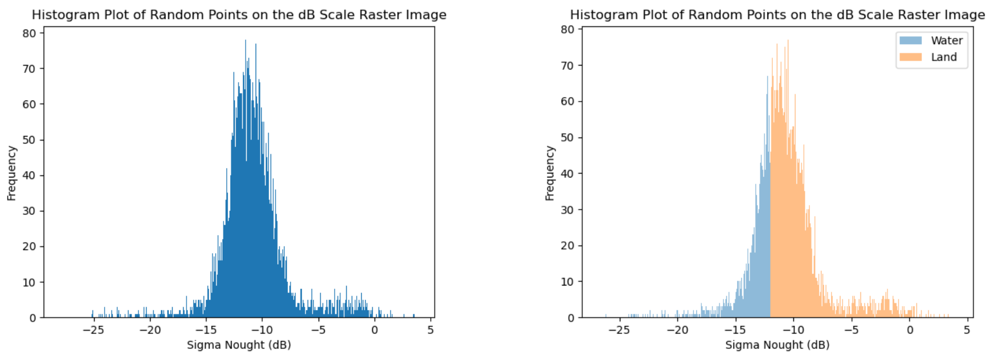

Figure 2.7 An adaptation of histogram-based thresholding method (Melkamu, Bagyaraj et al. 2022) applied on the VV-polarised scene of the Area of Interest (AOI) (01/09/2022)

Markert et al (2020) applied the Bmax Otsu and Edge Otsu- water mapping algorithms to the pre- processed Sentinel-1 datasets. Both of these algorithms are specific adaptation of the Otsu method that consider the maximum value of image pixels and edge information to determine the optimal threshold value, leading to more accurate results, especially when there is significant water surface reflectivity variation across the image.

Percentile thresholding is another technique in which the SAR imagery can be classified based on the statistical distribution of pixel values. The percentile values of pixel intensities are calculated within an image and these thresholds are applied for the segmentation of the image into different categories. Elkhrachy et al. (2021) used the 90th percentile and mean value for detecting water extent. The 90th percentile of threshold values extracted from histograms had a better performance compared to samples' median values (de Liz & Ribas, 2022; Elkhrachy et al., 2021). Percentile thresholding can possibly automate the thresholding process and perform image segmentation without the need for manual intervention; however, this technique is not used widely. The reason could be that a higher percentile threshold, such as the 90th percentile, could result in a more conservative classification, where only the pixels with the lowest backscatter values are classified as water. On the other hand, a lower percentile threshold, such as the 75th percentile, can result in a more inclusive classification, where some pixels with higher backscatter values may also be classified as water (Figure 2.8).

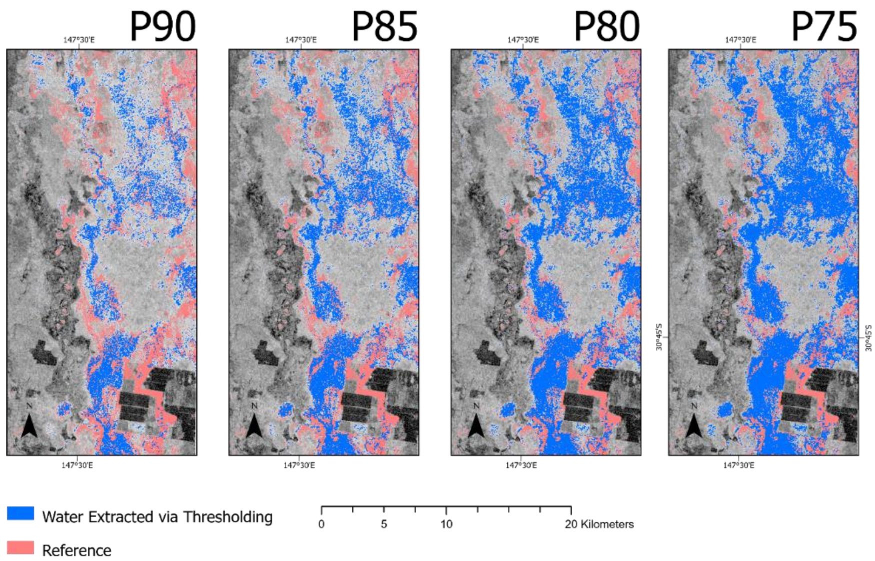

Figure 2.8: Water extracted from different percentiles in blue & the reference PlanetScope Image of the same date in coral colour. The background image is Sentinel-1 (acquired from Sentinel-1 2022))

In general, thresholding techniques are simple approaches, that can be rapidly applied to many images. However, a significant limitation of thresholding is the mapping of areas with similar low radar backscatter because all pixels with low radar backscatter are not covered with water (Andrew et al., 2023), and there is no universal thresholding value for water backscatter (Nemni et al., 2020). The classification of pixels into water and non-water strongly depends on their contrast that can misidentify sand patches, rough water surfaces, urban areas, etc. and to identify flooded vegetation, additional thresholds may be required (Helleis et al., 2022). Another alternative to tackle this issue is using the in-SAR change-detection approach or the machine learning algorithms especially the Convolutional Neural Networks (CNNs) and deep learning (DL) methods which can be employed to map floodwater in vegetated areas. However, ancillary data may be required for the image segmentation and classification, which may not be readily available (Andrew et al., 2023).

2.4.1.2 Object Based Classification

As an alternative, many studies have utilised Object-based classification (Gašparović & Klobučar, 2021; Sharifi, 2021; Zhang et al., 2021) as it delineates water with more accuracy and clearer edges compared to pixel-based methods (Guo et al., 2021) because of their effectiveness to reduce “salt and pepper” noise. An object-based random forest method can significantly improve the accuracy of flood information extraction. The RF algorithm does not require previous classification knowledge; instead, it forms classification rules based on the training sample set (Zhang et al., 2021). Despite the fact that most studies use pixel-based flood information extraction, this technique only takes pixels into consideration, overlooking texture, shape, neighbouring pixels, and spatial location of ground features. The object-based image (OBIA) classification technique considers the neighbouring pixels with homogeneous spectra and textures and spatial relationships, and unlike pixel-based techniques, OBIA is not vulnerable to speckle interference (Cai et al., 2020). Zhang et al. (2021) used the interferometric coherence (InSAR coherence (γ)), i.e., the cross-coherence between the two images and spatio-temporal information of the backscattering coefficient of Sentinel-1 time series in the classification. The backscattering coefficients of the different images were compared, and potential flooded regions were identified through the differences. Zhang et al. (2021) observed a strong influence of submerged vegetation on the extraction of flood information because there is a visible alteration of the vegetation to the backscatter signal, hampering the accurate detection of water. This limitation could be overcome with the use of high time-frequency and high spatial resolution quad-PolSAR data like Radarsat data. Grimaldi et al. (2020) noticed an increase in the double-bouncing effects in the presence of emerging vegetation due to increased permittivity and smoothness of water surface, resulting in a higher radar backscatter during floods. Wan et al. (2019) consider image segmentation as a time-consuming technique with little efficacy in a near real-time flood mapping. Also, the method is not completely automated as the semi-automatic water pixels need to be extracted under manual intervention. Gašparović and Klobučar (2021) applied object-based image analysis (OBIA) for flood mapping through integrating Sentinel-1 (during the flood period) and Sentinel-2 (pre-flood). In their study, the OBIA process consisted of combining the spectral signature, geometric and textural features, and vegetation indices. A multisource forest inventory, flood hazard map and habitat map were used as additional information sources for the assessment of accuracy and interpretation of results. The overall accuracy of the classification reported in that case was 94.94%. Gašparović and Klobučar (2021) applied five levels of data as the image classification input for flood mapping, involving initial segmentation and classification of VV imagery using statistical and geometric features followed by inclusion of statistical features of VH imagery into the classification input. The textural features of Sentinel-1 and Sentinel-2 were added at step-3 with an incorporation of vegetation indices at level 4 finally followed by statistical features of Sentinel-2. Support vector machines were used as a classifier. OBIA produces better results, but it demands knowledge and skills in the interpretation of satellite images along with the knowledge of the characteristics and environmental conditions of the area of interest (Tsyganskaya et al., 2018). The time required to produce a reliable flood map using OBIA should also be taken into consideration (Gašparović & Klobučar, 2021)

2.4.1.3 Change Detection

Histogram based thresholding like Otsu, split based thresholding and active contour models can identify flooded areas from a single sentinel image. However, Sentinel-1 has a huge catalogue of available data (Sentinel 1-A since 2014 and Sentinel 1-B since 2016) that can be used to emphasise changes in environmental conditions, for example, comparing a non-inundated image with a flooded one. With the subtraction of a reference image from the flood image, areas that have an increase in backscatter can be distinguishable from the areas with a negative shift in backscatter creating opportunities for flood mapping (Clement, 2020). The selection of the non-flooded reference image is important for the accurate derivation of the flood maps. Choosing the appropriate reference image can be challenging because it needs to be representative of the typical water extent in the area and taken during a similar season or time of year (could be previous year) but the land cover and the environmental condition should match with the flooded one as much as possible (Tupas et al., 2023). A key consideration in this process is to make sure that the two SAR images have the same viewing geometry/ alignment to reduce differences because of varying satellite capture angles, which can significantly influence the data interpretation and subsequent analysis (Zhou et al., 2023). The utilisation of SAR-based change detection approaches can advance the understanding of complex and dynamic ecosystems (Muro et al., 2016; Nasirzadehdizaji et al., 2019). With the comparison of SAR backscatter image potentially consisting of flood pixels with a reference SAR image with non-flooded conditions, the variations in spatial signals decrease which simplifies the task of acquiring optimal thresholds and model parametrisation for water detection. The chances of mislabelling of pixels with low backscatter values as flood can be reduced with the use of no-flood reference image (Tupas et al., 2023). There are multiple change detection algorithms such as Normalized Scattering Difference Index (NDSI), Standardised Residuals (SR), Shannon's entropy of NDSI (SNDSI), and Bayesian Inference method that normalise the issues of speckle and high variability among backscatter values. Tupas et al. (2023) found that the Bayes Inference (BI) method demonstrated the most consistent performance compared to NDSI, SNDSI and SR with an overall accuracy of 91%, and did not need to be tailor-fit while other change detection algorithms were significantly impacted with the input non-flood reference and the corresponding thresholding technique. Muro et al. (2016) applied SAR-based change detection technique to Fuente de Piedra and French Camargue to capture short-term changes in these highly dynamic and semi-natural areas using a set of Sentinel-1 images for 2014/2015 at a monthly resolution. (Muro et al., 2016) used the technique proposed by (Conradsen et al., 2016) that consists of carrying out simultaneous hypothesis testing of the homogeneity for SAR timeseries. The parametrisation of change detection models is less challenging compared to techniques that only use single SAR image to map floods, because these models can be applied to large and diverse domains. However, the choice of the reference images and the threshold for SAR pixels labelling in the change detection models can have a substantial impact on the accuracy of the flood maps (Tupas et al., 2023). Integration of change detection with other techniques can reduce the uncertainty stemming from low backscatter values over dry areas (Giustarini et al., 2012). Combining backscatter indices with the change detection approaches can also improve flood mapping accuracy (Pedzisai et al., 2023). Pedzisai et al. (2023) explore the value of combining change detection, thresholding and NDFI scenarios ensemble in mapping flood extent; the study demonstrated that multiple images (bi-temporal-S2, penta-temporal-S5 and deca-temporal-S10) can produce accurate flood mapping results within one calendar year, and especially the deca-temporal images produce better performance due to a longer temporal interval between the flooded images and the pre-flood/ driest reference image. This is also notable that with an increase in the number of images, the classification accuracy increases, and this also implies that high speed processers and computing environments may be required for the processing of large volumes of SAR images, though cloud-computing resources such as Google Earth Engine (GEE) can be leveraged for data accessibility, preprocessing and analysis (Al-Nasrawi et al., 2021).

2.4.1.4 Artificial Neural Networks

Several studies have explored the use of artificial neural networks to detect surface water using Sentinel-1 data (Andrew et al., 2023; Guzder-Williams & Alemohammad, 2021; Jiang et al., 2022; Mayer et al., 2021). Huang Lin (2021) proposed a Fully Convolutional Neural Network (FCN) Encoder method which is a deep learning model that is designed to consider both the pixel’s intensity and the spatial information of the pixel’s neighbourhood to detect water from SAR images. The So2sat dataset that consists of the patches of Sentinel-1 satellite SAR images was used to the train the neural the network for the detection of water from SAR images of several cities; the dataset consists of 17 classes but since the focus was only on water detection, therefore only the water patches were extracted and deployed as both the training and validation dataset initially. This approach worked better than the simple thresholding technique and the Random Forest that misclassified bridges as water. The proposed deep learning model with an accuracy of 98.38% surpassed the performance of CNN, Multilayer Perceptron (MLP), RF and SVM. Nallapareddy and Balakrishnan (2020) applied two neural network algorithms: Feed-Forward Neural Network & Cascade-forward back-propagation neural network. Both models were initially trained for detecting water bodies, and then they were used for water extraction and detection of flooded regions. Results when compared with the binary thresholding method of previous studies indicated that the Feed- Forward Neural Network performed with improved accuracy. Fraccaro et al. (2022) assessed using additional open access input layers as an AI model to detect water from Sentinel-1 images; however, the addition of extra input layers did not significantly improve the models’ performance. Mayer et al. (2021) used a deep learning approach to map surface water from Sentinel-1. A U-Net convolutional neural network was deployed using two automatic data labelling approaches of Joint Research Centre (JRC) surface water maps and Edge-Otsu dynamic threshold approach. Twelve different models using different settings were tested and the models that used the JRC data labels worked better. Water detection using ANNs and Sentinel-1 data can be highly accurate even in places with complex landcover (Guzder-Williams & Alemohammad, 2021). Guzder-Williams and Alemohammad (2021) applied a novel Convolutional Neural Network (CNN) model to Sentinel-1 observations for surface water detection at a global scale. Some studies have explored single-band based methods and probabilistic approaches to water segmentation (Bijeesh & Narasimhamurthy, 2020; Zortea et al., 2022). Deep learning techniques are promising for increasing flood mapping accuracy (Andrew et al., 2023); however, one of the limitations of using a CNN is the difficulty of hyperparameter tuning (Li et al., 2019). The convolution operation also often blurs water boundaries in segmentation tasks, and the CNN-based methods can sometimes be very computationally expensive if they try to retain sharp water bodies (Yang et al., 2022). CNNs require a large number of training parameters and datasets to be successful, and a small training dataset can result in the misidentification of water bodies (Yang et al., 2020).

2.4.2 Sentinel 2

The visible and infrared spectrum Sentinel-2 products can be easily accessed through different portals, for example they are available on the Google Earth Engine (GEE) (Wang, Ding et al. 2019) and Digital Earth Australia (https://www.dea.ga.gov.au/ accessed 18/06/2023). Sentinel data can be used to identify and map water bodies on the Earth's surface (Zhou, Dong et al. 2017). There are several methods for extracting information about water bodies from optical imagery, including the single-band threshold method (Jiang, Ni et al. 2021), the water index method (McFeeters, 1996; Xu, 2006), the remote sensing image classification method, the mixed pixel decomposition method, and the multisource data combination method. The water index method is regarded as the most convenient and accurate method and has been widely used in various applications (Jiang, Ni et al. 2021) due to the swift extraction and monitoring of surface water area. Within this method, various water indices have been developed for water detection (Table 2.3). The combination of visible and infrared bands through water indices enhance water and suppress non-water by setting a threshold value. The most effective indices for water detection in arid regions are the ones that use mid-infrared band (Thomas et al., 2015).

Table 2.3: Indices used by Fisher, Flood et al. (2016)

S. No.	Water Indices	Source	Equation
1.	AWEI $_{shadow}$	(Feyisa et al., 2014)	$Blue + 2.5 \times Green - 1.5 \times (NIR + SWIR1) - 0.25 \times SWIR2$
2.	AWEI $_{no\ shadow}$	(Feyisa et al., 2014)	$4 \times (Green - SWIR1) - (0.25 \times NIR + 2.75 \times SWIR2$
3.	TCWCrist	(Crist, 1985)	$0.0315 \times Blue + 0.2021 \times Green + 0.3102 \times Red + 0.1594 \times NIR - 0.6806 \times SWIR1 - 0.6109 \times SWIR2$
4.	NDWI	(McFeeters, 1996)	$\frac{(Green-NIR)}{(Green+NIR)}$
5.	MNDWI	(Xu, 2006)	$\frac{(Green-SWIR1)}{(Green+SWIR1)}$
6.	WI$_{2006}$	(Danaher & Collett, 2006)	$50 - 19\, ln\,(DNb2) - 52.18\, ln\,(DNb3) + 83.32\, ln\,(DNb4) - 14.78\, ln\,(DNb5) + 11.875\, ln\,(DNb7) + 14.135\, ln\,(DNb2)\, ln\,(DNb3) - 13.95\, ln\,(DNb2) ln\,(DNb4) + 3.935\, ln\,(DNb2)\, ln\,(DNb5) - 0.77\, ln\,(DNb2)\, ln\,(DNb7) - 3.785\, ln\,(DNb3)\, ln\,(DNb4) + 7.37\, ln\,(DNb3)\, ln\,(DNb5) - 4.675\, ln\,(DNb3)\, ln\,(DNb7) - 5.41\, ln\,(DNb4)\, ln\,(DNb5) + 1.08\, ln\,(DNb4)\, ln\,(DNb7) + 1.265\, ln\,(DNb5)\, ln\,(DNb7)$ *
7.	WI$_{2015}$	(Fisher et al., 2016)	$1.7204 + 171 \times Green + 3 \times Red - 70 \times NIR - 45 \times SWIR1 - 71 \times SWIR2$

*WI$_{2006}$ used top-of-atmosphere reflectance scaled linearly to an 8-bit digital number (DN) (Fisher et al., 2016)

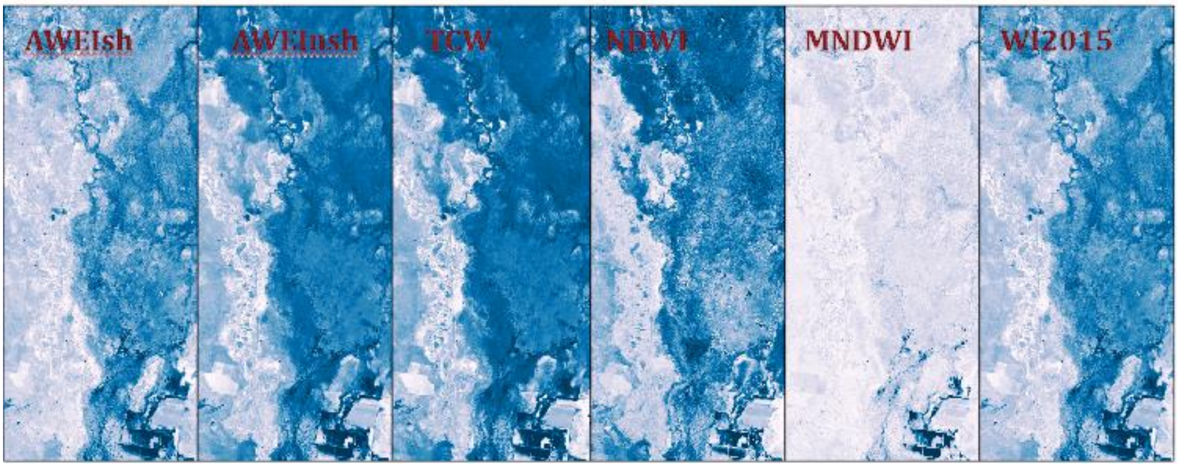

Figure 2.9: Figure showing the indices used by Fisher et al., 2016 applied to a Sentinel-2 Mosaic image of Macquarie Marshes for the year 2022

Fuentes et al. (2019) applied different algorithms to MODIS imagery (Table 2.4), including, the Brakenridge algorithm for single images (BRAK) and composite images (BRAKC), and Normalized Difference Indices for the temporal analysis and flood extent inundation in the Namoi River basin, and found that the results of Islam methodology (ISL) were the most promising with respect to spatial dynamics. There was reasonable accuracy for all algorithms in capturing the discharge peaks. As another example, Mueller et al. (2016) developed the Water Observation from Space (WOfS) product using 27 years of data from Landsat-5 and Landsat-7, spanning from 1987 to 2014. This water detection algorithm was based on combining water indices with a decision tree classifier, and the WOfS product provided a classified output, giving the probability of water for every available Landsat image (Krause et al., 2021).

Table 2.4: Indices used by (Fuentes et al., 2019)

S. No.	Water Indices	Source
1.	Open Water Likelihood (OWL)	(Guerschman et al., 2011)
2.	Islam methodology (ISL)	(Islam et al., 2010)
3.	Brakenridge algorithm for single images (BRAK)	(Nigro et al., 2014)
4.	Brakenridge algorithm for composite images (BRAKC)	(Nigro et al., 2014)

MODIS, which has a relatively high temporal resolution, can delineate inundation extent over large areas; however, the low spatial resolution (500x500m) of MODIS does not allow accurate delineation of inundation over small scales, which is a drawback (Li, Sun et al. 2013). Other high-spatial-resolution multispectral imagery can enable accurate detection and delineation of the water surface area (Pôssa and Maillard 2018). The disadvantages of using some of the high spatial resolution satellites, such as Landsat TM/ETM+, ALOS, SPOT, and ASTER, for delineating the extent of the water surface are the long return periods of the satellites and narrow scanning coverage between successive satellite overpasses (Wu and Liu 2015). However, the launch of Sentinel-2 has provided higher spatial resolution (10-20 meters) and spectral resolution (13 spectral bands), making it possible to detect and map floods in more detail. Also, a higher revisit time enables more frequent, accurate and up-to-date information on flood extent and dynamics. The water indices that were previously used with Landsat and MODIS data, Normalized Difference Water Index (NDWI), Modified Normalized Difference Water Index (MNDWI), AWEI were therefore simply applied to Sentinel-2 data (Abazaj, 2020; Wang & Xu, 2020; Yang et al., 2017). Table 2.2 shows a wide range of techniques used for surface water, wetlands, floodwater mapping based on Sentinel-2 including the geographic distribution of the coverage area, and the accuracy techniques used in these papers for the verification of results.

2.4.2.1 Water Indices

Sekertekin et al. (2018) used NDWI and MNDWI for mapping water extent of reservoirs related to Çatalan and Yedigoze Dam in Turkey. NDWI gave better results than MNDWI. MNDWI misrepresented non-water pixels as water pixels. The optimum thresholding values were 0.2627 & 0.3647 for NDWI and MNDWI respectively. Güvel et al. (2022) also applied the Modified Normalized Difference Water Index in the Berdan Plain in Turkey for the analysis & estimation of flooding in agricultural areas. Contrary to Sekertekin, Cicekli et al. (2018), Yang and Chen (2017) found that the performance of NDWI was good for a large homogeneous lake in China but could not identify some parts of river and many ponds due to shadow and built-up areas. This suggests that NDWI works well for homogenous water bodies like reservoirs, lakes, etc. but its performance is less certain with respect to shadows and clouds (Mialhe et al., 2008). Yang and Chen (2017) experimented with both SWIR bands for calculating MNDWI. AWEInsh and MNDWI (with band 11) almost gave similar results addressing sparsely distributed noise well. High-rise buildings and tree form shadows were not addressed well by NDWI and AWEIsh. Milczarek et al. (2017) also found that the AWEInsh provided the best land cover class distinction; they also proposed a new index Sentinel Water Mask (SWM) which uses blue, green, Near Infrared and SWIR bands. With optimal thresholds ranging from 1.4 to 1.6, the new SWM performed well compared to other indices. Jiang et al. (2021) proposed a further water index, a Sentinel-2 water index consisting of Band 5 and 11. They applied SWI and NDWI on the regions of Taihu Lake, Yangtze River, Chaka Salt Lake, and Chain Lake in China to conduct a water body extraction performance and found that the contrast value of the SWI was larger with respect to distinctive water types like purer water, turbid water, salt water, and floating ice, SWI performed better for enhancing and extracting water bodies with higher overall accuracy compared to NDWI.

2.4.3 Fusion of Optical with SAR Data

Optical imagery from sensors like Landsat or Sentinel-2 can be fused with SAR data to improve the accuracy of flood mapping. Optical imagery can provide additional information on the water and land cover characteristics, which can help differentiate water from other land cover types based on SAR data. Wangchuk and Bolch (2020) applied a rule-based image segmentation technique using multi-source data- Sentinel-1, Sentinel-2, DEM, and a random forest classifier model for mapping glacial lakes. The NDWI threshold values were 0.05, 0.3 and 0.6 for the optical images, while a backscatter intensity threshold of less than −14 dB was used for the Sentinel-1 image. This technique detected and delineated glacial lakes with high accuracy and more than 95% also predicted the correct class labels via random forest classifier model (RFCM). The integration of Sentinel-1 & 2 observations offer increased accuracy for mapping permanent surface water as compared to a mono-date approach (Bioresita et al., 2019). Van Deventer et al. (2022) put forward that a fusion between the radar and optical images enables reducing the omission errors associated with the optical data as demonstrated through other studies (Bioresita et al., 2019; Manakos et al., 2020; Muro et al., 2020). Vanderhoof et al. (2023) developed surface inundation algorithms for Sentinel-1 and Sentinel-2 and applied this to 12 diverse hydrologic and vegetation landscapes across the United States for a 5-year time-series. The images were classified into open and vegetated water, and non-water at 20 m resolution. The study demonstrated that the algorithms of Sentinel-1 and Sentinel-2 can be combined to enhance temporal resolution across all 12 sites and highlighted that the inclusion of topographic and weather variables enhanced the model’s performance. However, the difference in the sensitivity of these two sensors, such as to vegetation structure and pixel colour pose a major challenge of data integration when working with mixed-pixel, vegetated water, which would be important for analysing wetland flooding dynamics.

2.5 Synthesis of approaches and novel research directions

SAR has an operational advantage for flood mapping because of its ability to penetrate clouds. Delineating open surface water extent using Sentinel-1 images is a well-considered and explored domain. Pixel-based and object-based algorithms have been developed for identifying open water from SAR images, which emphasise the specular radar signal’s reflection (Clement, 2020; Pedzisai et al., 2023). As reviewed, other techniques include applying a local water histogram threshold change detection approach by image ratio (Shilengwe et al., 2023), using a deep learning model like Fully connected Convolutional Neural Network (FCNN) for delineating flooded areas with nominal human intervention (De La Cruz et al., 2020), integration of both Sentinel-1 & 2 for the inundation & extent mapping of floodwater and seasonal fluctuations (Morelli et al., 2019), active-passive surface water classification, i.e., integration of Sentinel-1 and Landsat satellite leveraging machine learning techniques and cloud-based computing resources for the delineation of monthly 10-m-resolution water body maps (Slinski et al., 2019), Interferometric Synthetic Aperture Radar (InSAR) (Slinski et al., 2019), and automatic Otsu thresholding for time series analysis for flood water extent detection in near-real-time (Tran et al., 2022). Each technique has its own advantages as well as limitations, for instance, the technique proposed by Liang and Liu (2020) showed improved accuracy compared to traditional methods by applying an intersection operation to combine water maps derived from two different polarizations (VV and VH) of an image. However, the accuracy of a method depends on the geophysical characteristics of the study area (Sherjah & Sajikumar, 2021). For instance, deep learning model like CNN-based semantic segmentation may not succeed in accurate classification of pixels around narrow river channels (Li & Demir, 2023). Otsu's method is also the most used method in surface water detection (Bijeesh & Narasimhamurthy, 2020) but reliance of most thresholding techniques on a single threshold may not be appropriate for every scene (Liang & Liu, 2020), especially because it relies on a strong bi-modal response. For Sentinel-2 many of the indices build on earlier spectral satellite indices. NDWI, MNDWI, AWEI, Moisture Stress Index (MSI) are already being used for mapping wetlands. MNDWI, AWEI dominate most water bodies mapping applications (Sarp & Ozcelik, 2017). Integration of multiple frameworks, and traditional processing techniques can help reducing the chance of false classifications. However, the primary challenge is still the identification of inundation under vegetation (Clement, 2020). Improving sensing in wetlands and dense vegetative areas is important because of the increased need to understand the impact of flood events in these areas. Time-based flood inundation maps derived from SAR images (or hybrid) can provide information for the analysis and assessment of wetland ecosystem conditions aided by spatio-temporal water information (Melkamu et al., 2022).

After looking at satellite approaches more generally, this section focuses on the specific application of these methodologies to the Macquarie Marshes, which being a complex wetland system, present a distinctive set of characteristics and challenges that make them an ideal case study for the implementation of satellite-based techniques for the surface water extent monitoring. Despite the availability of research on Macquarie Marshes estimating the water extent for time series analysis using Landsat, MODIS (Huang et al., 2014; Mueller et al., 2016; Senanayake et al., 2023; Thomas et al., 2015; Thomas et al., 2011) or Landsat/Sentinel-2 (Tulbure et al., 2022) (Table 2.5, Figure 2.10), not much work has been done to produce long-term, time-dense inundation maps using the data fusion of the Sentinel-1 derived flood extents and Sentinel-2 (Vanderhoof et al., 2023).

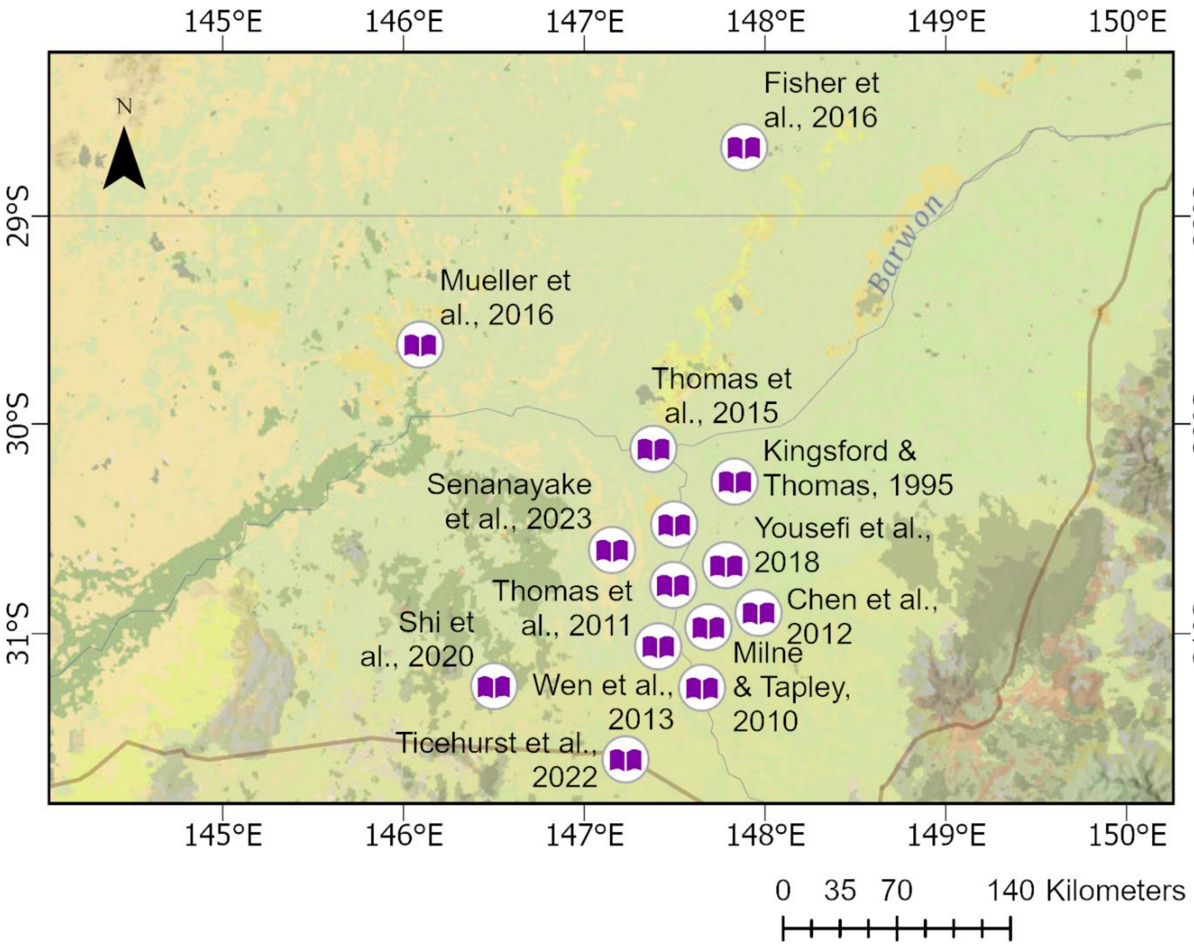

Figure 2.10: Map showing studies with a coverage of Macquarie Marshes

Table 2.5: Studies with a coverage of Macquarie Marshes

S.no.	Author	Article	Sensor	Year	Approach
1	(Thomas et al., 2015)	Mapping inundation in the heterogeneous floodplain wetlands of the Macquarie Marshes, using Landsat Thematic Mapper	Landsat 5 TM and Landsat 7 ETM+ images	1989–2010	Classification of three inundation classes: water, mixed pixels and vegetation, later merged to map inundated areas from not-inundated areas (dry land)
2	(Thomas et al., 2011)	Landsat mapping of annual inundation (1979–2006) of the Macquarie Marshes in semi-arid Australia	Landsat images MSS and TM	1979-2006	Mapping inundation pattern over long timeframes to investigate the variability of inundation in this heterogeneous floodplain wetland

3	(Fisher et al., 2016)	Comparing Landsat water index methods for automated water classification in eastern Australia	Landsat TM/ETM +/OLI	1999-2002	Assessment of the accuracy of different water index methods for water classification
4	(Shi et al., 2020)	Discharge Estimation Using Harmonized Landsat and Sentinel-2 Product: Case Studies in the Murray Darling Basin	Landsat 8 OLI, Sentinel-2 MSI	2017- 2018	Application of the Calibration/Measurement method for discharge estimation in the small rivers in Murray Darling Basin using the Harmonized Landsat and Sentinel-2 (HLS) surface reflectance product
5	(Senanayake et al., 2023)	A Random Forest-Based Multi-Index Classification (RaFMIC) Approach to Mapping Three-Decadal Inundation Dynamics in Dryland Wetlands Using Google Earth Engine	Landsat 5 Thematic Mapper (TM), Landsat 7 Enhanced Thematic Mapper (ETM+), Landsat 8 Operational Land Imager (OLI), and Thermal Infrared Sensor (TIRS) surface reflectance (SR) image collections	1987-2020	A random forest-based multi-index classification algorithm (RaFMIC) to map inundation extent
6	(Yousefi et al., 2018)	Assessment of channel expansion and contraction using crosssection data from repeated LiDAR acquisitions in the Macquarie Marshes, NSW	LIDAR	2008, 2014	Analysis of the changes in channel width and depth in the Macquarie Marshes utilising the cross-section data obtained from repeated LiDAR acquisitions
7	(Sandi et al., 2018)	Predicting floodplain inundation and vegetation dynamics in arid wetlands	River discharge data, Hydrodynamic Model, Aerial Photographs	1991-2008	Hydrodynamic model to calculate daily inundation patterns using discharge records from gauging station and analysis of vegetation patches according to water depth, percent exceedance time and frequencies of inundation.

8	(Ticehurst et al., 2013)	Using MODIS for mapping flood events for use in hydrological and hydrodynamic models: Experiences so far	TERRA and AQUA MODIS	2010	Generation of Surface Water Extent maps
9	(Chen et al., 2012)	Spatial modelling of potential soil water retention under floodplain inundation using remote sensing and GIS	MODIS	2000-2011	Estimation of potential maximum soil water retention under floodplain inundation from an ecologically significant flood return period
10	(Kingsford & Thomas, 1995)	The Macquarie Marshes in Arid Australia and their waterbirds: A 50-year history of decline	Landsat TMM/ MSS	1983-1993	Assessment of the relationship between total annual waterflow in the Macquarie River and the flooding extent in the northern Macquarie Marshes and trends in waterbird populations
11	(Milne & Tapley, 2010)	Wetland monitoring of flood-extent, inundation patterns and vegetation, Mekong River Basin, Southeast Asia, and Murray-Darling Basin, Australia	Radar dataset	2008	Application of SAR to map and monitor changes in wetlands hydrology and differentiate between different wetland cover types hydrology and
12	(Mueller et al., 2016)	Water observations from space: Mapping surface water from 25 years of Landsat imagery across Australia	Landsat-5 and Landsat-7	1987-2014	Water detection algorithm was used based on a decision tree classifier, and a comparison methodology using a logistic regression.
13	(Ticehurst et al., 2022)	Development of a Multi-Index Method Based on Landsat Reflectance Data to Map Open Water in a Complex Environment	Landsat 5, 7, 8	2007-2013	Development of a new approach (multi-index) for mapping open water in complex environments using Landsat reflectance data

14	(Wen et al., 2013)	From hydrodynamic to hydrological modelling: Investigating long-term hydrological regimes of key wetlands in the Macquarie Marshes, a semi-arid lowland floodplain in Australia	Hydrodynamic model (MIKE FLOOD)	1991-2009	A coupled 1D/2D MIKE FLOOD floodplain hydrodynamic model to simulate the daily behaviours of inflow/outflow, volume, and inundated area

Key within this process is the accounting for uncertainty as the high-resolution Sentinel-1 & 2 images would likely have reduced errors. It is also crucial that many of the methods in the literature have been fine-tuned for specific areas, as this is often necessary to achieve optimal results (Muro et al., 2016). Additionally, some methods, such as those that rely on SAR backscatter or multi-temporal analysis, may be more robust to differences in environmental conditions across locations (Mayer et al., 2021). The same is the case with Sentinel-2 as the Normalized Difference Water Index, Modified Normalized Difference Water Index, Automated Water Extraction Index, Sentinel Water Mask, Water Ratio Index, and Water Index are all effective indices for surface water identification and mapping in different environmental settings using remote sensing data. But the most significant aspect is that a thorough consideration of the environmental conditions and characteristics of study area is essential before the selection of appropriate indices. The reason is that some indices perform well in open waters (Du et al., 2016), or in lakes (Doña et al., 2021), while some perform better in wetlands (Kaplan & Avdan, 2017; Lefebvre et al., 2019; Pena-Regueiro et al., 2020). Machine learning models, such as Random Forest and Support Vector Machine, have been shown to effectively classify surface water (H. Li et al., 2021), especially in complex environments with mixed pixels or varying water depths, however, these methods will be location and image specific and would retraining to be applied more globally. A further problem with these methods is the need for a high-quality observed dataset. In many cases this is not available at large scales. Change detection or time series analysis has been an effective technique for monitoring and assessing changes in surface water extent and distributions over time (Bioresita et al., 2019). The combination of these techniques like the remote sensing indices and machine learning models might improve accuracy and efficiency in surface water extent mapping and monitoring.

2.6 Summary and conclusions of literature review

To conclude, mapping the extent of surface water during flooding events is crucial (Huang et al., 2018; Mueller et al., 2016). Despite the considerable progress made in wetland inundation studies using Sentinel-1 and Sentinel-2 data since their launch in 2014/2015, work that would easily apply to the Macquarie Marshes in New South Wales (NSW), Australia is limited. Numerous studies have investigated the inundation patterns in various wetlands worldwide, including some regions in the US, Europe, and Africa and demonstrated the utility of time-series analysis using the hybrid model of Sentinel-1 and Sentinel 2 for wetlands with improved accuracy (Gargiulo et al., 2020; Jamali et al., 2021; Kaplan & Avdan, 2018; Manakos et al., 2020; Slagter et al., 2020; Vanderhoof et al., 2023). There are very few direct observations of shallow water beneath vegetation using relatively finer spatio-temporal satellite observations, and in effect there is a lack of research and significant uncertainties addressing the temporal changes in the accuracy of satellite flood mapping observation, and the quantification of these uncertainties is essential (Vervoort et al., 2022). While the practice of managing environmental flows in the Macquarie Valley has been in operation for more than 40 years to restore and maintain the natural ecological balance of the wetlands (Mason et al., 2022), and there is substantial research available from multiple datasets, the challenge is to support the environmental watering with accurate flood mapping over time that integrates finer resolution satellite sensors. Since there is an increase in data volumes as an added feature of an increase in finer spatial scales as well as temporal frequency, the gap of multi-scale spatial–temporal analysis of wetlands with improved accuracy might be filled with the development of improved ML models with the fusion of Sentinel-1 and Sentinel-2.

3 Extraction of Surface Water Extent

As discussed earlier in Chapter 2, a wide range of water indices has been reported as effective in detecting water bodies. Due to the powerful capabilities and public availability of both Sentinel-1 and Sentinel-2 products, these data products have been used in many studies including mapping and monitoring of flooding (Goffi et al., 2020; Meyer et al., 2022) and near-real time evaluation of catastrophic floods (Caballero et al., 2019; Tarpanelli et al., 2022). Different approaches to evaluate the accuracy of Sentinel water detection results have been developed. One approach is visual interpretation, in which the results are compared to known reference data or ground truth data (Markert et al., 2020). Markert et al. (2020) used Planet Scope data as a validation dataset by visually interpreting water and no water areas for a particular sample within each scene. Tarpanelli et al. (2022) conducted a real case analysis for the validation of the reliability of their results. They assessed the flood-mapping capability of Sentinel-1 and Sentinel-2 satellites in Europe by conducting a synthetic analysis based on the river discharge data from multiple sites and different satellite revisit time configurations to estimate the percentage of potential inundation events using these satellites. They focus on three specific monitoring stations where river discharge data were available during the operational period of Sentinel-1 and Sentinel-2 satellites. These monitoring stations allow them to compare their satellite-based observations with actual river discharge data, ensuring the accuracy of their flood event detection methodology. An absence of reference data can be challenging for validation of the results (Fichtner et al., 2023).

Overall, the verification of the accuracy of satellite observations has proven to be elusive, making accurate estimation of surface water extents still difficult. For instance, a mismatch occurs with Landsat OLI-8 and Sentinel-2 data (Phiri et al., 2020) and there can be discrepancies between the resolution of Sentinel images and the validation data. Particularly, the validation data may not always have the same high spatial resolution as Sentinel products, which can make it difficult to compare. For example, there can be up to 38m difference between Landsat8 and Sentinel-2 geolocation (Storey et al., 2016). Limited availability of ground-truth data for validation purposes is another challenge (Fichtner et al., 2023). The timeframe of the ground data may also not match with the duration of the Sentinel missions' lifespan (Tarpanelli et al., 2022). Despite the wealth of research in this area (Fuentes et al., 2019; Meyer et al., 2022; Thomas et al., 2015; Thomas et al., 2011; Ticehurst et al., 2022), there are two further unresolved challenges, particularly for complex wetland areas with shallow water including different types of vegetation, such as dense emergent vegetation, floating vegetation, overhead canopies and standing tall vegetation obscuring wetland boundaries (Dronova, 2015; Gxokwe et al., 2020). The first relates to the stability of the thresholds that are needed to separate water and non-water pixels. There has been little research to confirm that this threshold is stable between different images and situations. The second relates to how well the different indices can be assessed relative to each other, considering the uncertainty in the thresholds. In other words, while different indices have been identified as being superior relative to others for different study areas, there is no consistent comparison over a long time series of images for a complex study area.

3.1 Methods

3.1.1 Area description

The case study area, the Macquarie Marshes is located in the lower catchment area of the Macquarie River in South-East Australia between latitude 30.551°S and 30.840°S and longitude 147.45°E and 147.606°E (Figure 3.1). Consisting of interrelated lagoons, swamps, marshes and branching channels, the RAMSAR listed Macquarie Marshes are of great ecological importance (Kingsford & Thomas, 1995). The marshes offer habitat to different animals and plants, which are dependent on floods including Red Gum forests, grasslands, reed beds, water couch, and different species of fish, frogs and waterbirds (Rogers et al., 2010). The Macquarie River flows are primarily dependent on rainfall and runoff induced flooding in the upper catchment in the southeast (Herron et al., 2002) and not on the local rainfall. However, due to river regulation, diversions in the river water and water allocations in the last few decades, flooding frequency has changed, and particularly decreased, in the Marshes resulting in the deterioration of the environmental assets and biodiversity of the Macquarie Marshes (Bowen, 2019; Ralph et al., 2015). Since local precipitation is not the main water source, the Macquarie Marshes are mainly influenced by water that originates from outside the immediate area, i.e., rainfall, runoff and flooding in the catchment upstream, which is a crucial hydrological perspective while assessing the water dynamics of Macquarie Marshes and also justifies the focus of this study on integrating remote sensing data, enabling a comprehensive analysis of external hydrological influences on the inundation patterns of Macquarie Marshes.

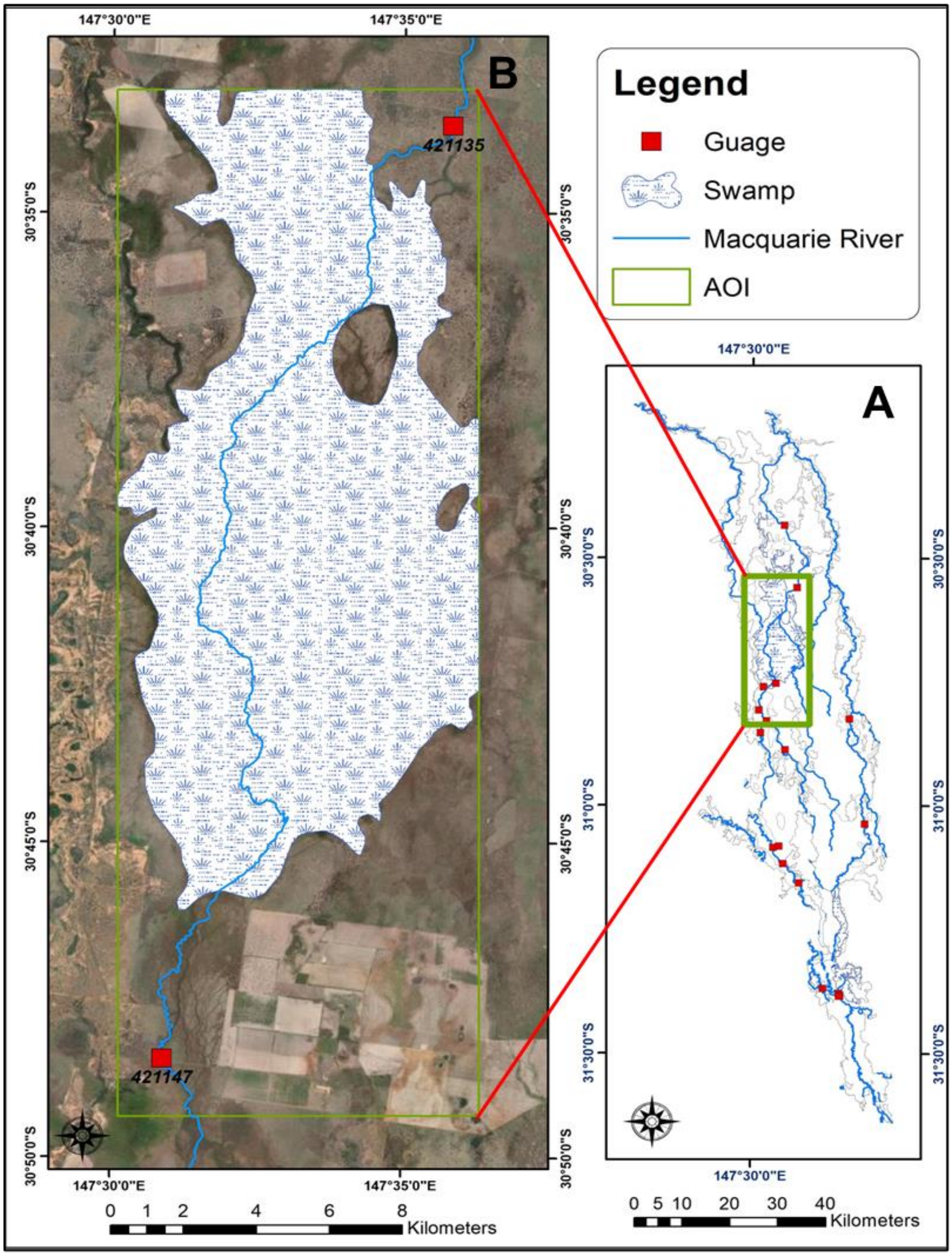

Figure 3.1: (A) The Macquarie Marshes Floodplain with its main River Macquarie River and Gauges and Swamps (B) Location of the Study Area within the Macquarie Marshes Indicating the Macquarie River and its Gauges

Land cover is a substantial factor for the flood analysis for the AOI, as it affects water flow and flood intensity. Areas with high percentages of vegetation, such as wetlands or forests, are capable of more water absorption and retention than areas with less vegetation, decreasing the amount of surface runoff and mitigating flood risk. The landcover map gives an overall picture of the area. The Landcover map was acquired from https://livingatlas.arcgis.com/landcover/ which is derived from Sentinel-2 and then clipped to the AOI extent (Figure 3.2). If we compare the landcover classifications with the EVI and NDVI map, the spatial distribution of vegetation types from the landcover map is matched with the density of vegetation as indicated by the EVI and NDVI data (Figure 3.9).

As can be seen from Figure 3.2, flooded vegetation has increased in the Macquarie Marshes in the year 2022, after a drought in the past. The drought between 2017 and 2019 steadily decreased the water volume in the Marshes over the period (Schweizer et al., 2022), and there was such a degradation of the state of the Marshes that there were concerns of losing their status of Ramsar Listing (OEH, 2013). However, the recent flood in 2022 led to the revival of the wetlands (Regulator, 2022), and is also regarded as "wettest period in living memory" (Jose, 2022).

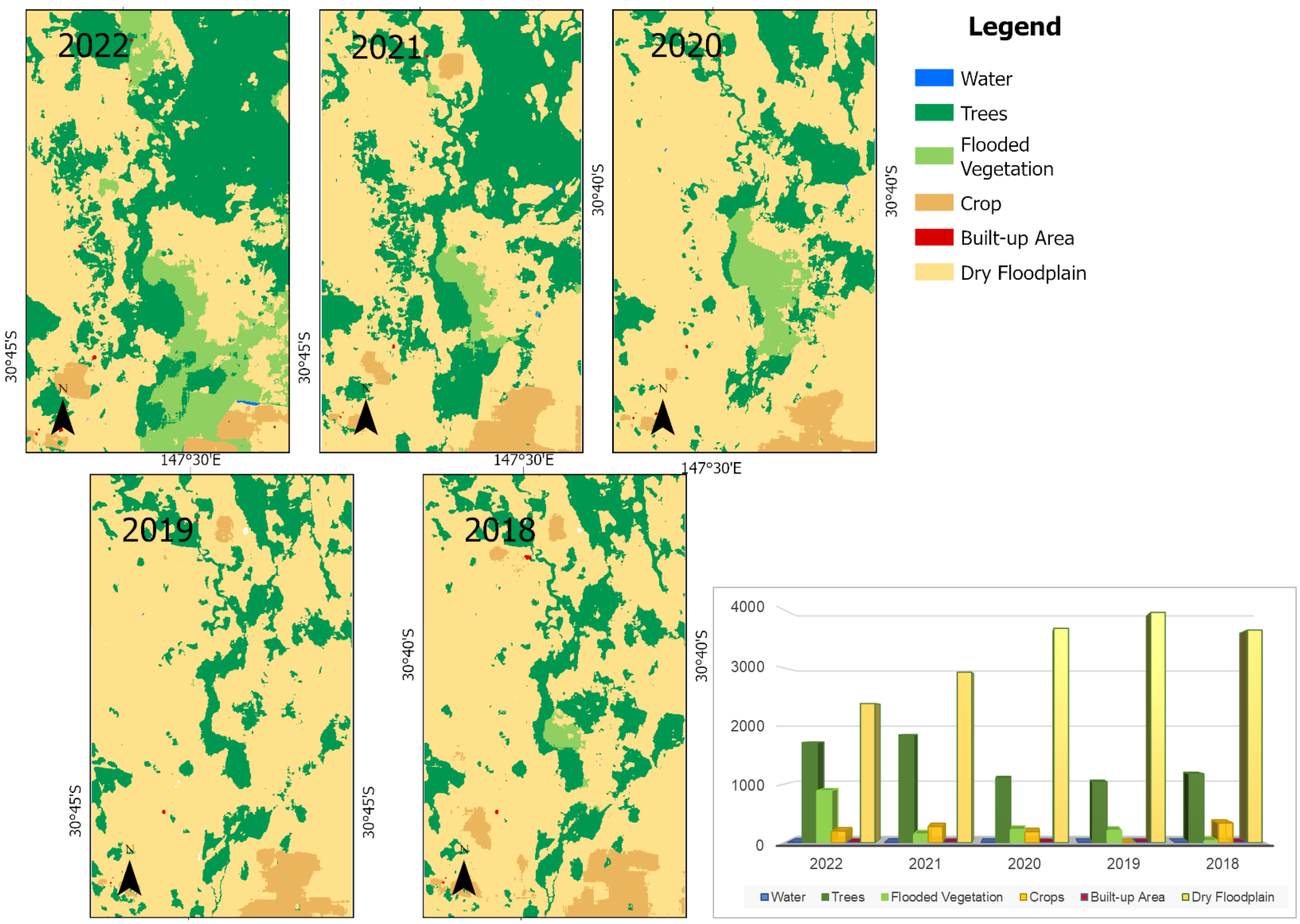

Figure 3.2: Landcover of Macquarie Marshes for the Years 2018, 2019, 2020, 2021, 2022. The Landcover Maps for the last 5 years were acquired from https://livingatlas.arcgis.com/landcover/

3.2 Objectives

The aim of this research is to estimate flood area and volumes using different satellite derived indices to assist with monitoring environmental watering events focusing on a case study in the Macquarie Marshes. The sub-objectives of this study are:

1. To develop and evaluate the accuracy of a toolbox of algorithms to delineate flooded area testing variation in time across multiple images.
2. To evaluate the spatio-temporal dynamics of flood extent and volumes derived using Sentinel 1 and Sentinel 2 satellite data compared to gauging data.

The rationale for using Sentinel for this study is its capacity to provide fine spatial and reasonable temporal resolution multi-spectral and SAR imagery for mapping water bodies (Caballero et al., 2019; Du et al., 2016; Yang et al., 2017). The Macquarie Marshes have been selected as a case study area as they represent a complex, shallow water, wetland system with dense vegetation in pockets of the area, where satellite derived indices traditionally struggle.

3.2.1 Description of the data used

The range of different (publicly accessible) spatial and temporal data sources are used in this study. This includes satellite data such as Sentinel 1 and 2, the commercially available Planet Imagery, as well as daily discharge data of upstream and downstream gauges, rainfall and a digital elevation model (Table 3.1). Figure 3.3 demonstrates the methodological framework for this study.

Table 3.1: Data Sources used in this study

Data	Year	Spatial Resolution	Temporal Resolution	Data Source
Sentinel 1 SAR Data	2022	10m - 20m	12 Days	www.asf.alaska.edu/data-sets/sar-data-sets/sentinel-1/
Sentinel 2- Optical	2022	10m - 60m	Up to 5 days	GEE
PlanetScope Imagery-Optical	2022	3m	Daily	www.planet.com/explorer/
Discharge Data for Macquarie River at Miltara (421135) and Macquarie River at Pillicawarrina (421147)	2022	N/A (point data)	Daily	www.bom.gov.au/waterdata/
DEM (Digital Elevation Model)	2014	1 m	N/A	www.elevation.fsdf.org.au
Rainfall	2022	N/A	Daily	https://www.longpaddock.qld.gov.au/silo/gridded-data/

Water Observation from Space	2022	30 m	Up to 16 days	https://explorer.dev.dea.ga.gov.au/products/ga_ls_wo_3/2022
NSW Inundation Maps	2022	10 m	Up to 5 days	https://datasets.seed.nsw.gov.au/dataset/inundation-maps-for-nsw-inland-floodplain-wetlands

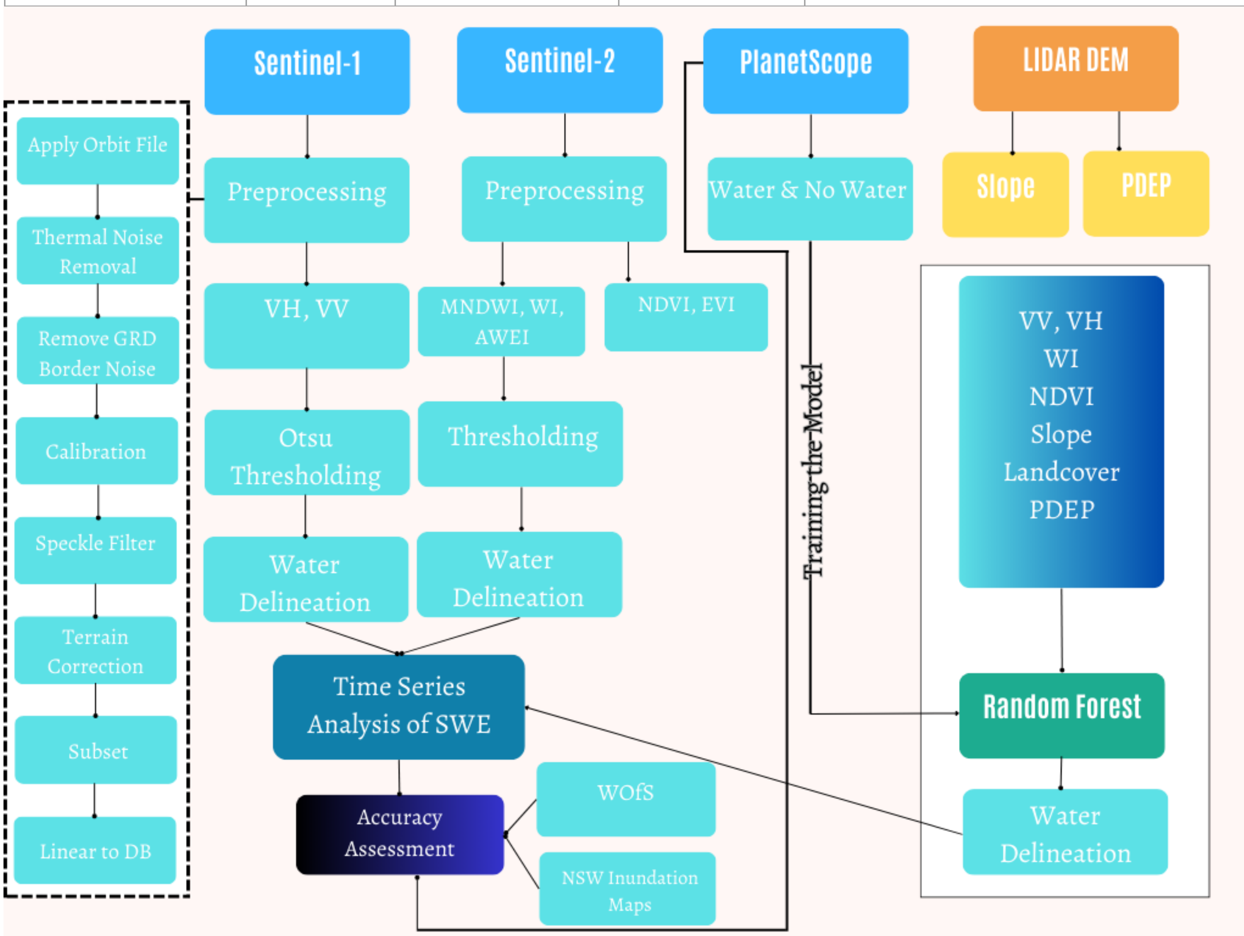

Figure 3.3: Methodological Framework

Water maps derived from Sentinel-1 and Sentinel-2 were analysed independently employing distinct sources of validation for each (Table 3.2). The water maps derived from Sentinel-1 were compared with the NSW inundation maps, whereas the water inundated maps derived from Sentinel-2 were compared with the WOfS data and manually demarcated points on multiple scenes of PlanetScope imagery. The Random Forest (RF) model was trained using the PlanetScope imagery while it was compared against the WOfS and NSW inundation maps.

Table 3.2: Sensors & RF Model Validation Against the Reference Datasets

Sensors & Approaches Used	**Reference Datasets**		
	WOfS	**PlanetScope**	**NSW Inundation Maps**
Sentinel-1 – Otsu			✓
Sentinel-2 – Water Indices	✓	✓	
RF Model	✓		✓

3.2.1.1 Sentinel-1

Twenty-eight Sentinel 1 scenes from the 1st January 2022 to 31st December 2022 were downloaded from www.asf.alaska.edu/data-sets/sar-data-sets/sentinel-1/. All these images were pre-processed using the SeNtinels' Application Platform (SNAP) software which is an earth observation data processing software used for analysis of satellite imagery data (*Science Toolbox Exploitation Platform*)(www.step.esa.int/main/toolboxes/snap).

The workflow used for the pre-processing of the Sentinel-1 images using the Sentinel-1 toolbox in the SNAP) software was demonstrated in Figure 3.3. All 28 Sentinel-1 scenes were Level-1 ground range detected (GRD) data acquired in the interferometric wide swath (IW) mode, which is the predefined mode over land with the VV and VH polarizations in the descending orbit direction. As the above flowchart demonstrates, a series of standard corrections was applied to all the downloaded scenes of Sentinel 1, including the precise acquisition orbit, removal of thermal and image border noise, radiometric calibration, speckle filtering and application of range doppler terrain correction. Speckle filtering is a procedure to reduce the speckle in the image and to increase image quality. There are multiple single product speckle filters operators available in SNAP; however, the refined Lee filter is regarded as the most effective one due to its capability of preserving edges, texture information and features (Rana & Suryanarayana, 2019). Range Doppler terrain correction is a method used to correct the topography induced geometric distortions, for example, foreshortening and shadowing (Bayanudin & Jatmiko, 2016). A 1 arc sec SRTM DEM was used for the correction of each image pixel. The Sentinel 1 scenes were subsequently masked to the Area of Interest and then converted into decibels (dB) using a logarithmic transformation provided in SNAP.

3.2.1.1.1 Thresholding of Sentinel-1 Images

Thresholding is an image segmentation technique, that implies setting a threshold value which divides an image on the basis of their grey level distribution in an image. There are multiple techniques for determining a threshold value, including histogram-based methods, clustering-based methods, entropy-based methods, and iterative techniques. Otsu thresholding was applied in this study for the classification of the observed pixels of the Sentinel-1 images into binary classes (water and non-water). Ottinger et al. (2017) applied different thresholding techniques for the classification of SAR images and found the Otsu thresholding results superior compared to other techniques (Ottinger et al., 2017). Otsu's thresholding technique finds the optimal threshold value for an image by classifying the input image and establishing a threshold that provides the best separation between the classes. Pixels with a backscatter value less than the estimated Otsu threshold were classified as water, while the pixels with a value greater than or equal to the estimated Otsu threshold's backscatter value were classified as non-water. An example is provided in Figure 3.4. The Otsu threshold requires a clear bi-modal histogram distribution to work correctly, and although there is plenty of open water in Macquarie Marshes, this is also worth mentioning here that the presence of various types of vegetation, such as emergent and floating vegetation, can lead to a more complex and less clearly bi-modal histogram, which can pose challenges for the application of the Otsu method, and can influence the effectiveness of the Otsu method (Liang & Liu, 2020).

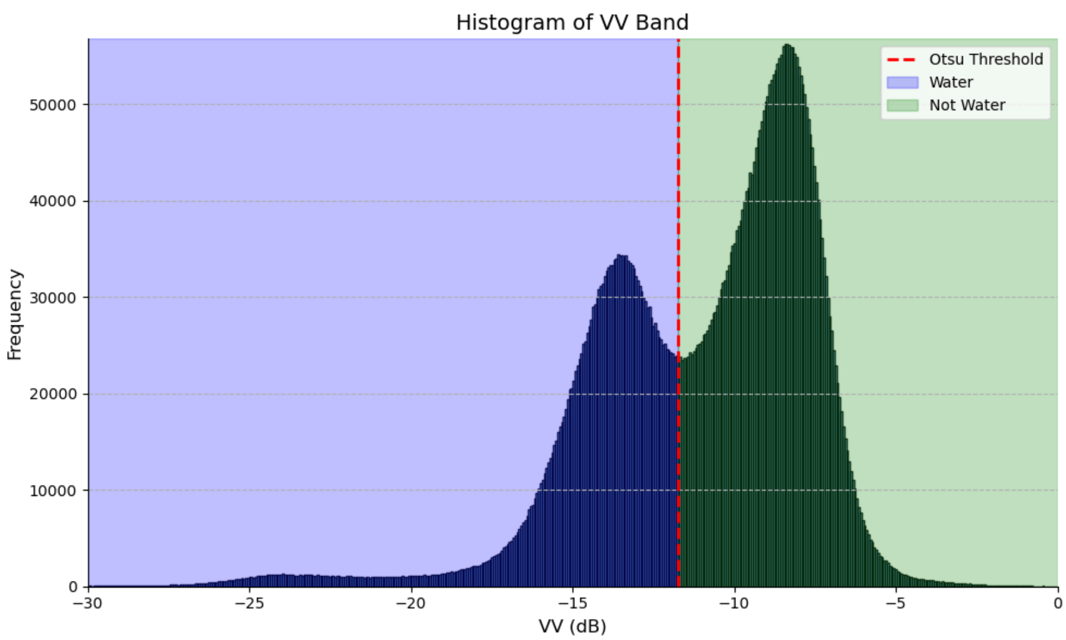

Figure 3.4: Example of the Histogram using Otsu thresholding on the VV band of a Sentinel-1 image acquired on 06/12/2022 for water and non-water pixel classification

3.2.1.2 Sentinel-2

Data from the Sentinel-2 satellite mission of the European Space Agency (ESA) was used in this study as a dataset for spectral indices. The data considered are from January 2022 to December 2022. The Sentinel-2 mission consists of two satellites, Sentinel-2A and Sentinel-2B, which have a temporal resolution of 5 days, allowing for efficient temporal analysis of the data. The atmospherically corrected Sentinel-2 data (level 2A) was utilised in this study. The Sentinel-2 multi-spectral instrument (MSI) has 13 different spectral bands. The high resolution of Sentinel-2 allows for more precise identification of features on the Earth's surface. However, clouds can be an obstacle for spectral images (Figure 3.5), therefore the spectral cloud layer (SCL) band was utilised to mask out the clouds in the Sentinel-2 images.

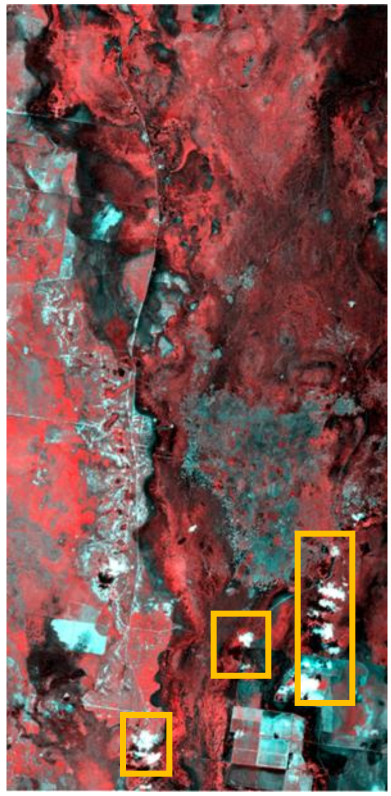

Figure 3.5: Clouds over the scene acquired on 09/10/2022

Water detection using Sentinel-2 images involves using the satellite's spectral bands. Different indices were used based on the Sentinel-2 images to differentiate the water from non-water pixels and these indices were discussed in the previous chapter. Among those indices the Automated Water Extraction Index (AWEI) (Feyisa et al., 2014), the Normalised Difference index $_{\text{modified}}$ (MNDWI)(Xu, 2006) and the Water Index (WI_{2015}) (Fisher et al., 2016) were selected (Table 3.3). The rationale for choosing these indices is that Macquarie Marshes are a group of shallow water bodies and with highly turbid water and past studies have indicated the efficiency of the selected indices (Table 3.3) in the detection of shallow water bodies.

Table 3.3: Description of Spectral Algorithms based on Sentinel-2 used in the Study

Water Index	**Source**	**Equation**	**Recommended Threshold***
Normalised Difference Water Index *modified* (MNDWI)	(Xu, 2006)	$\frac{(Green-SWIR1)}{(Green+SWIR1)}$	0
Automated Water Extraction Index *no shadow* (AWEInsh)	(Feyisa et al., 2014)	$4 \times (Green - SWIR1) - (0.25 \times NIR + 2.75 \times SWIR2$	0

Automated Water Extraction Index $_{shadow}$ (AWEIsh)	(Feyisa et al., 2014)	$Blue + 2.5 \times Green - 1.5 \times (NIR + SWIR1) - 0.25 \times SWIR2$	0
Water Index (WI_{2015})	(Fisher et al., 2016)	$1.7204 + 171 \times Green + 3 \times Red - 70 \times NIR - 45 \times SWIR1 - 71 \times SWIR2$	0

*Adapted from Table-2 (Page 63) of (L. Li et al., 2021)

In Sentinel-2, the visible, near-infrared (NIR), and short-wave infrared (SWIR) bands are used to detect and monitor water bodies. Generally, the blue (Band-2), green (Band-3), red (Band-4), NIR (Band-8) and SWIR (Band-11) are commonly used for water detection in Sentinel-2 (Table 3.3).

3.2.1.2.1 Thresholding of Spectral Indices

The spectral indices have preferred thresholds that vary based on applications, considering factors like vegetation cover, soil colour, soil moisture, and water colour (Kordelas et al., 2018). There is not a single fit for all situations or images or a universal index or threshold (Ticehurst et al., 2022). As a result, each study applying these spectral indices should find an optimal threshold. Optimal thresholding means obtaining the best threshold value to separate water and non-water areas with the highest accuracy, considering the remote sensing data's characteristics (image contrast, presence of noise) and the classification objectives. Misclassification of water or non-water areas can be the result of either a too high or a too low threshold, resulting in lower accuracy. The indices used in this study (WI, MNDWI, AWEIsh, AWEInsh) are calculated using the spectral reflectance values of different bands, and thresholding is required to perform a binary classification of water and non-water areas (Figure 3.6). Most of the water indices require user-defined thresholds to be set for water extraction (Chen et al., 2022), but AWEI is designed to automatically set the threshold to 0 to extract water without any need for a manual threshold (Feyisa et al., 2014). The AWEI uses coefficients to improve the separability of water and non-water pixels, and 0 can be used as a default threshold (Feyisa et al., 2014; L. Li et al., 2021). However, according to Vinayaraj et al. (2018), AWEI also needs a regional optimal threshold to get better results. The Water Index (WI_{2015}) is composed of the green, red, NIR and SWIR bands and uses six empirical coefficients, and the theoretical range of WI is from − 50 to +50, and the recommended threshold for WI is also 0 (L. Li et al., 2021). MNDWI is regarded as the most preferable water index (Laonamsai et al., 2023; Ticehurst et al., 2022) and the recommended threshold for MNDWI for delineating water bodies is considered to be above 0 (Fisher et al., 2016). The thresholding value for water delineation using the Modified Normalised Difference Water Index (MNDWI) appears to vary depending on the specific study area. For instance, Sims et al. (2014) found a threshold of -0.3 to be effective in capturing water extent at different regions along the Murrumbidgee River. The similar threshold value was used to delineate permanent and flooded water bodies in Northern Australia (Sims et al., 2016), floodwater in Western Australia (Karim et al., 2018) and the northern Murray Darling Basin (Dutta et al., 2016). However, in a study in the area of central Australia, the negative thresholding value tended to overestimate surface water extent and 0 appeared a more appropriate threshold for accurate water delineation (Ticehurst et al., 2022). In a study based in central Georgia by Ji et al. (2009) aimed at detection of open water and vegetated wetlands, -0.504 was selected as the threshold value for MNDWI to detect inundated vegetated areas (25% water & 75% vegetated water) and 0.12 for only water pixels. The drawbacks of selecting low thresholding values can be increased commission errors or false positives (Ji et al., 2009; Jones, 2015).

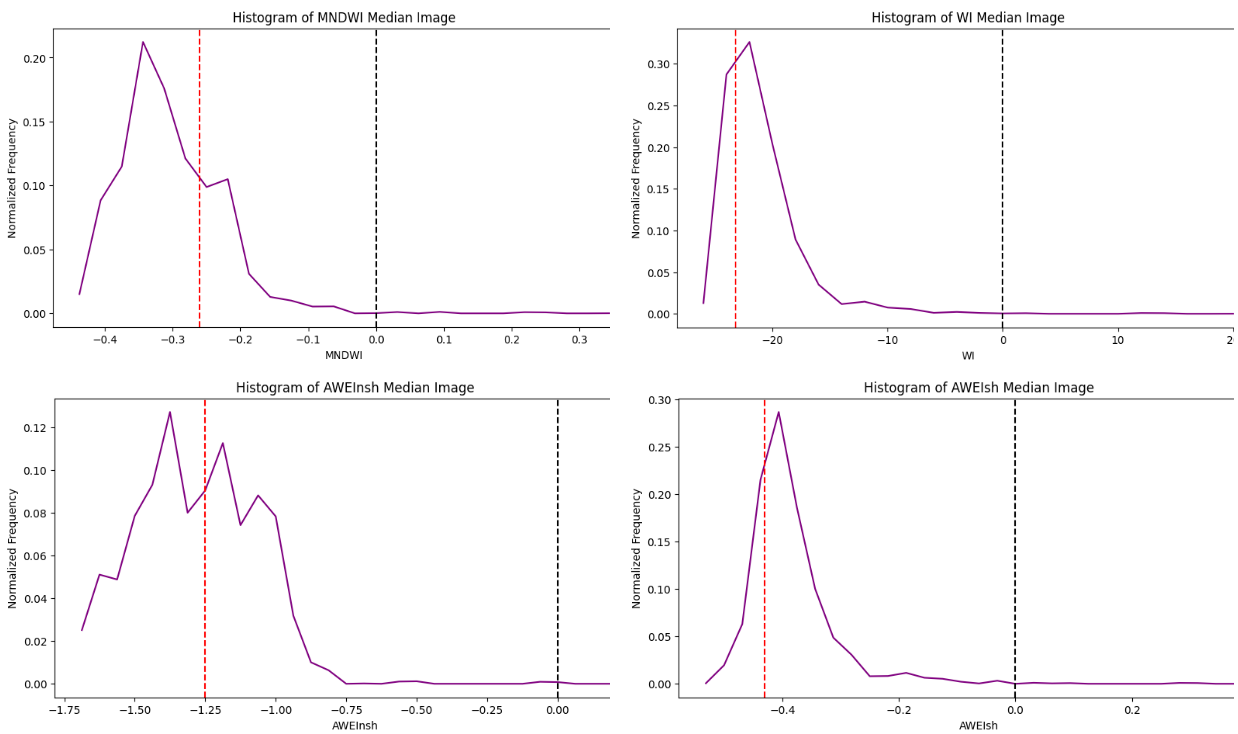

Figure 3.6: Histograms showing the median values of MNDWI, WI and AWEInsh and AWEIsh for image collection of Sentinel-2 for the year 2022 applied in this study. The Water Indices were calculated across the whole collection and then the median was calculated for the accurate representation. Black dotted shows the recommended threshold while the red like shows the estimated threshold

There are multiple techniques, for example Adhikari (2019) used the Otsu as binary thresholding technique for water surface delineation in the St. Croix Watershed area. Laonamsai et al. (2023) also determined the optimum threshold of NDWI, MNDWI, SAVI, WRI and AWEI on the basis of the Otsu threshold method to achieve the highest overall accuracy for river boundary extraction. Additionally, indices with better extraction abilities may be combined to enhance the separability between water and non-water surfaces, as determined by evaluation matrices. Fuentes et al. (2019) determined the threshold for OWL's algorithm with the selection of the median of the maximum kappa values for each image which was found to be 0.87. Zhai et al. (2015) utilised a sample points technique for the selection of the appropriate thresholds. This makes this index less applicable on a larger scale. This study also made use of a similar technique, the mean of the MNDWI index for the water feature is used as the threshold for delineating water and non-water features. The thresholding value for MNDWI was found to be -0.19 (Figure 3.7 and Figure 3.8).

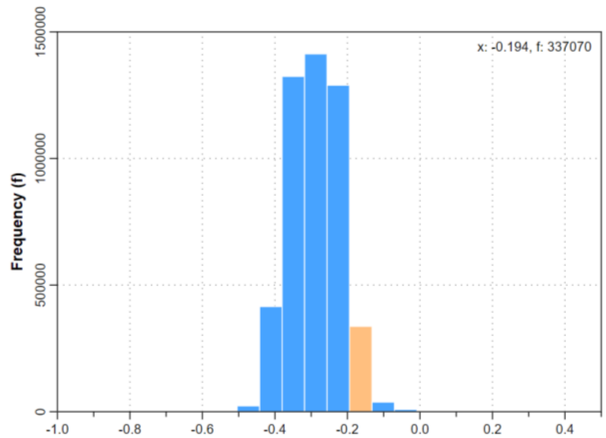

Figure 3.7:Histogram of MNDWI for the Mean Image of Macquarie Marshes for the Year 2022

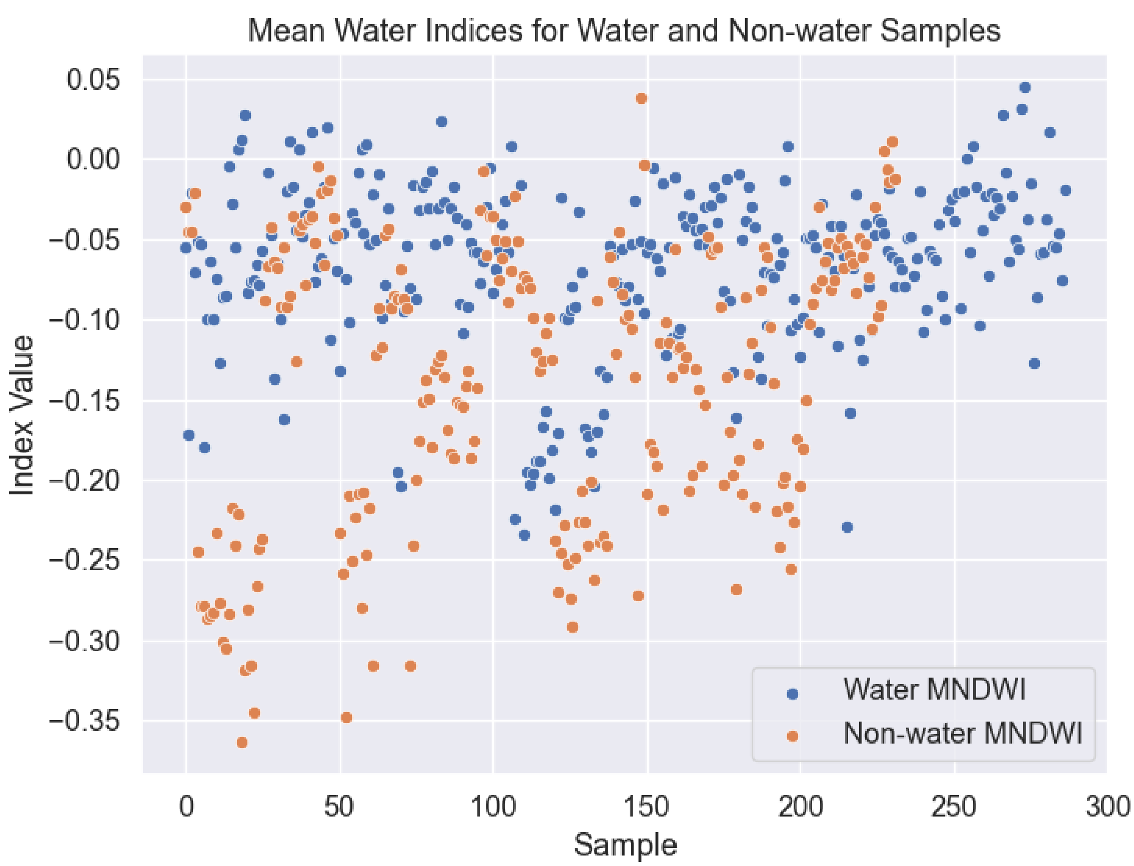

Figure 3.8: MNDWI values for Water and Non-Water Pixels (Water pixels generally lies between -0.2 to 0.05, while non-water pixels fall within the range of -0.35 to 0)

3.2.1.3 Vegetation Indices

Dense vegetation such as in the Macquarie Marshes absorbs and reflects a lot of light, making it difficult to see the water underneath using the optical sensors on the Sentinel-2 satellite. In addition, the visibility of the water is also affected by the depth of the water beneath the vegetation. With shallower water, more light will be absorbed and scattered by the vegetation, making it even more difficult to detect the water. Therefore, vegetation indices (NDVI and EVI), indicating vegetation greenness and vigour (Billah et al., 2023) were therefore also determined from the satellite data to get a completer picture of the area. A median value of NDVI and EVI were calculated using Sentinel 2. The NDVI values generally range from -1 to 1, where negative values indicate non-vegetation like water, and values closer to 1 indicate dense vegetation (Observatory, 2000). Low NDVI values could also be an indication of dry vegetation. The NDVI values in Figure 3.9are ranging from -0.6 to 0.1 which are within the expected range for vegetation indices. (Observatory, 2000) The enhanced vegetation index (EVI) is an 'optimal' vegetation index (also considered as a modified form of NDVI) that combines the red, blue and NIR bands to highlight vegetation while minimizing influences from soil, atmosphere, and biomass, and shadows (Glenn et al., 2008). The range of EVI is typically from -1 to 1, with higher values indicating denser and healthier vegetation. The EVI values in Figure 3.9 range from -0.19 to 0.77 suggesting a variation in vegetation density and health across the imaged area. NDVI, despite being a vegetation index, has been used in different studies for water mapping as the water bodies are generally negative or closer to zero in the NDVI index (Lekhak et al., 2023; Thomas et al., 2015). NDVI is more frequently used compared to other vegetation indices that asserts the significance of global vegetation monitoring (Kaplan & Avdan, 2017).

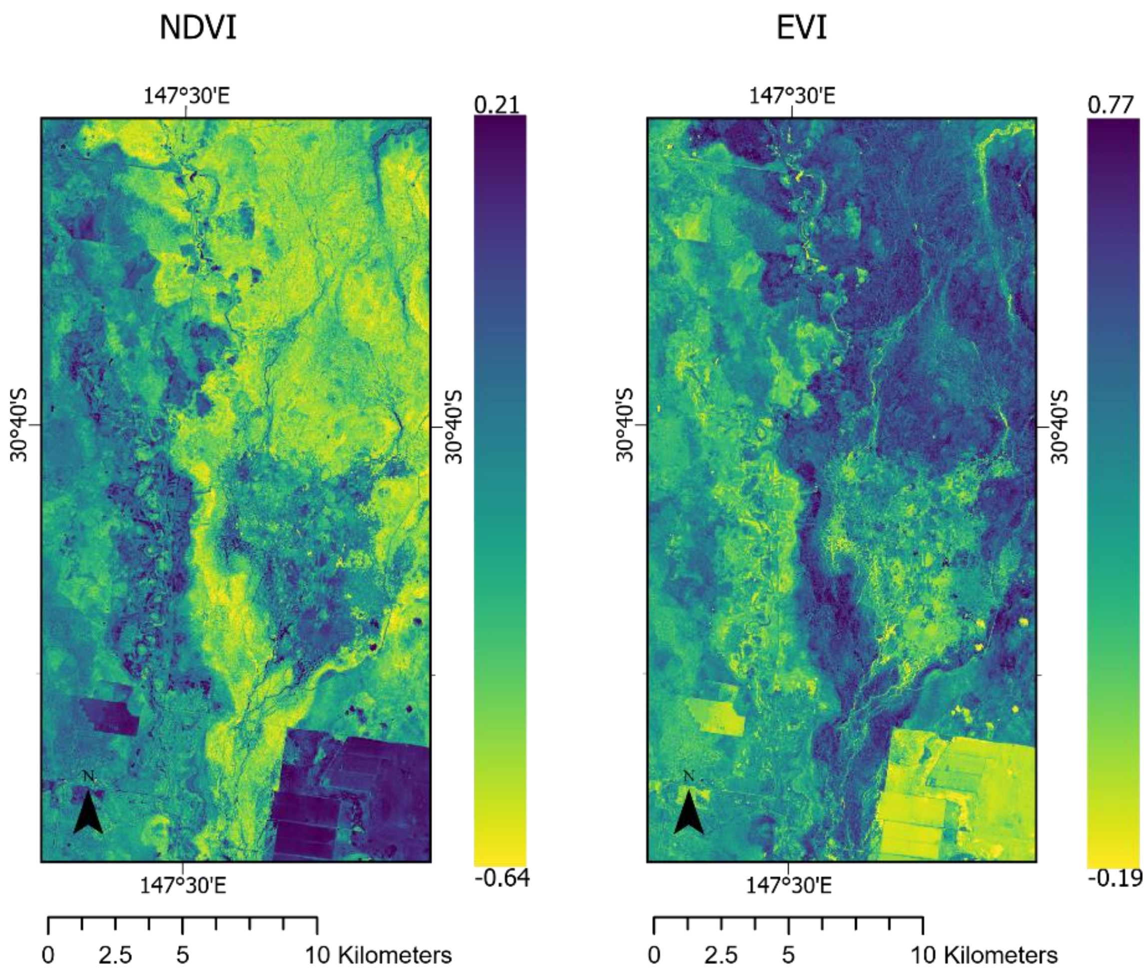

Figure 3.9: Comparison of vegetation indices: (left) Normalized Difference Vegetation Index (NDVI) ranging from -0.64 to 0.21, and (right) Enhanced Vegetation Index (EVI) ranging from -0.19 to 0.77. The colour scale represents the index values, with green indicating high vegetation cover and yellow indicating low vegetation cover. Both of the maps are median values for the year 2022.

3.2.1.4 Flow Discharge and Volume

Flow discharge and volume indicate the amount of water moving through a river or stream per unit time and the total amount of water available. Gauging station data for surface water (daily stream level and discharges) was obtained from www.realtimedata.waternsw.com.au for the upstream and downstream stations for the Macquarie Marshes area (Table 3.4).

Table 3.4: Gauging Stations within the AOI

Gauging Station	Station Name	Zero Gauge meters (m)	Start Date	End Date
421135	Macquarie River At Miltara	132.027	01/01/2022	31/12/2022
421147	Macquarie River At Pillicawarrina	141.430	01/01/2022	31/12/2022

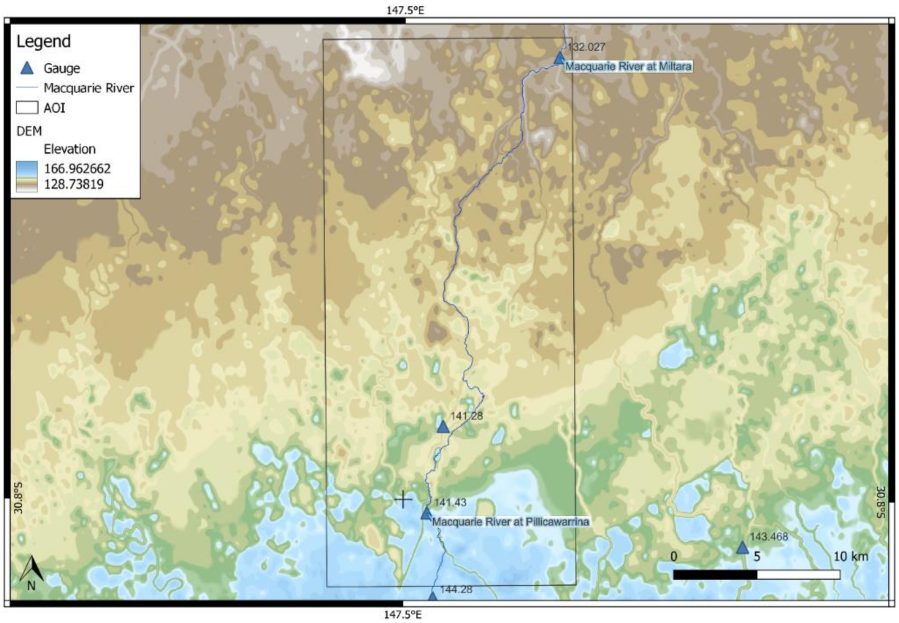

Figure 3.10: Map showing Gauges within AOI (with SRTM DEM as the base map)

3.2.1.5 Rainfall

The daily rainfall data for the year 2022 was acquired from SILO (www.longpaddock.qld.gov.au/silo/gridded-data). This data was aggregated by averaging the rainfall measurements across all pixels in the AOI, resulting in a time series of total daily rainfall values across the area (Figure 3.11).

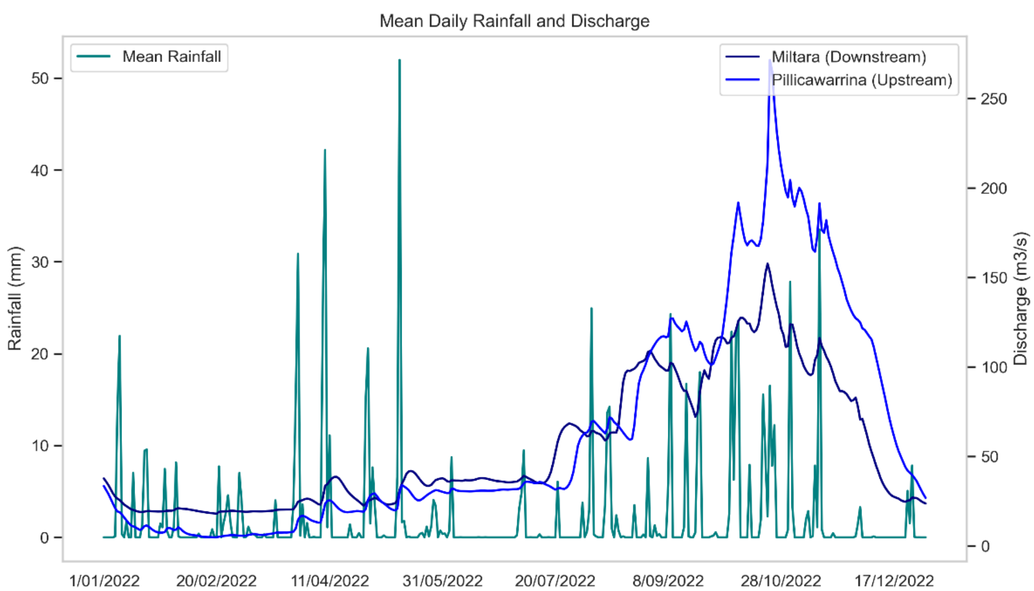

Figure 3.11: Time Series of Daily Rainfall and Discharge in Macquarie Marshes for the Year 2022

For the RF model, the delayed impact of rainfall on water accumulation over multiple days is included, which means a lagged/ cumulative rainfall variable is included in the analysis. The cumulative rainfall over the past 3 days were chosen as the time window, and then lagged rainfall layer was included in the RF model.

3.2.1.6 Digital Elevation Model

A digital elevation model (DEM) of the case study area was derived from a 1m LiDAR dataset that was downloaded from the Elvis - Elevation and Depth - Foundation Spatial Data resource (https://elevation.fsdf.org.au/, accessed 24/06/2023)/. The LiDAR was captured between November 2013 and May 2014 (LiDAR metadata). The tiles were mosaiced to form a seamless raster. This DEM was used to produce the depression probability distribution and slope map of the Macquarie Marshes (Figure 3.12). A high-resolution DEM can enable accurate identification and analysis of water features, but since the area has dense vegetation, there are some potential errors due to interpolation (sparse ground points cause errors) (www.elevation.fsdf.org.au).

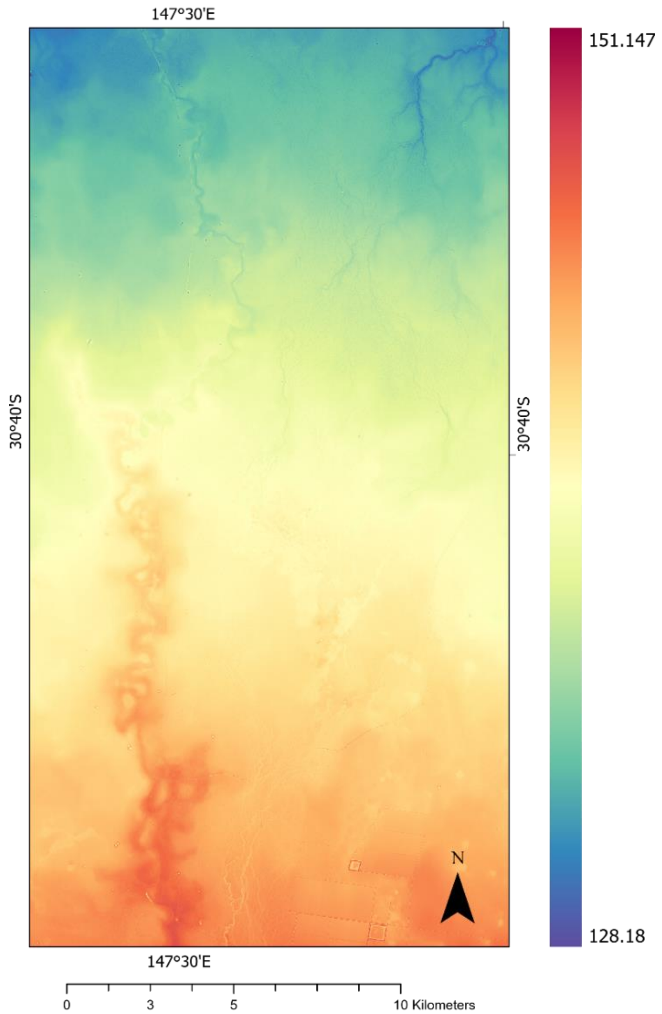

Figure 3.12: 1m Lidar of the Study Area indicating the Flat Area (Data sourced from ELVIS (Elevation and Depth - Foundation Spatial Data resource) captured between 2013/2014

Stochastic probability can be used for water depth calculation (Kuchment & Gelfan, 2011; Yu et al., 2013). It is often used in the flood modelling for the prediction and assessment of flooding likelihood at a certain region. Digital Elevation Models (DEMs) are used to develop multiple stochastic rainfall scenarios and simulate the resulting surface water flow, which lead to generate a probability distribution of water depth at different locations. This information can be utilised for the identification of most vulnerable areas to flooding. Stochastic probability can be combined with inundated water extent data from remote sensing data to further enhance flood modelling accuracy. With the integration of satellite remote sensing, flood models can provide more detailed information about the extent and severity of flooding in a particular area. Digital elevation models, in combination with optical remote sensing imagery can deal with the complexity of wetlands and limitations of optical remote sensing to develop operational surface water extent mapping with more accuracy (Rossi & Vervoort, 2022).

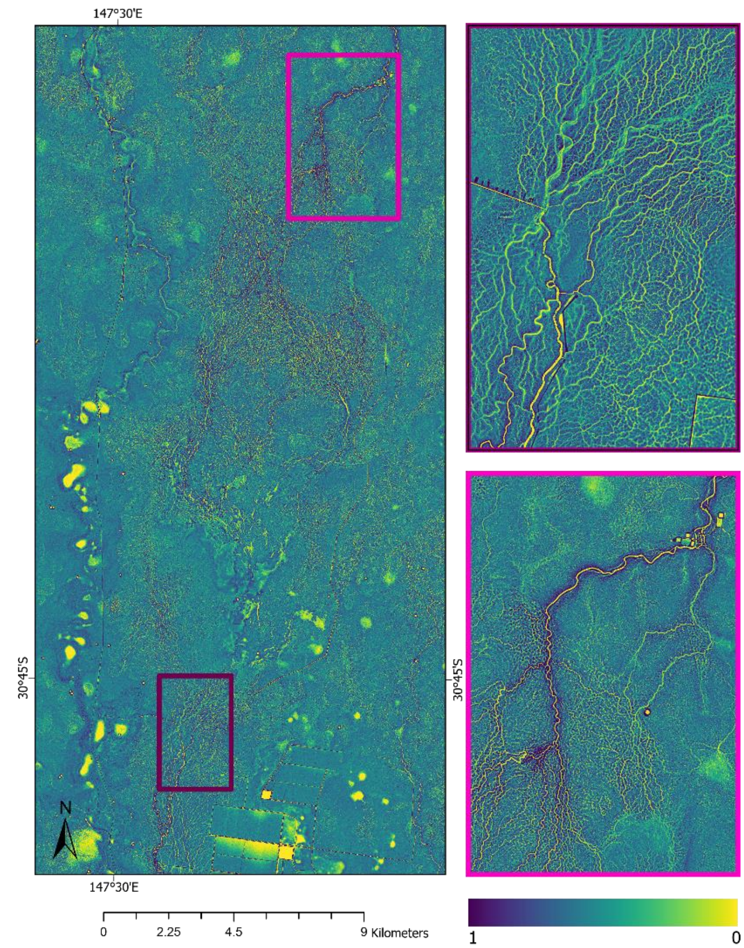

Figure 3.13: Probability of Depression Map, showing the Depression in the Marshes. The Top Right shows a zoom image of Upstream, whereas the bottom right shows the downstream area

The stochastic analysis of depression was carried out (Figure 3.13) using the stochastic depression analysis tool that performs a Monte Carlo simulation to determine the probability of each cell in a dem (Lindsay & Creed, 2005). Parameterising the stochastic depression tool can be tricky especially the dem root mean square error (RMSE) parameter as the tool is more sensitive to RMSE as compared to range of autocorrelation error. The vertical accuracy of LIDAR dem (0.3m) (https://elevation.fsdf.org.au/, accessed 24/06/2023) was considered as the dem RMSE while the range of autocorrelation error was set as five times to the resolution of LIDAR dem, i.e. 5m.

3.2.1.7 PlanetScope Imagery

PlanetScope (PS) images used in this study were acquired by the (PS2.SD) Dove satellites designed to capture high-resolution images. The PS images are processed by the PlanetScope Lab (PBC, 2022), which performs geometric (through Ground Control Points and DEM) and radiometric corrections on the raw images to produce reliable and accurate data. The images are also atmospherically corrected to surface reflectance using sensor telemetry and a sensor model, which removes atmospheric interference and improves the accuracy of the data. The spatial resolution of the PS images is 3m, and because the satellite has a daily flyover schedule, it is available every day, allowing for near-real-time monitoring. PlanetScope satellites capture eight spectral bands, including the coastal blue, blue, green I, green, yellow, red, red edge, and near-infrared bands (www.planet.com accessed 19/06/2023). The spectral bands that are most commonly used for water delineation using PlanetScope imagery are blue, green, red and near infra-red bands (Mullen et al., 2023).

The Planetscope image was used as a reference to manually demarcate water and non-water pixels. A total of around 1200 points were manually demarcated as water and non-water pixels to provide an independent validation dataset (Figure 3.14). Because this was a manual process, the accuracy of the manual classification is unknown. There is no reliable observed field data to assess this. It was later used for the performance assessment of indices used for surface water mapping using Sentinel 1 & 2. The points were initially marked using the 3-meter data. To ensure their accuracy, their precision was double-checked by comparing them with the Sentinel-2 and resampled 10-meter PlanetScope data (Figure 3.15). This helped to verify the water pixels are aligned with the 10m image as well and to manage the scale difference between the satellites.

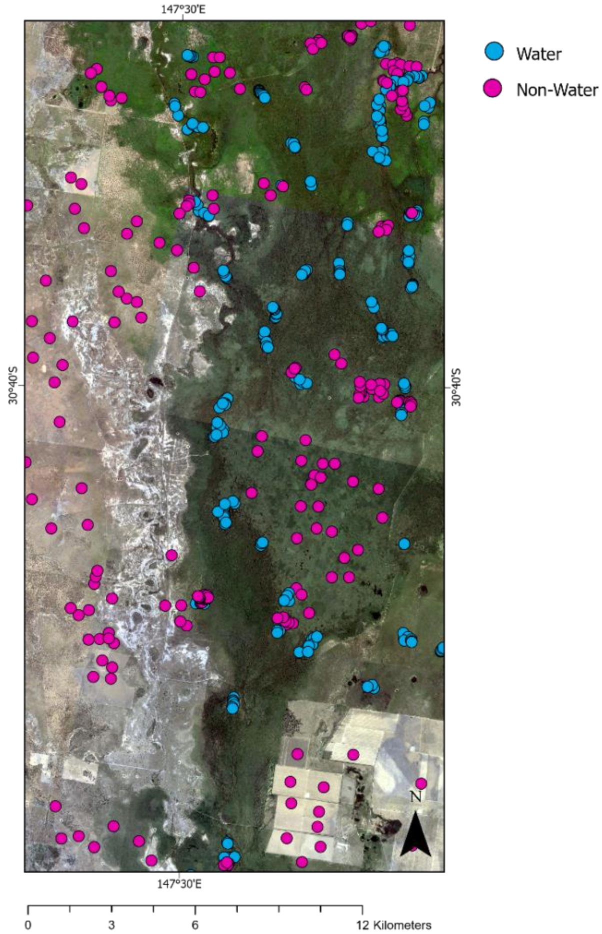

Figure 3.14: Superimposed Manual Points Digitised Over PlanetScope Image

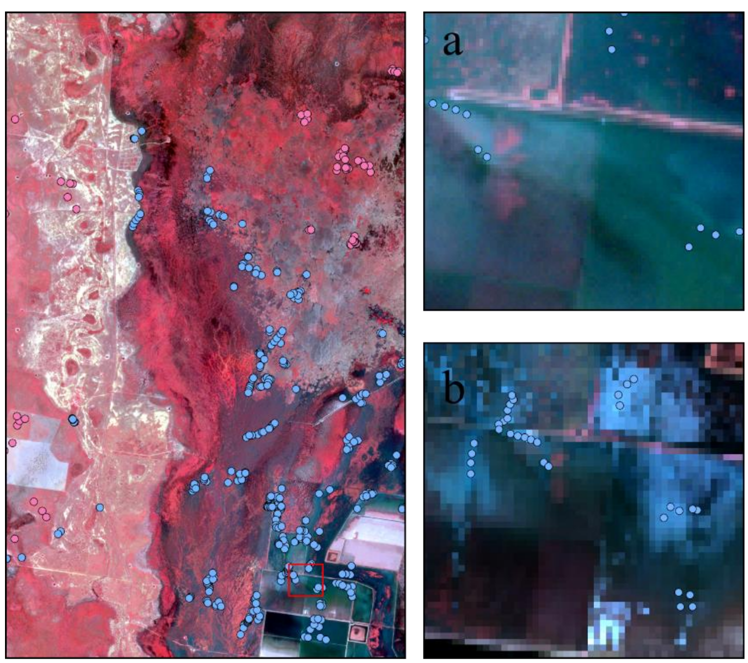

Figure 3.15: Cross-referencing manually marked water points (Blue represents Water & Pink points represent Non-Water) with the resampled 10-meter (10m) PlanetScope (a) and Sentinel-2 data (b)

3.2.1.8 Water Observation from Space (WOfS)

The WOfS product developed by Mueller et al. (2016) is based on 27 years of data from Landsat-5 and Landsat-7, covering the period from 1987 to 2014. WOfS is available as a geospatial dataset developed by Geoscience Australia that includes information on the presence and recurrence of surface water across Australia (Law et al., 2021). The WOfS product has since been updated to include data from Landsat-8 and Sentinel-2 and provide more frequent and higher-resolution observations. The WOfS time-series data was used as further validation data in this study. The Water Observations from Space (WOfS) dataset is designed to map open surface water, and as such, it may not effectively identify flooded vegetation. The WOfS method focuses on detecting open water, and its accuracy may decrease in areas with mixed water and vegetation pixels. While WOfS is valuable for detecting open water, it may underestimate water in mixed-signal pixels, particularly in wetland areas. Therefore, when using the WOfS dataset, it is important to consider its limitations in capturing inundated vegetation, especially in areas with thick vegetation or mixed water and vegetation pixels. Other methods, such as the Tasseled Cap Wetness index, may be used to complement WOfS for a more comprehensive analysis of water and vegetation dynamics in wetlands.

3.2.1.9 Inundation Maps for NSW Inland Floodplain Wetlands

Inundation maps for NSW inland floodplain wetlands Murray-Darling Basin are derived from Landsat and Sentinel-2 and available for the period between July 2014 and June 2022, and are developed using a modified version of Thomas et al. (2015). Water Index (Fisher et al., 2016) and NDVI were calculated for each satellite observation to allocate inundated pixels to multiple classes, i.e., open water, mixed water and vegetation, and inundated dense vegetation cover. As Figure 3.16 demonstrates, final inundation classes include non-inundated regions (0), inundated areas (1), off-river storages with water (2), cloud shadows that often erroneously misclassify as water (3). Though this study does not intend to eliminate cropped areas but Thomas et al. (2015) coded the cropped areas with similar spectral properties of wetlands vegetation as zero. In order to use this dataset these images were reclassified to binary imagery as non-water (0) and water (1) (off-river storages with water were considered as inundated too).

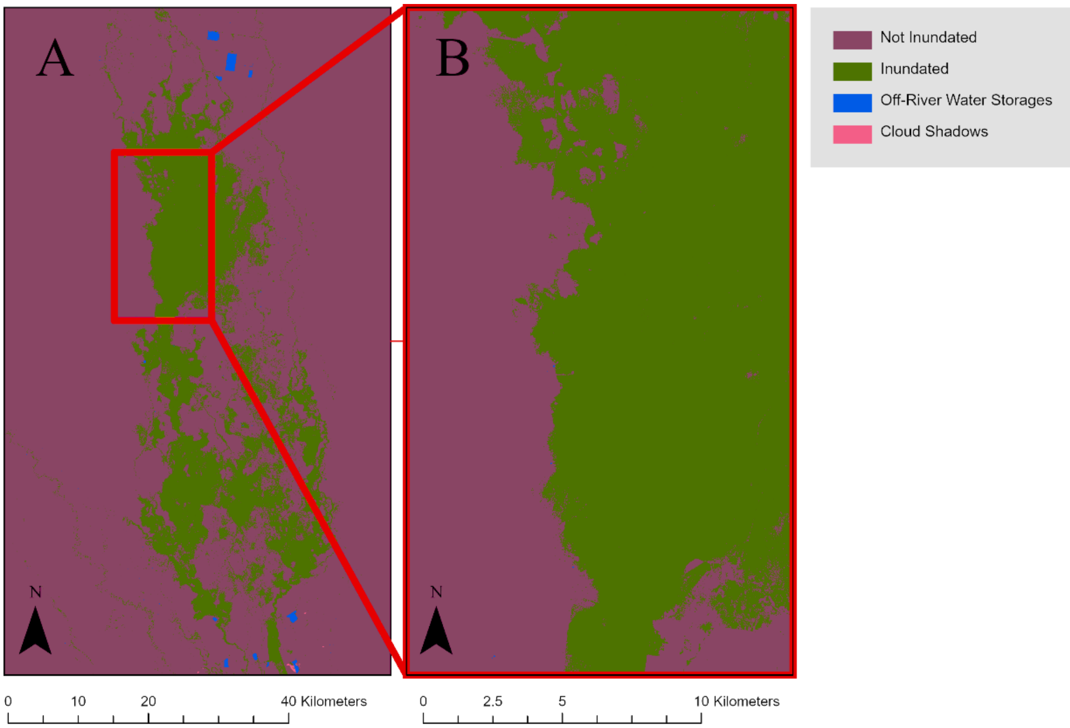

Figure 3.16: Inundation Maps for NSW Inland Floodplain Wetlands for Macquarie Marshes (03/03/2022) (A) while (B) shows the clipped and reclassified image of Area of Interest

3.2.1.9.1 Fusion of Sentinel-1 & Sentinel-2

To enable fusion of the datasets, the Sentinel-1 and Sentinel-2 images, corresponding to similar dates (Table 3.5), were stacked together at the pixel level. This stacking process involved merging the data from both sensors to create a composite representation at overlapping dates (Table 3.5), resulting in only 5 dates. A Random Forest (RF) algorithm was applied to the stacked images to classify the pixels into water and non-water categories but involved including additional covariates. The RF model was executed in Python, using the scikit-learn library's '**RandomForestClassifier**' module comprised of 100 decision trees with default parameters such as maximum depth. The outputs from the RF model include the inundated maps and the probability maps which provide the probability of each pixel belonging to the water or non-water category. As outlined in the literature review, the fusion of Sentinel-1 and Sentinel-2 data and applying RF for water delineation combines the strengths of both sensors to improve the accuracy of water delineation. The input data for classifiers included the VH and VV bands of Sentinel-1, Fisher's Water Index, NDVI from the Sentinel-2, Rainfall from SILO, and Slope and Probability of Depression raster images based on the Digital elevation model. NDVI was chosen as the preferred vegetation index as it has been widely used in the water and flood mapping; however, it is worth mentioning that NDVI is not specifically optimised for detecting water surfaces (Foroughnia et al., 2022), but in conjunction with other Water Indices, the limitations of NDVI in water surface analysis can be mitigated, for example Thomas et al. (2015). All the images were aligned and resampled to a final resolution of 10 meters. All the pre-processing steps were conducted on the

Sentinel Application Platform (SNAP) and GIS software. Due to the difference in revisit time of Sentinel-1 and Sentinel-2, all the satellite images were not available for the exact same dates, and the different revisit times of these two satellite systems posed a challenge for data synchronisation. In order to resolve this issue, a two-tiered approach was adopted, i.e., priority was given to the dates where S1 and S2 images were available on the exact same day (Table 3.5 coloured cells) and secondly for dates, where no coinciding S1 and S2 images were available, those images were selected that were closely aligned in time, with a maximum allowable difference of 3-4 days between them. This approach was chosen to balance the need for temporal proximity with the availability of data. Images that were more than with a time difference exceeding 4 days were excluded from analysis to minimise the impact of significant temporal discrepancies on the analysis and to ensure consistency.

Table 3.5: Table showing the closeby acquisition dates of Sentinel-1 and Sentinel-2 used for RF Modeling. Coloured cells indicate dates of images acquired from Radar & Optical Sensor on the similar date

S. No.	Sentinel 1	Sentinel 2
1	04/01/2022	05/01/2022
2	16/01/2022	15/01/2022
3	28/01/2022	30/01/2022
4	**9/02/2022**	**9/02/2022**
5	21/02/2022	19/02/2022
6	05/03/2022	03/03/2022
7	17/03/2022	18/03/2022
8	10/04/2022	12/04/2022
9	04/05/2022	05/05/2022
10	**21/06/2022**	**21/06/2022**
11	15/07/2022	14/07/2022
12	27/07/2022	24/07/2022
13	**8/08/2022**	**8/08/2022**
14	**20/08/2022**	**20/08/2022**
15	01/09/2022	04/09/2022
16	25/09/2022	27/09/2022
17	07/10/2022	09/10/2022

18	31/10/2022	27/10/2022
19	24/11/2022	26/11/2022
20	**06/12/2022**	**06/12/2022**
21	18/12/2022	16/12/2022
22	30/12/2022	28/12/2022

Table 3.5 demonstrates that we specifically considered the dates when Sentinel-1 and Sentinel-2 images overlapped within the desired time frame.

3.2.1.9.2 Water Depth Maps Calculation

Water depth of the inundation water extent was calculated using the Digital Elevation Model (DEM) and a Boolean mask identifying inundated areas. The maximum elevation in each inundated area was calculated, and then the water depth was derived by subtracting DEM values from water table elevations. The resulting water depth raster was then used to calculate the volume of water in m^3.

3.3 Results

3.3.1 Surface Water Mapping Using Sentinel 2

As discussed, the recommended threshold value for Water Indices of WI, AWEIsh, and AWEInsh is typically set to 0 to identify surface water (Figure 3.17). However, in some cases, this threshold value may not be optimal for detecting water in certain images, and despite using the recommended thresholds, using a single threshold resulted in difficulties in detecting water in certain images. Therefore, to maximise the performance of the WI, AWEInsh, AWEIsh and MNDWI algorithm, the Kappa coefficient was calculated for a range of threshold values to determine which threshold value provides the best agreement with the reference image and use that value to detect water in the image collection (Figure 3.18). Previously we calculated the threshold of MNDWI using another technique (Section 3.2.1.2.1), and the value derived from that technique (-0.19) can be validated by this approach as well (-0.2 in this scenario).

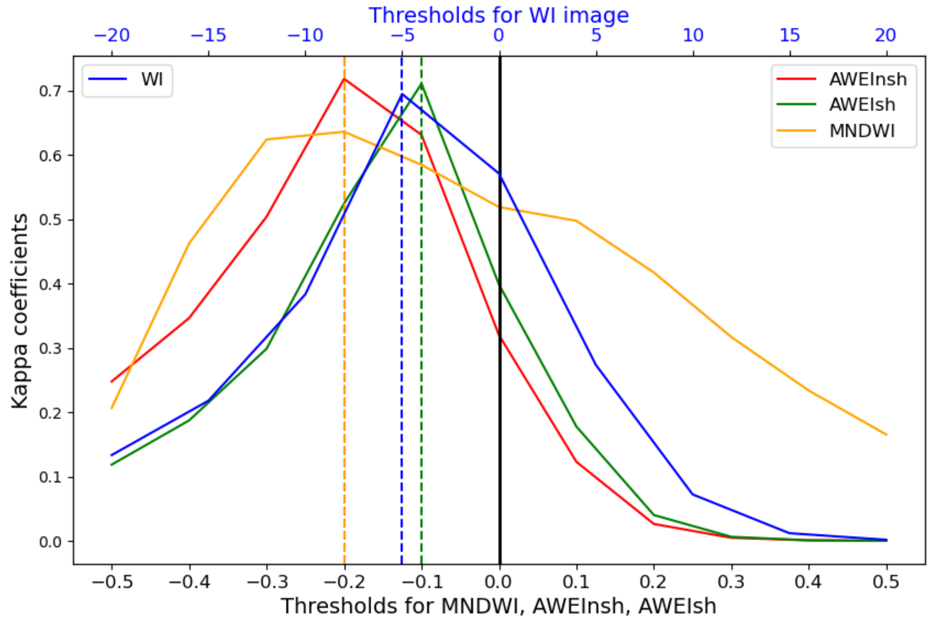

Figure 3.17: Kappa coefficients of the Water Indices (WI, AWEInsh, AWEIsh, MNDWI) calculated on the Sentinel-2 image with the WOfS (Water Observations from Space) image. Both Sentinel-2 and WOfS are of same date (06/12/2022). The black line shows the recommended threshold for Water Indices in some literature.

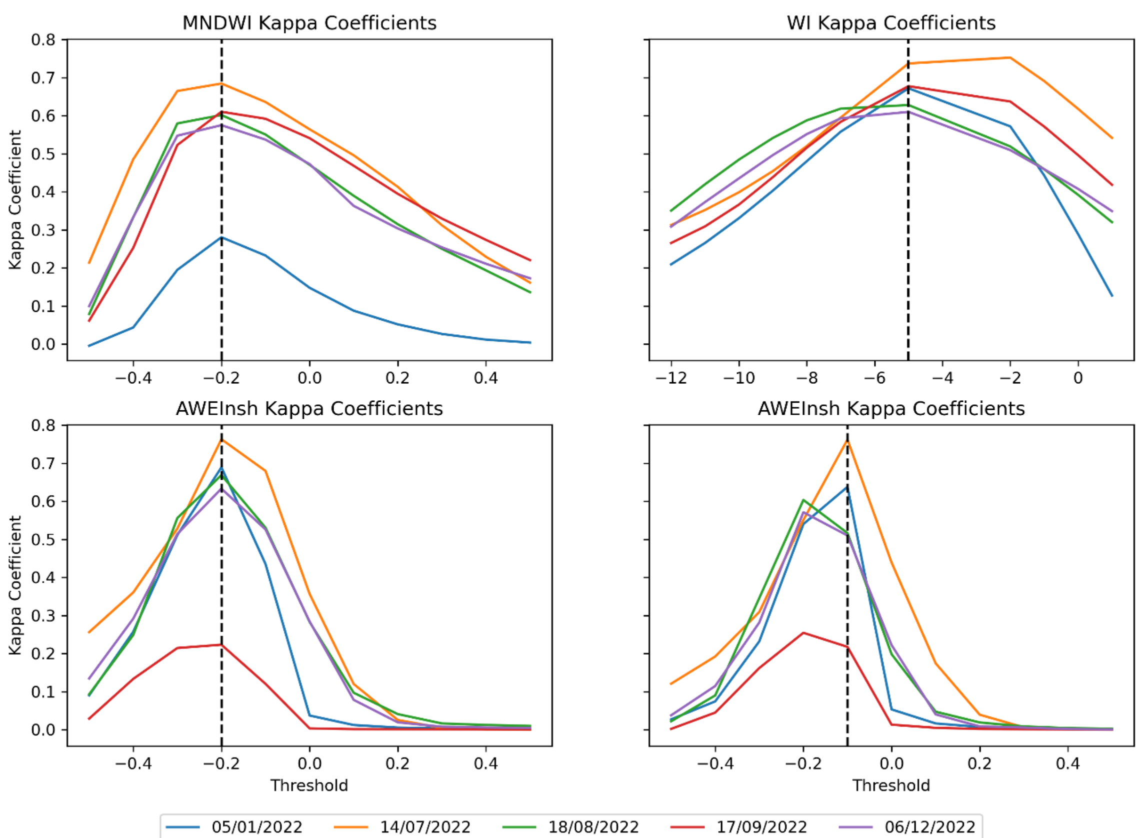

Figure 3.18: Kappa coefficients of the MNDWI, WI, AWEInsh, AWEIsh compared with WOfS using different thresholds for different dates. The dotted black line shows the estimated threshold

Figure 3.18 shows the Kappa coefficients computed for MNDWI, WI, and AWEI using the WOfS images of the similar dates as the reference. The comparison was done by applying different thresholds to these indices. As demonstrated in Figure 3.18, this gives us an optimal threshold, i.e., the threshold at which the algorithm achieves the highest accuracy in classifying water pixels. By finding the optimal threshold for each algorithm, the accuracy of water detection in Sentinel-2 images using these water indices can be enhanced, overall improving the reliability of water monitoring and analysis.

3.3.1.1 Temporal Analysis of Water Extent

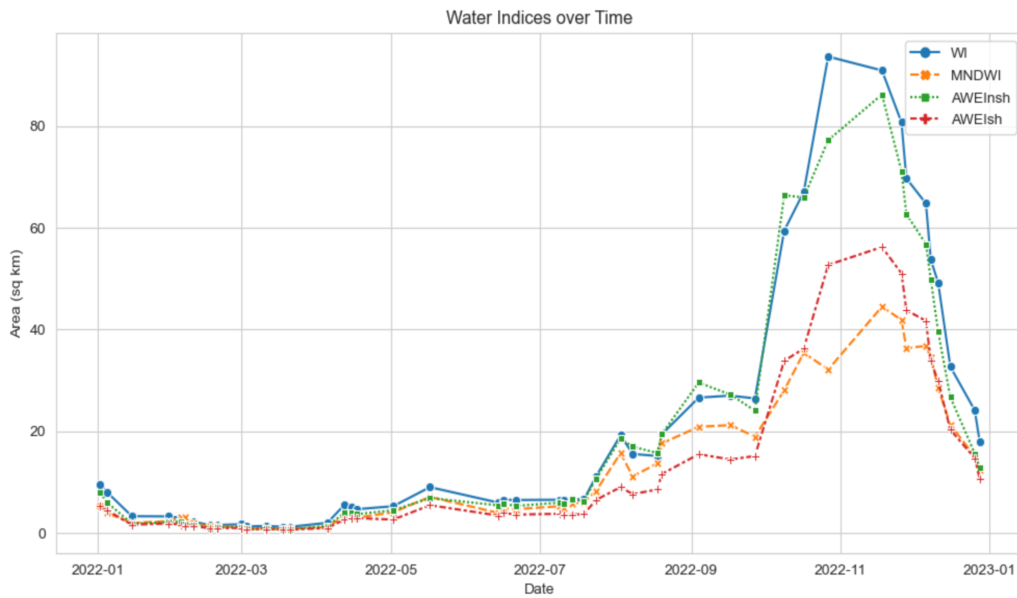

Figure 3.19: Area of Surface Water Delineated using Different Indices for the year 2022

Figure 3.19 demonstrates the trends in the water delineated using multiple indices over the year 2022. WI shows notable peaks in October and November 2022. The MNDWI values vary between 0.71 and 44.5 sq km, and it delineated a lower surface water extent compared to other indices, implying that it may not be the best choice for detecting water bodies compared to other indices (Albertini et al., 2022). This in contrast to the fact that it has performed well in some other studies through enhancing water bodies and reducing noise from built-up land, vegetation, and soil (Buma et al., 2018). Figure 3.20 presents the distribution of inundated areas using a boxplot, across 47 Sentinel-2 images from January 2022 to December 2022, applying various algorithms:

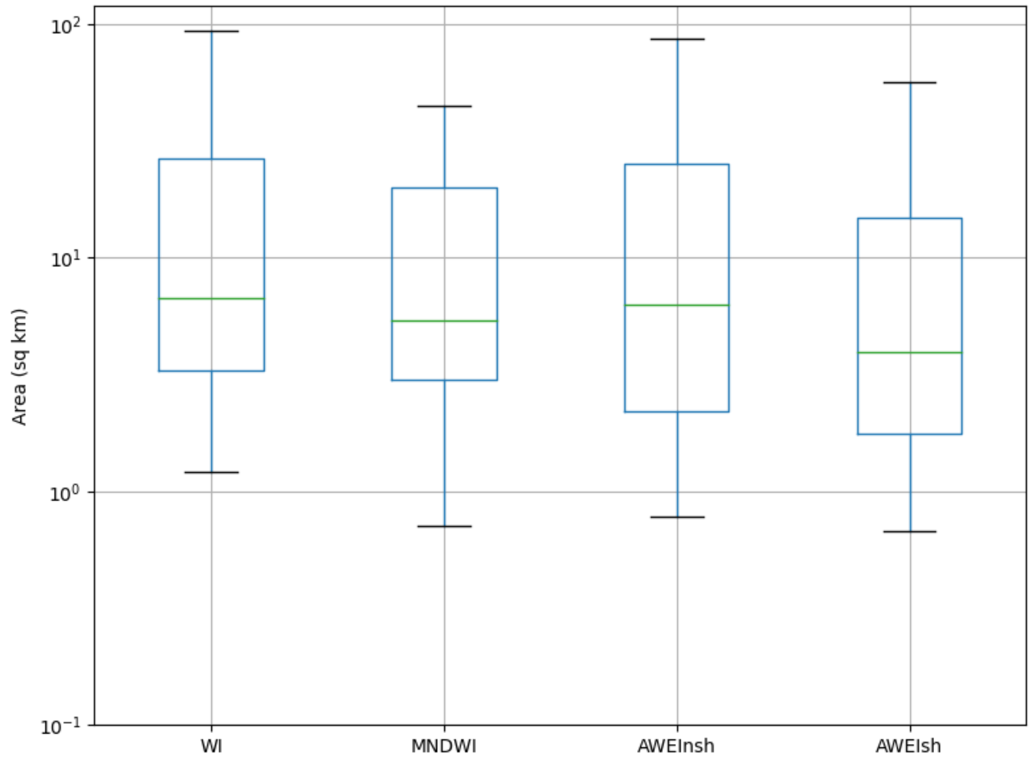

Figure 3.20: Boxplot of the distribution of surface water areas calculated using different water indices

The WI algorithm estimated the highest maximum inundated area, whereas AWEIsh estimated the smallest maximum inundation area in relation to other indices. The WI values have a larger IQR (53.87) and the values tend to deviate from the mean further compared to MNDWI, AWEInsh, and AWEIsh values. The median values of MNDWI, AWEInsh, and AWEIsh are 8.37, 7.65 and 4.88 while the IQR values are 29.19, 24.765 and 17.495. A lower IQR of AWEIsh compared to other indices predicts a smaller range of inundated extents. The IQR is not heavily influenced by extreme values or outliers in the dataset. The smaller IQR in Figure 3.20 suggest that the AWEIsh on the average might underestimate areas during large flood events. However, all algorithms have limitations in detecting all flood events and further analysis and validation may be necessary to determine the most effective water index for flood detection in this area. In addition, there is a relatively low difference in the overall distributions of the different indices (Figure 3.20). ANOVA (Analysis of Variance) test was performed to find the statistical significance of the differences between group means. The results of ANOVA test show a P-value of about 0.09, suggesting only weak evidence that significant differences between the means of the different water indices (MNDWI, WI, AWEInsh, AWEIsh).

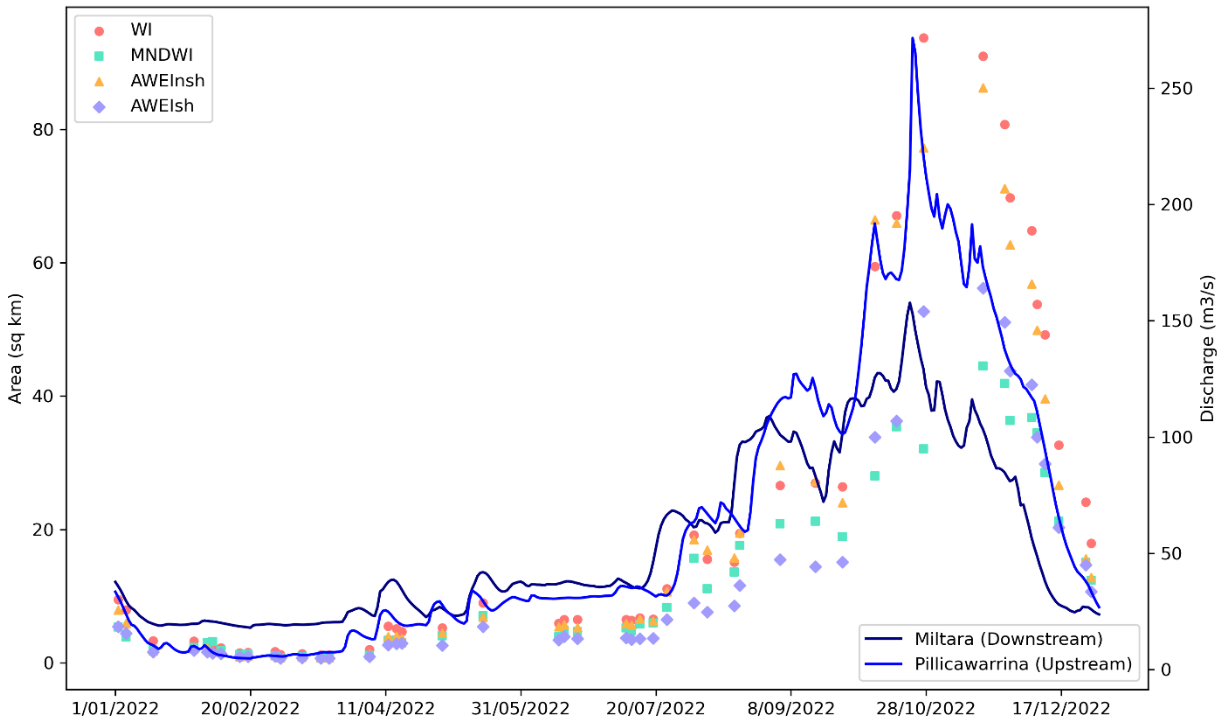

Figure 3.21: Surface water extracted using water indices including (MNDWI, WI, AWEInsh, AWEIsh) and daily discharges at Pillicawarrina (421147)- Upstream & Miltara (421135)- Downstream

Figure 3.21 shows the time series of area of surface water extracted using different indices and daily water discharge data at the upstream and downstream gauges from January 2022 to December 2022. In general, the inundated areas identified by WI and AWEInsh have a similar pattern in time as the discharge peaks recorded at the gauging stations with a sharp peak during the major flood event. However, some discharge peaks also resulted in no peaks in the inundated areas even using WI and AWEInsh, and some flood detection occurred with no associated peak in discharge. In addition, the other indices show a much flatter pattern in time relative to the discharge peaks. We would expect to see at least some correlation between the area of surface water extent and water discharge which might be used to quantify the association between the river discharge data and water indices. The Pearson correlation coefficient between Water Indices (WI, MNDWI, AWEInsh, AWEIsh) and Water Course Discharge (upstream) was 0.75, 0.76, 0.8 and 0.72 respectively for the upstream while the correlation of the indices is relatively higher with downstream discharge. Since the Pearson correlation coefficients between MNDWI, WI, AWEInsh, AWEIsh and Water Course Discharge are all positive, this indicates that there is a positive linear relationship between these variables. There is also a variation in the strength of the correlations between the indices at the upstream and downstream water discharge, with downstream having the strongest correlation (Figure 3.22). This makes more sense as downstream gauges generally receive increased amounts of the accumulated flow upstream in the catchment, and the downstream gauging station generally exhibit a better representation of the overall hydrological behaviour (Fuentes et al., 2019), leading to greater cross-correlation between the surface water extent and daily water discharge at the gauging station. However, in the downstream gauging station, there can be a notable delay in the flood-discharge response (Figure 3.23) if there are more complex interactions, backwater effects, and delays in water movement (Zhang & Werner, 2015). This is because downstream stations would capture the cumulative effects of water flow, delays, and interactions as they progress through the system. Discharge peaks can occur several days prior to the flood response, but this can actually present an opportunity to explore whether inundation images could potentially yield advance information on downstream flooding conditions. However, as De Lavenne et al. (2019) put forward the behaviour of main river discharge masks the hydrological behaviour of the downstream, and the upstream naturally supplies more water volume compared to downstream (as can be viewed in Figure 3.21).

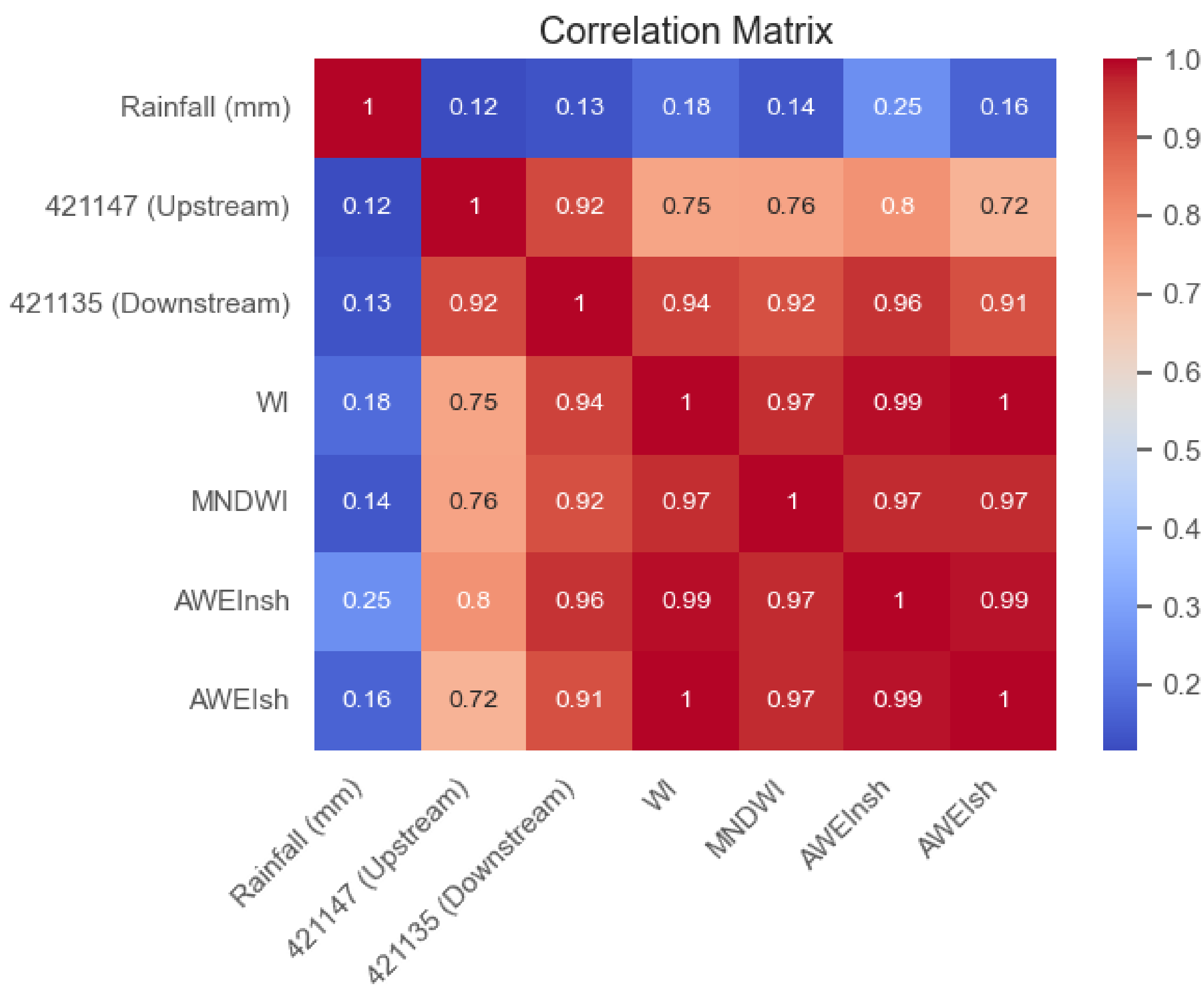

Figure 3.22: Correlation Matrix suggesting a strong positive linear relationship between MNDWI, AWEInsh, AWEIsh and Water Discharge

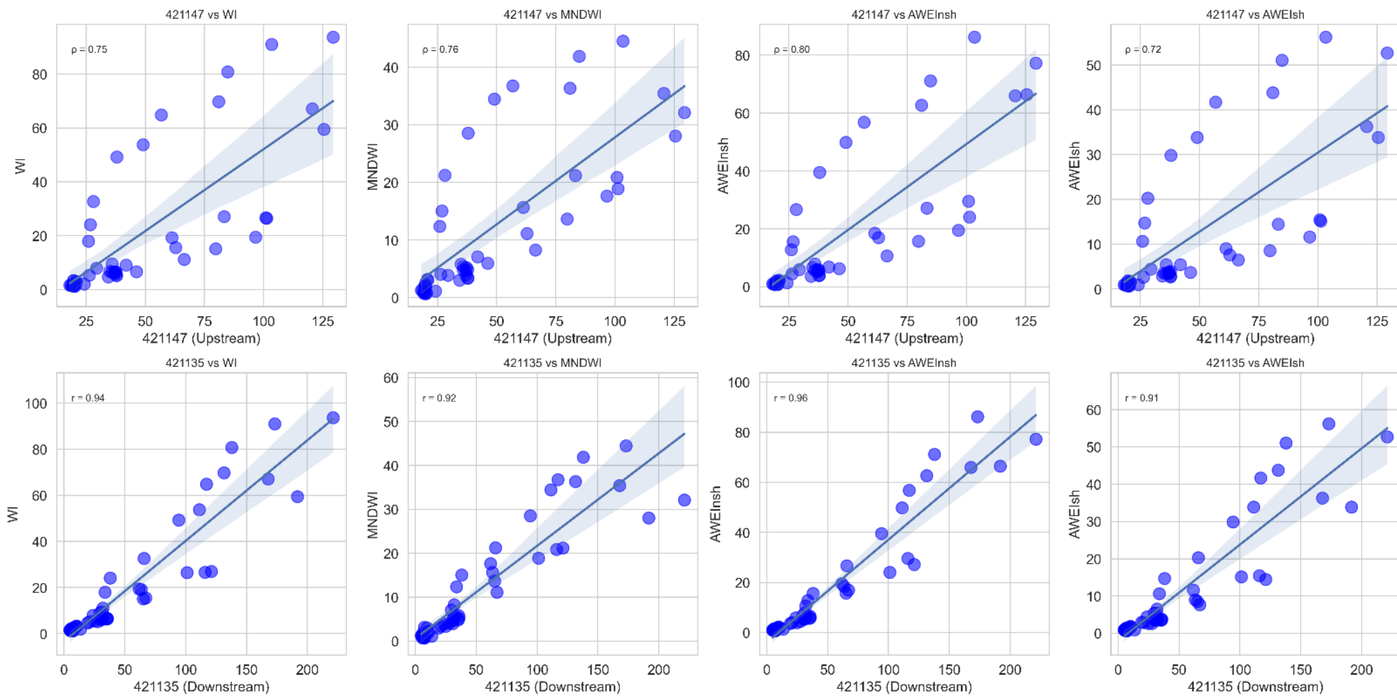

Figure 3.23: Scatterplots between daily discharge and inundated areas obtained from the different Water Indices at two gauge stations located in the Macquarie River, at Pillicawarrina (a), and at Miltara (b), and their correlation coefficients. The line is the linear fit

The AWEInsh has the highest correlation with the river daily discharges, followed by the WI and MNDWI. These correlation coefficients indicate reasonably strong associations between the discharge and flood extents at the downstream gauge stations. However, the linear associations as in Figure 3.23 are an approximation of the relationship between the discharge and surface water extent delineated through these water indices, and the linear approximation may oversimplify the complex nature of the data (Fuentes et al., 2019). The discharge is a flux (a volume per time) while the flood extent (or volume) is a state variable, which means that some sort of water balance needs to be used to estimate the exact relationship. In addition, numerous environmental factors like topography, land cover types, and soil properties also play substantial part in influencing the correlation between river discharges and inundation patterns.

3.3.1.2 Performance Assessment of Water Indices Against WOfS

As indicated, WOfS data was used as one of the independent datasets to assess the performance of the different indices using their derived optimal thresholds. The indices (WI, MNDWI, AWEI) were compared against WOfS using performance assessment metrics, such as commission/omission or users/producers accuracy. Table 3.6 suggests that all the algorithms achieved relatively high accuracy scores, and altogether the performance of the different water indices ranges from moderate to substantial agreement. Figure 3.24 illustrates a bar chart showing the comparison between the area inundated using the WOfS and different water indices.

Table 3.6: Evaluation of accuracy between Landsat-based WOfS and different Sentinel-2 Water Indices.

Date	**Approach**	**Accuracy**	**Kappa**	**F1 Score**	**Commission**	**Omission**	**Area Delineated (sq km)**	**WOfS area (sq km)**
05/01/2022	WI	0.98	0.54	0.55	0.009	0.05	7.95	6.19
	MNDWI	0.98	0.21	0.22	0.0065	0.75	3.9	
	AWEInsh	0.99	0.64	0.64	0.006	0.09	5.95	
	AWEIsh	0.99	0.67	0.67	0.003	0.21	4.42	
14/07/2022	WI	0.99	0.50	0.50	0.008	0.17	6.74	7.12
	MNDWI	0.99	0.54	0.54	0.007	0.18	5.83	
	AWEInsh	0.99	0.55	0.55	0.008	0.106	6.57	
	AWEIsh	0.99	0.55	0.55	0.003	0.38	3.61	
18/08/2022	WI	0.97	0.53	0.54	0.018	0.23	15.14	16.01
	MNDWI	0.98	0.54	0.55	0.015	0.25	13.65	
	AWEInsh	0.97	0.54	0.55	0.018	0.18	15.73	
	AWEIsh	0.98	0.55	0.55	0.008	0.43	8.55	
17/09/2022	WI	0.96	0.55	0.56	0.033	0.076	27.01	21.16
	MNDWI	0.97	0.56	0.58	0.02	0.17	21.21	
	AWEInsh	0.97	0.27	0.28	0.007	0.78	27.2	
	AWEIsh	0.97	0.28	0.28	0.004	0.80	14.45	
06/12/2022	WI	0.93	0.63	0.67	0.06	0.04	36.78	49.66
	MNDWI	0.96	0.71	0.73	0.02	0.24	64.80	
	AWEInsh	0.94	0.68	0.71	0.05	0.06	56.81	
	AWEIsh	0.96	0.74	0.76	0.02	0.16	41.71	
Mean	**WI**	0.96	0.55	0.56	0.025	0.11		
	MNDWI	0.97	0.51	0.52	0.013	0.31		
	AWEInsh	0.97	0.53	0.54	0.017	0.24		
	AWEIsh	0.97	0.55	0.56	0.007	0.39		

The WI achieved an accuracy of 0.96 with a relatively high kappa coefficient of 0.55, indicating a moderate level of agreement in detecting surface water extent in the AOI based on WOfS. The AWEIsh (with an accuracy of 0.97 and a kappa coefficient of 0.55) also demonstrated reasonable performance, and comparable to the WI. However, AWEIsh indicates the highest omission error of 0.39 that indicate a higher rate of false negative detections. The MNDWI algorithm, with an accuracy of 0.97 and a kappa coefficient of 0.51, showed slightly lower performance compared to WI and AWEIsh. The AWEInsh algorithm performed similarly to the MNDWI algorithm, with an accuracy of 0.97 and a kappa coefficient of 0.53. The MNDWI algorithm also has a slightly higher commission error of 0.013 and a higher omission error of 0.31 that shows an increased rate of false positive detections and somewhat false negative detections.

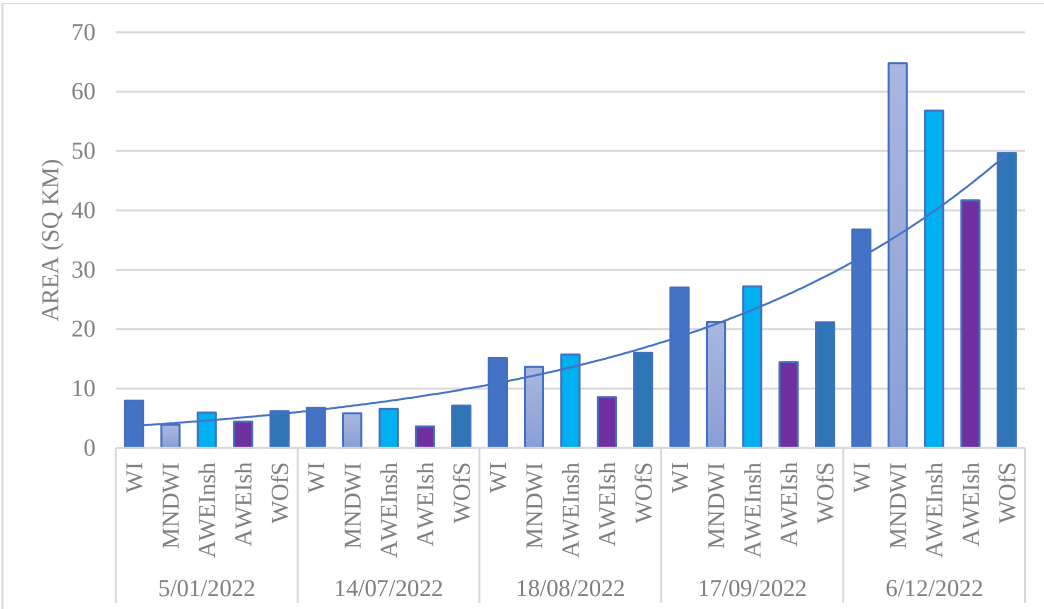

Figure 3.24: A bar chart showing comparison between the Predicted and Observed values.

The WI and AWEIsh algorithms demonstrated the highest agreement in detecting surface water extent based on WOfS, as indicated by their high accuracy and kappa coefficients. A qualitative ranking of the different indices is in Table 3.7.

Table 3.7: Qualitative Ranking of Water Indices

Water Indices	Overall Performance	Ranking Based on Correlation Coefficient	General Ranking
WI	1	2	1
MNDWI	3	2	3
AWEInsh	2	1	1
AWEIsh	1	3	2

The ranking is based on how well the indices performed against the reference WOfS-derived water extent, and how well they captured the flood dynamics relative to the gauge discharges. The indices that performed the best are ranked first, and the index that performed the worst is ranked third. Based on the performance against the flood occurrence from the Landsat based WOfS images and considering the mean kappa values (Table 3.7), indices ranked first have mean kappa coefficients greater than or equal to 0.55, index ranked second has mean kappa coefficient of 0.53, and algorithms with mean kappa coefficient lower than 0.53 was ranked third. Then, based on the mean correlation coefficients between inundated areas and discharges at the Miltara & Pillicawarrina (Figure 3.22), indices that have mean correlation coefficients greater than 0.8 are ranked first, mean correlation coefficients between 0.75 and 0.8 are ranked second, and mean correlation coefficients smaller than or equal to 0.75 are ranked third. As per the final ranking, WI and AWEInsh perform better compared to other indices.

3.3.1.3 Performance Assessment of Water Indices Against PlanetScope

While we conducted a performance assessment of water indices against WOfS images that were for the same day or dates that were very close, it is important to note that WOfS has been known to underestimate water in certain cases. Therefore, we also incorporated PlanetScope imagery into our analysis to further determine the accuracy and reliability of delineated water. This can further validate our results of Water Indices considering the potential limitations of the WOfS data.

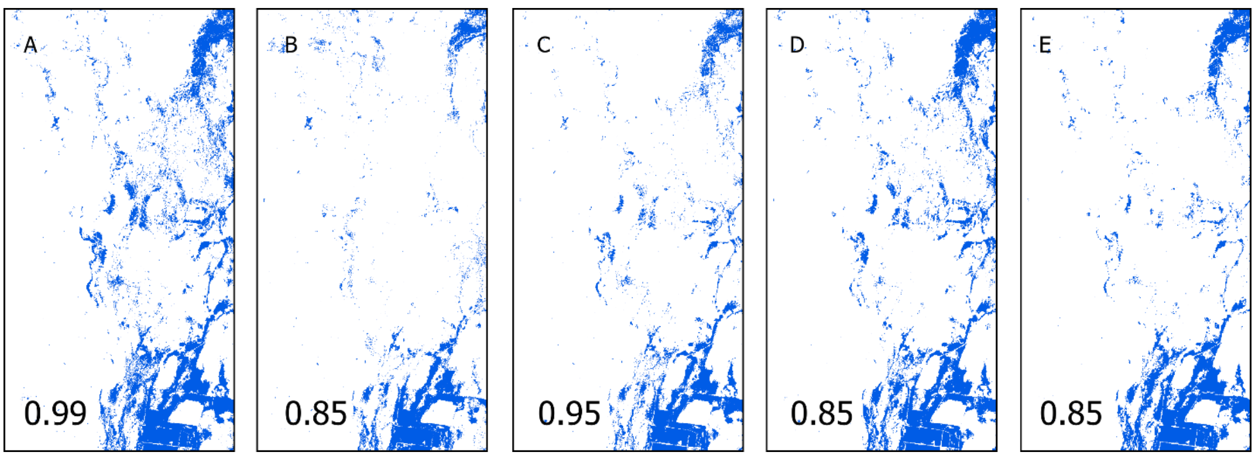

Figure 3.25: Surface Water Extent Delineated from Different Water Indices Water Index (A), MNDWI (B), AWEIsh (C), AWEInsh (D) & (E) WOfS alongwith their respective Kappa Coefficient. Water Indices were applied on Sentinel-2 acquired on 06/12/2022, WOfS is also of the same date.

Figure 3.25 demonstrates that the performance of the Water Index (WI) and AWEIsh was better than other indices when compared to the Water Observations from Space (WOfS) algorithm. This observation was consistent comparing WI with the PlanetScope dataset. In both cases, WI and AWEIsh demonstrated better performance in identifying and characterising water features. Both the quantitative and qualitative results emphasise the effectiveness of the WI in accurately detecting water bodies especially in wetlands.

3.3.1.4 Spatial Relationship Analysis for the Sentinel-2 results

This is important to understand the spatial relationship between flood water and different covariates, such as, vegetation, elevation, and probability of depression, etc. This can help understand the influence of topography on water accumulation, and the proximity of water bodies to vegetation areas. Also, an understanding of these patterns can enable predictions about how similar relationships might play out in other areas.

Table 3.8: Cross tabulation of water and non-water predicted and observed classes

Observed	**Predicted**	
	Water	No Water
Water	A	B
No Water	C	D

For this analysis, the results are split into 4 classes (Table 3.8). Class A denotes areas where both the observed and predicted data indicate the presence of water. Class B represents areas where the observed data indicates the presence of water, but the predicted data suggests the absence of water. Class C includes areas where the observed data indicates the absence of water, but the predicted data suggests its presence. Class D classifies areas where both the observed and predicted data indicate the absence of water.

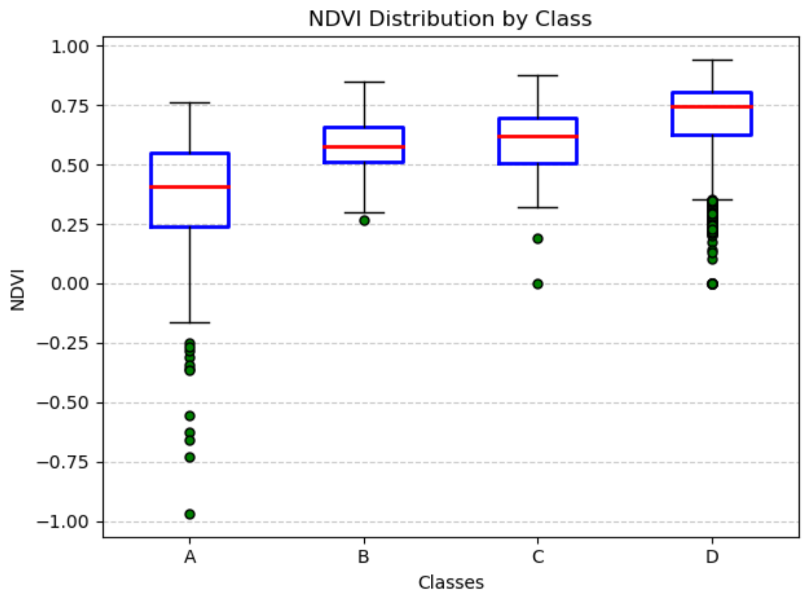

Figure 3.26: NDVI Distribution by Class

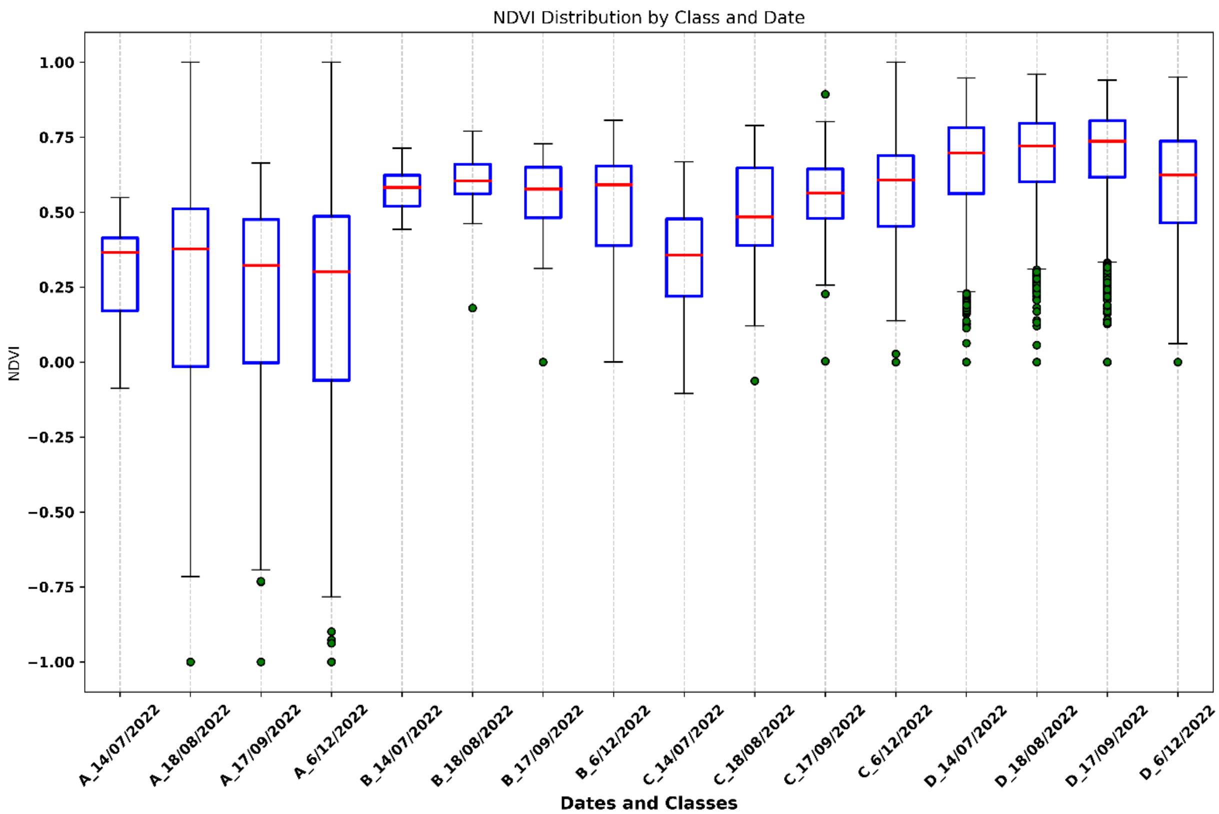

Figure 3.27: NDVI Distribution of Class for Multiple Dates

As demonstrated in Figure 3.26 and Figure 3.27, there are significant differences among the classes in the NDVI values. In Figure 3.26, the median value for class A is 0.4 while the mean value is 0.3. The class D where no water was detected either in the predicted or observed image, the NDVI median value is 0.75 while the mean value is 0.7 (Figure 3.26). This is consistent with the idea that water bodies typically have lower or negative NDVI values while higher NDVI values are indicative of healthy vegetation. However, it also indicates that mis-classifications are concentrated in areas where pixels are more mixed and the NDVI values fall in between the two extremes. This confirms the notion that identifying water under vegetation is more difficult (Brinkhoff et al., 2022; Mueller et al., 2016).

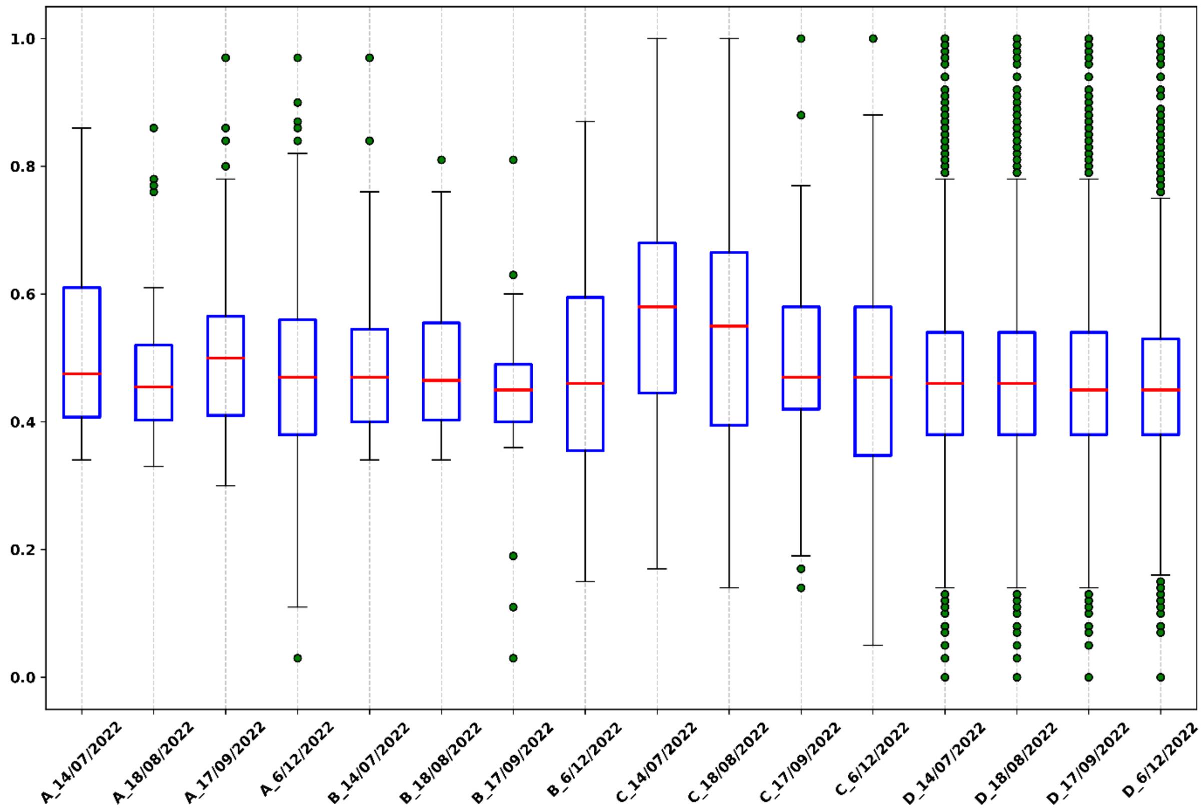

Figure 3.28: Probability of Depression Distribution for Different Time-period

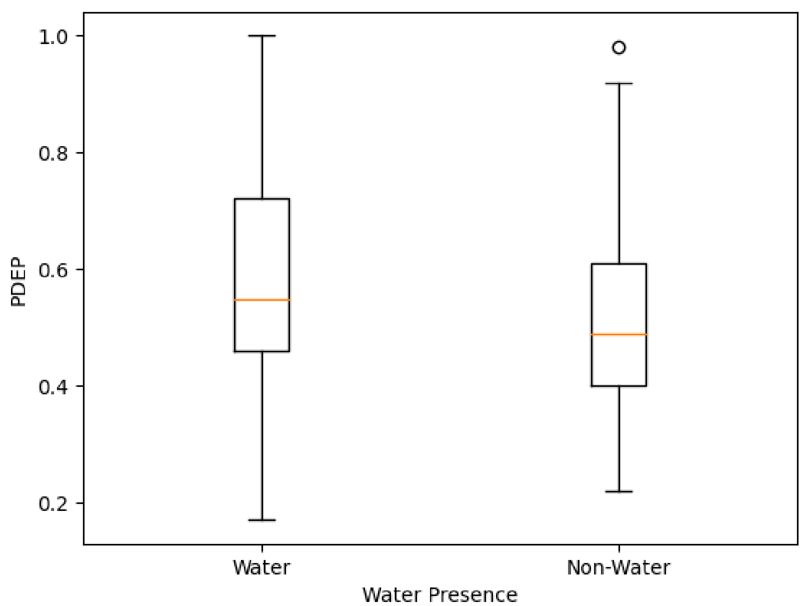

Figure 3.29: Distribution of Probability of Depression for Water & Non-Water Pixels

There is no real relationship between the water presence in an area and probability of depression, even though the probability of depression tends to increase in the areas with water (Figure 3.29) but no significant conclusion can be derived from Figure 3.28. For the NDVI, a moderate to strong relationship between NDVI and the presence of water in the wetlands exists ($r^2 = 0.5$). As can be seen in Figure 3.26, the likelihood of water presence tends to decrease with an increase in NDVI. Although the literature suggests that slope can play a significant role in determining drainage patterns (Ayalew & Yamagishi, 2005), which can indirectly affect water presence, there was no impact of slope on water presence in the study area as channel and floodplain slopes in this system are all very low.

3.3.2 Surface Water Mapping Using Sentinel 1

Figure 3.30 shows dynamic thresholds that were determined using the automatic Otsu thresholding algorithm on the time series of Sentinel-1 images from January 2022 to December 2022 in Macquarie Marshes. The VV values (ranging from -12.9 to -7.91) are higher than the VH values (ranging from -20.20 to -15.66), which is typical for Sentinel-1 data (Villarroya-Carpio et al., 2022). There are occasional spikes in the VV and VH values. There is no general trend, but the threshold for VH polarised scenes was constantly lower in the flood event (September to November) compared to other seasons. The reason could be that the surface water is generally much deeper and apparent during the flooding event, resulting in a lower backscatter intensity acquired by Sentinel-1 satellites. However, with the fluctuation of the VV and VH values over time, with some values being higher or lower than others, there can be a potential issue of fixing a constant threshold for the whole duration (Tran et al., 2022).

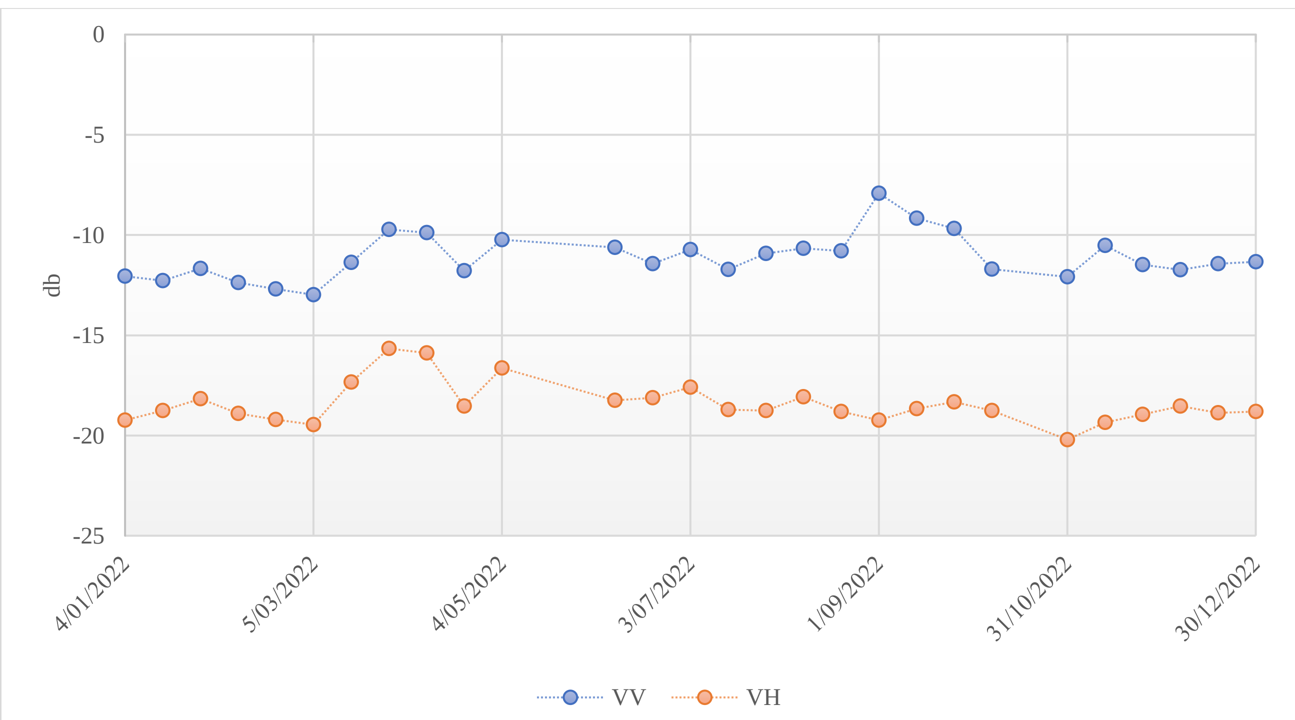

Figure 3.30: Automatic thresholding Values for Sentinel 1 images Acquired for AOI in 2022.

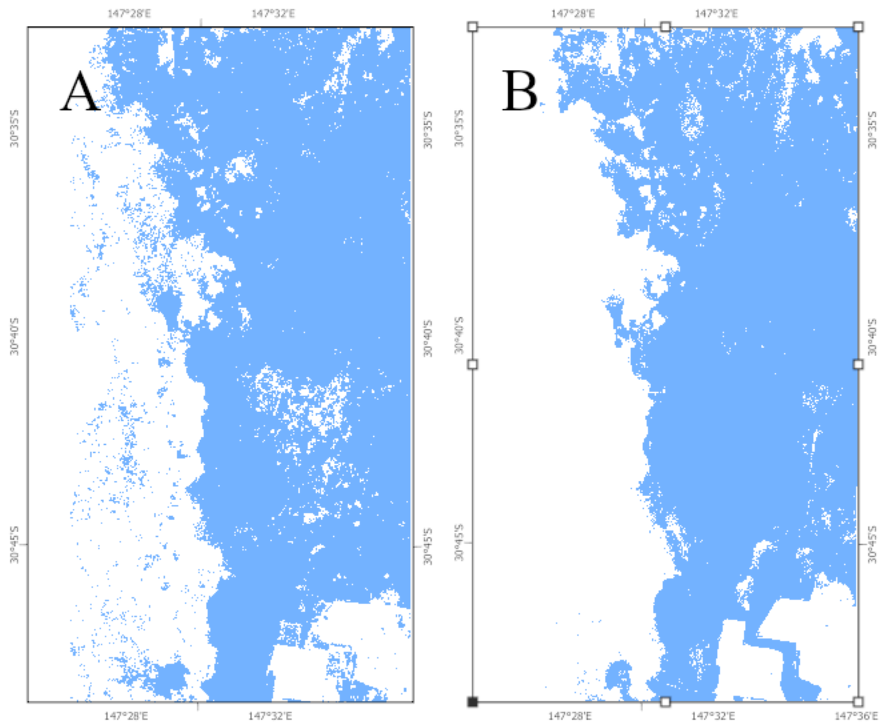

Figure 3.31: A showing water delineated using Otsu thresholding technique applied on Sentinel-1 acquired on 04/01/2022, B shows the NSW inundation map of Macquarie Marshes of 02/01/2022 (2021-2022 inundation maps, 2023)

Figure 3.31 demonstrates coherence between the results acquired from Otsu thresholding and the NSW inundation map. Figure 3.32 also displays the consistency between the two sets of results which is interesting in a way that the water delineated using multiple water indices applied on Sentinel-2 do not match with the Otsu results which was initially attributed to sensor variations. But the somewhat alignment of Otsu results with the NSW inundation maps (executed through the same Sentinel-2 platform) suggest that the results are valid (with an overall accuracy of 85%). Table 3.9 presents the accuracy assessment of the Otsu Thresholding technique applied to Sentinel-1 imagery. The results obtained from this technique are compared against the NSW inundation maps, which serve as the reference dataset for validating the accuracy of the flood delineation.

Figure 3.32: Area of delineated water acquired using the Otsu thresholding technique, based on Sentinel-1 imageries compared with NSW inundation map (reference dataset)

Table 3.9: Accuracy Assessment of Otsu Thresholding Technique applied to Sentinel-1 imagery compared against the NSW inundation maps

Commission Error	0.249
Omission Error	0.05
Overall Accuracy	0.85
Kappa	0.69
F1 Score	0.86

The commission error, also known as the false positive rate, is 0.24 that indicates 24% of the time Otsu technique incorrectly classified non-water as water. The omission error, also known as the false negative rate, is about 5.5% which means Otsu incorrectly classified water as non-water. Overall accuracy measures of how well the classification model performs across all classes, which 85% in this case. A Kappa value of 0.69 suggests substantial level of agreement between predictions and actual labels. An F1 score of 0.86 also indicates a good balance between precision and recall.

3.3.3 RF Model and Fusion Results

The RF model determines the importance scores for multiple variables (Table 3.10). As observed in the case of Sentinel-2, rainfall did not have a significant correlation with surface water availability in the region, likewise here rainfall has a relatively lower significance in the analysis. This was because local rainfall does not really have a strong effect on flooding in Macquarie

Marshes, as these wetlands source most of their water from the upstream catchment, not local rainfall (Ndehedehe et al., 2021). As a result, rainfall was excluded from further considerations.

Table 3.10: Variable Importance in RF Analysis

Variables	**Score**
WI	0.51
NDVI	0.30
Sentinel VV Band	0.057
Landcover	0.049
Sentinel VH Band	0.037
PDEP	0.025
Slope	0.007
Cumulative Rain	0.0045

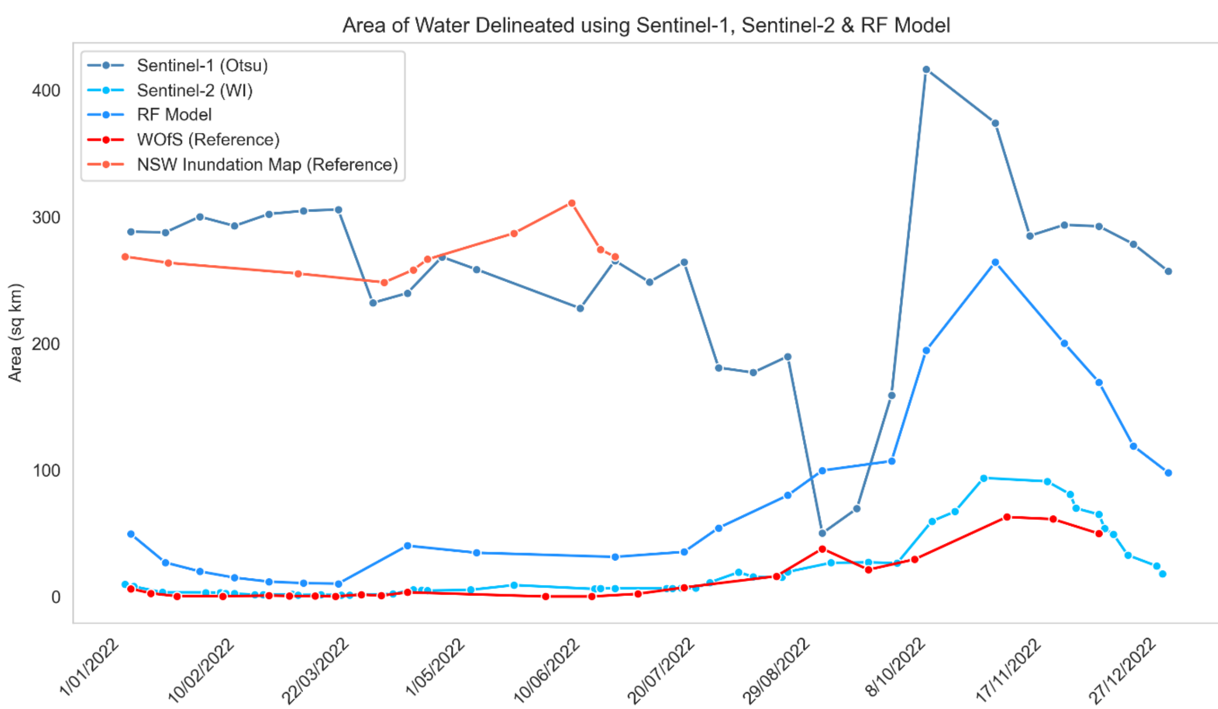

Figure 3.33: Area of Water Delineated using Sentinel-1, Sentinel-2 and RF Model

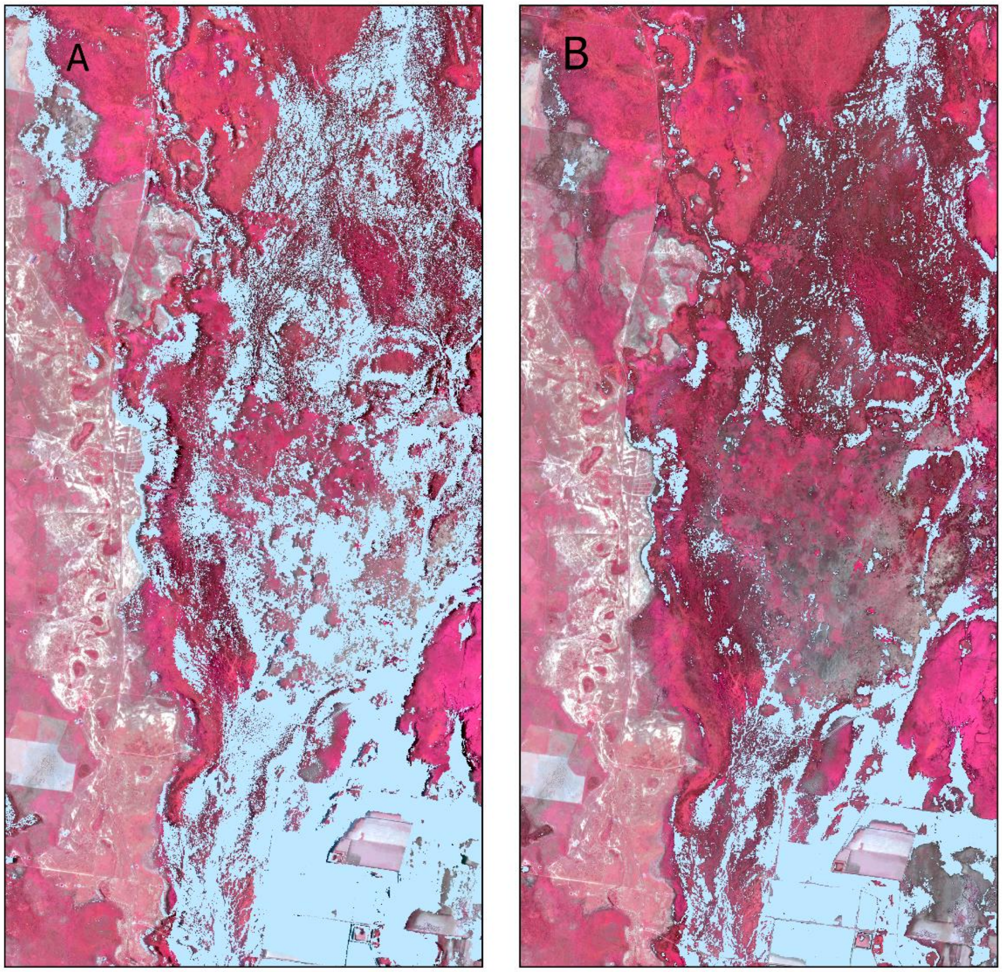

Figure 3.34: Figure A shows water delineated using RF while Figure B shows the water delineated using Water Index on Sentinel-2 acquired on 06/12/2022

As Figure 3.33 & Figure 3.34 demonstrates that the RF model tends to significantly increase the extent of observed water in the study area as compared to WI and WOfS. In order to improve the accuracy of RF model, the adjustments in the hyperparameters of the model could be made. By fine-tuning the hyperparameters, the model's performance could be optimised for accurate water predictions within the study area. However, a major challenge is the limited availability of ground truth data, which has made it difficult to assess the true accuracy of the RF model and make adjustments of hyperparameter. The Inundation Maps for NSW Inland Floodplain Wetlands 2021-2022 can be used as a verification data for the similar date. Figure 3.35 shows the PlanetScope image (A), Sentinel-1 (B), Sentinel-2 (C), the Inundation Maps for NSW Inland Floodplain Wetlands (D) were acquired of the same date (21/06/2022) whereas close by WOfS data was available for 29/06/2022. A comparison with the Inundation Maps for NSW Inland Floodplain Wetlands (Thomas et al., 2015) indicates that the model underestimates the inundated area. There is a mismatch between the satellite and the ground truth data and there is also a lack of a reliable benchmark data to evaluate the progress of the RF model.

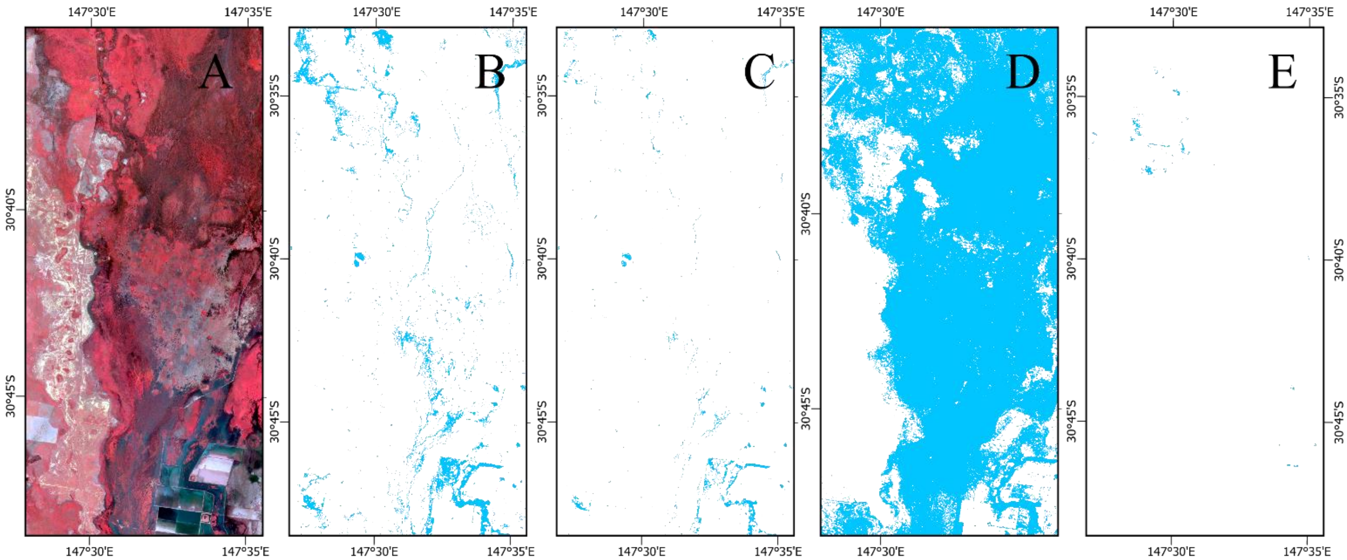

Figure 3.35: PlanetScope image acquired on 21/06/2022 (A), Water delineated using RF-21/06/2022 (B), WI-21/06/2022 (C), Inundation Maps for NSW Inland Floodplain Wetlands-21/06/2022 (D), WOfS-29/06/2022 (E)

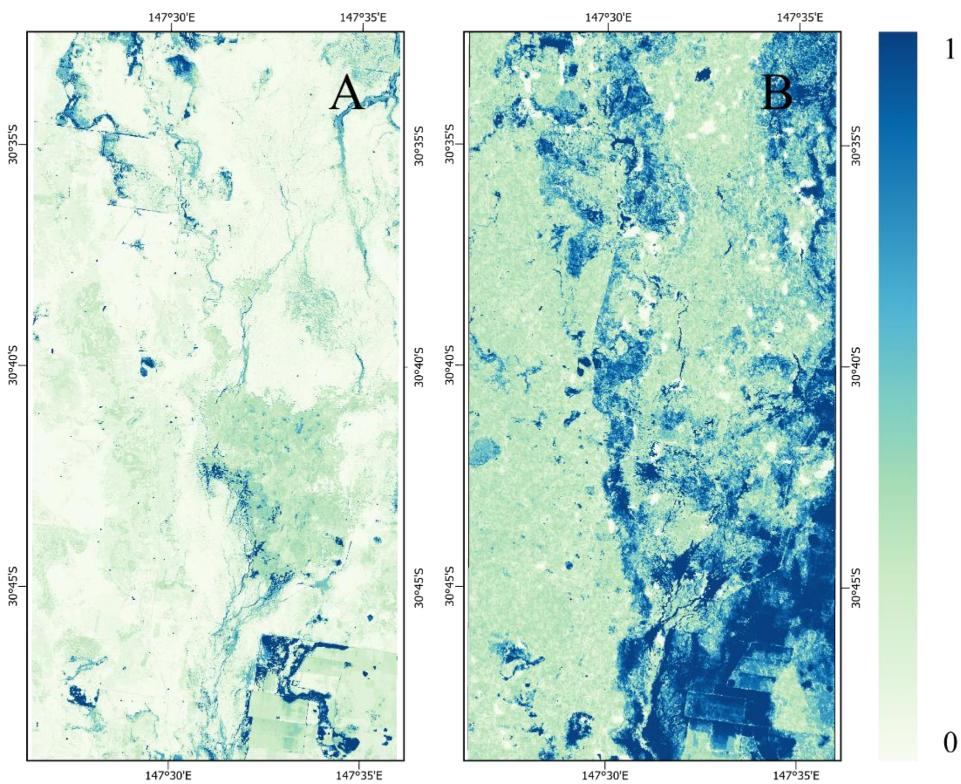

Figure 3.36: Figure showing comparison between the probability of water calculated using RF with the WOfS probability map.

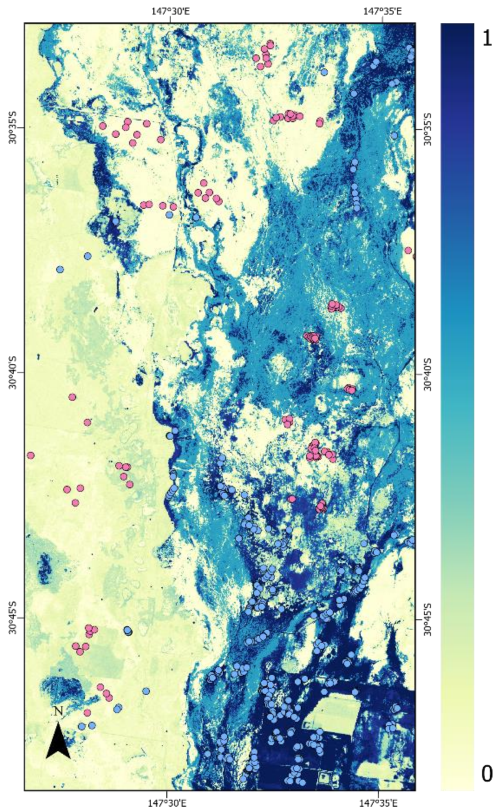

Figure 3.37: Probability of Water Occurrence using the RF Model (The stacked image was of 06/12/2022). Manually demarcated water and non-water points derived from PlanetScope data are also visible in the map

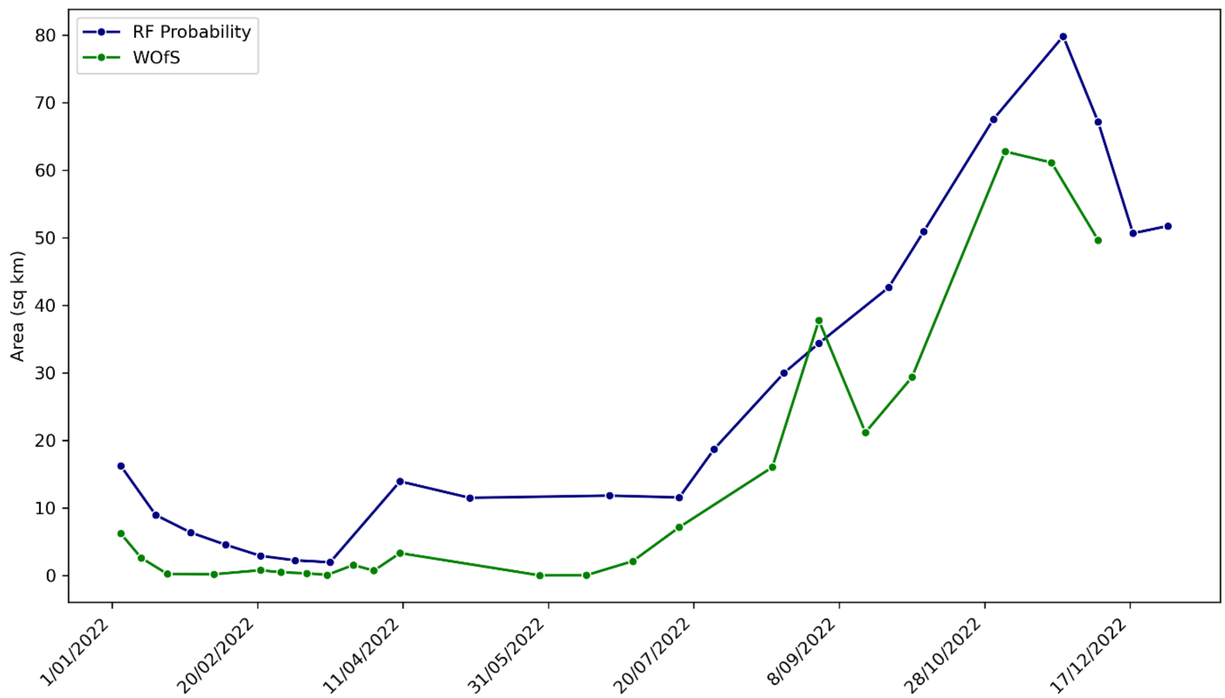

Figure 3.38: A comparative graph showing area calculated using probability maps (>80%) and WOfS

As is demonstrated by Figure 3.33, the RF model consistently overestimates the surface water extent in the AOI (if compared with the WI and WOfS), which may indicate a bias in the training data. Multiple factors can influence the RF model accuracy to make predictions, including quality and quantity of training data and hyperparameters of the model. In this study, around 1200 training points of water and non-water features were demarcated, which can be increased for more accurate results. The probability estimates of Figure 3.34 suggest that certain areas with overestimated predictions actually have a lower water occurrence probability (Figure 3.37). And another approach could be identification of areas with high water occurrence probability (like setting a threshold probability of > 80%) and finding the surface water extent of the areas for which the model is more confident. This may result in reducing the overestimation of water delineated area. As it can be seen in Figure 3.38, the area with high water occurrence probability is congruous to the area delineated using the WOfS.

3.3.3.1 Accuracy Assessment of RF Model

3.3.3.1.1 Confusion Matrix

The confusion matrix for the RF model was calculated, using the PlanetScope data as a validation dataset. Comparing the results of RF model with validation data provided a measure of how well RF Model performs in relation to ground truth data. The overall accuracy was calculated using the confusion matrix, that is, the ratio between correctly classified pixels and total pixels.

$$P_{\circ} = \frac{C_p}{n}$$

where P_o, C_p and n denote the overall accuracy, correctly classified pixels, and the total number of pixels respectively.

Table 3.11: Accuracy Assessment of RF Model

Commission Error	0.06
Omission Error	0.87
Overall Accuracy	0.90
Kappa	0.04
F1 Score	0.09

Considering the Kappa and F-1 score, Table 3.11 shows almost no agreement at all between the predicted water using RF model and the reference image. However, the overall accuracy indicates that the model achieved an accuracy of 90%, i.e., 90% of the points were correctly classified.

3.3.4 Estimation of Water Volume using RF Delineated Water

Figure 3.39 shows the water depth maps with an estimated volume in cubic meters for the corresponding dates.

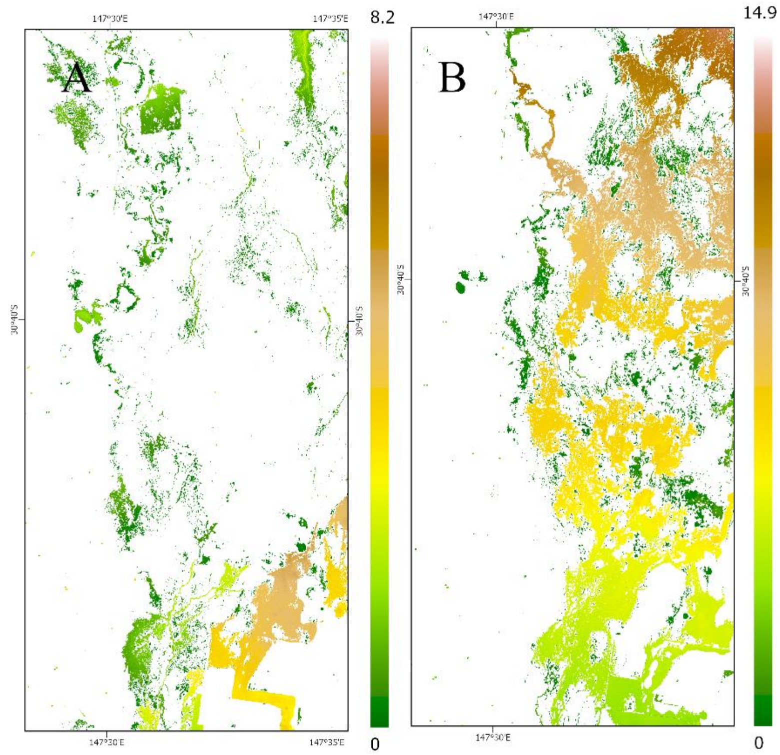

Figure 3.39: Water Depth Maps of Macquarie Marshes 04/01/2022 (A) & 30/12/2022 (B) with an estimated water volume of 52746450 m^3 and 97989725 m^3

Figure 3.40 demonstrates the inundated volume time series and portrays a temporal perspective on the water availability in the region. This also highlights the recurring pattern of changes in inundated volume that correspond to seasonal fluctuations and also somewhat matches with the gauge data (an increase in discharge value implies an increase in the water volume in the region and vice versa) shedding light on the hydrological behaviour, including the interplay between different flow rates and the broader seasonal trends influencing water levels.

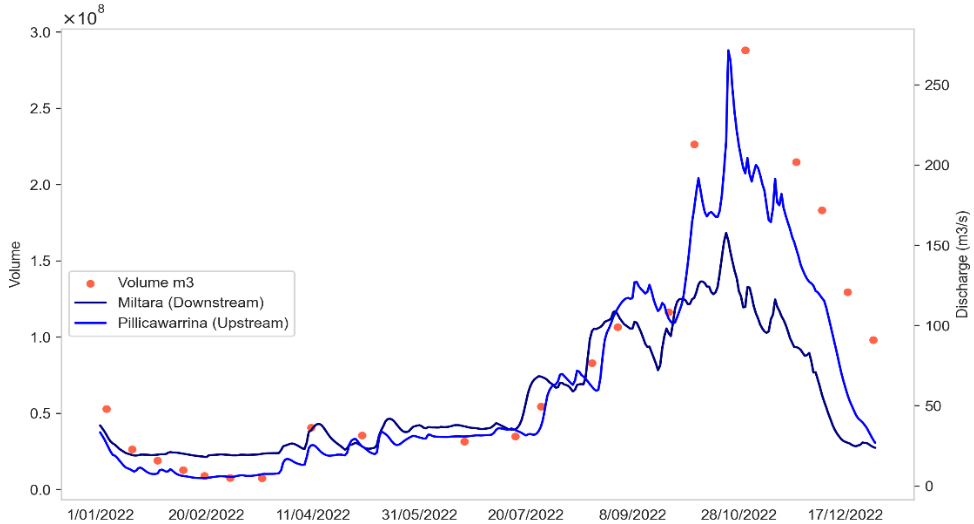

Figure 3.40: Time series of volume of water bodies delineated using RF and discharge data at the upstream and downstream gauges

Figure 3.41 shows the water balance in the wetlands at the very elementary level.

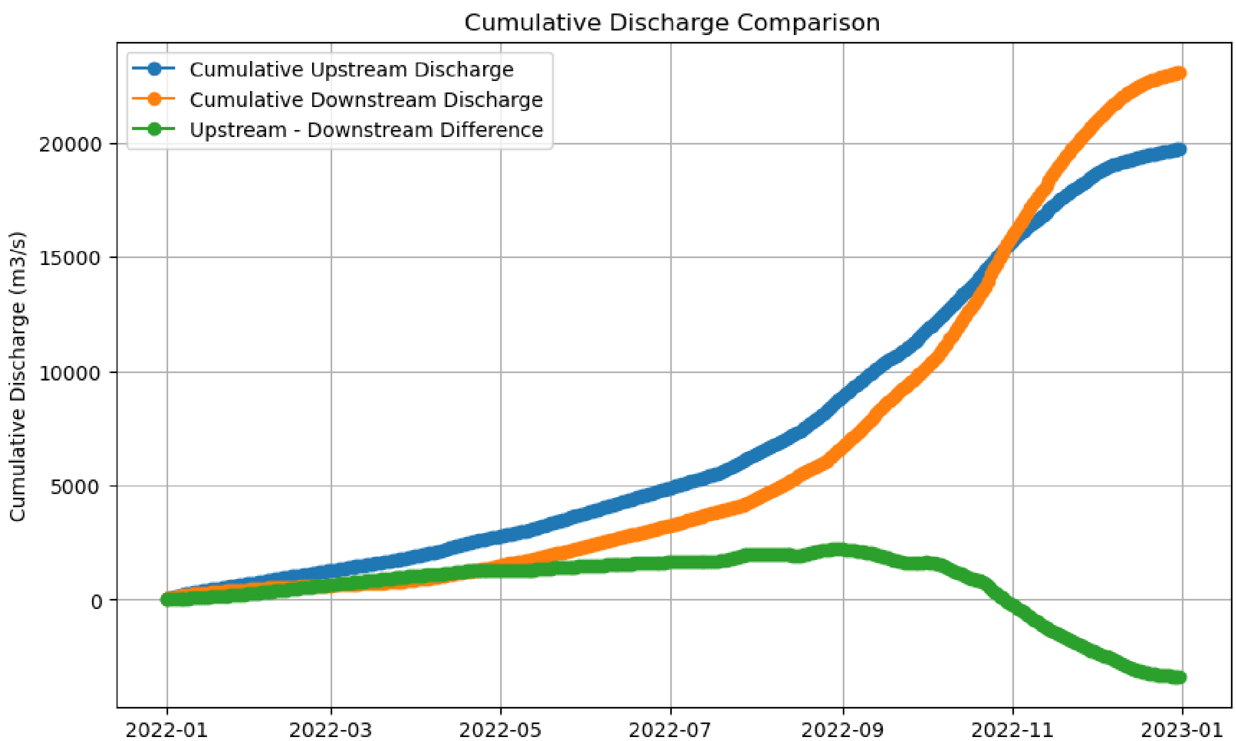

Figure 3.41: Cumulative discharge at the upstream and downstream and the difference between upstream and downstream cumulative discharge

The difference in upstream-downstream cumulative sum of river discharge is trending downwards (below zero since November), which indicates that the downstream flow is greater than the upstream flow, or in other words, it can be said that at the downstream, Macquarie River is experiencing a net outflow/ water loss compared to what is being contributed by upstream. For a more detailed water balance analysis in Macquarie Marshes, a broader range of factors and variables need to be considered including climatic variables, runoff, and evapotranspiration (Daly et al., 2019; Vervoort et al., 2014).

3.4 Discussion

3.4.1 General Findings

The Macquarie Marshes have experienced substantial changes over time, with recent La Niña periods playing a crucial role in providing the necessary water for the survival of the Macquarie Marshes, which has resulted in an ecological response. There are multiple challenges of surface water extent delineation with accuracy from dense time series of satellite imagery, including the varying duration of water features demanding a per-image classification (Vanderhoof et al., 2023). As there are both permanent and seasonal/ variably inundated water bodies in the region, this requires a classification per image. Image classification tends to produce results with more accuracy when it is based on the changes between multiple images (Chuvieco et al., 2019). Non-availability of properly gauged flow data is another challenge in the semi-arid wetland ecosystems (Kennard et al., 2010).Sentinel-1 and Sentinel-2 are regularly captured, making them suitable for monitoring and quantification of the variability of inundation patterns within the Macquarie Marshes. Sentinel-1 can see through clouds (Mayer et al., 2021) and rain at any time whether it’s day or night which give it a competitive edge over the Sentinel-2 and makes it exceptionally beneficial for floods monitoring (Luo et al., 2023). However, a drawback of Sentinel-1 images is their speckle noise that can obscure surface water identification. That’s why, the focus of many studies is on optical remote sensing sensors for water body extraction because of their capabilities at capturing fine details and textures. There is also recent trend of combining radar and optical sensors to complement the limited precision offered by optical and radar sensors individually to produce more reliable and accurate results (Saghafi et al., 2021).

The aim of this research study was to evaluate different methods of inundation mapping utilising optical and radar sensors on an individual level and also to synergise them to produce potentially accurate results across one year timeframe for the Macquarie Marshes. For Sentinel-1, Otsu thresholding was used, while different water indices were used using Sentinel-2. The idea was to have continuous time-series data collection because the Sentinel-1 can be available conveniently throughout the year without being affected by cloud and light rain (the C-band wavelength allows for convenient availability throughout the year without being affected by cloud cover and light rain, heavy rain can still pose challenges for this frequency) so it will fill up the gap in between the Sentinel-2 observations during the rainy season. In case of non-availability of optical-image data, adding the frequency of inundation in the timeseries using the Sentinel-1 can help analyse changes in the richness of the landscape in the wetlands during fluctuations in water levels. However, this idea did not give the desirable result due to the difference in the recording principle of radar and optical sensors, and a deviation was observed in the water extent delineated from Sentinel-1 and Sentinel-2. Water areas were possibly underestimated by the optical sensors as they receive signals from the bottom of a water body under clear water conditions and unable to delineate with accuracy in shallow water areas. On the other hand, Sentinel-1 tends to overestimate the water look-alike areas. Also, inaccurate water delineation in areas with dense partially inundated vegetation is a known limitation of both optical and radar-based water detection.

Overall, 28 scenes of Sentinel-1 and 47 scenes of Sentinel-2 were used to acquire the information about the inundation pattern in the area. The initial idea of this study was to produce a timeseries of water delineated using Sentinel-1 and Sentinel-2 but as it can be seen in Figure 3.42, the overestimation of Sentinel-1 and underestimation of Sentinel-2 could not produce a reliable timeseries data that can be interpolated for the whole year.

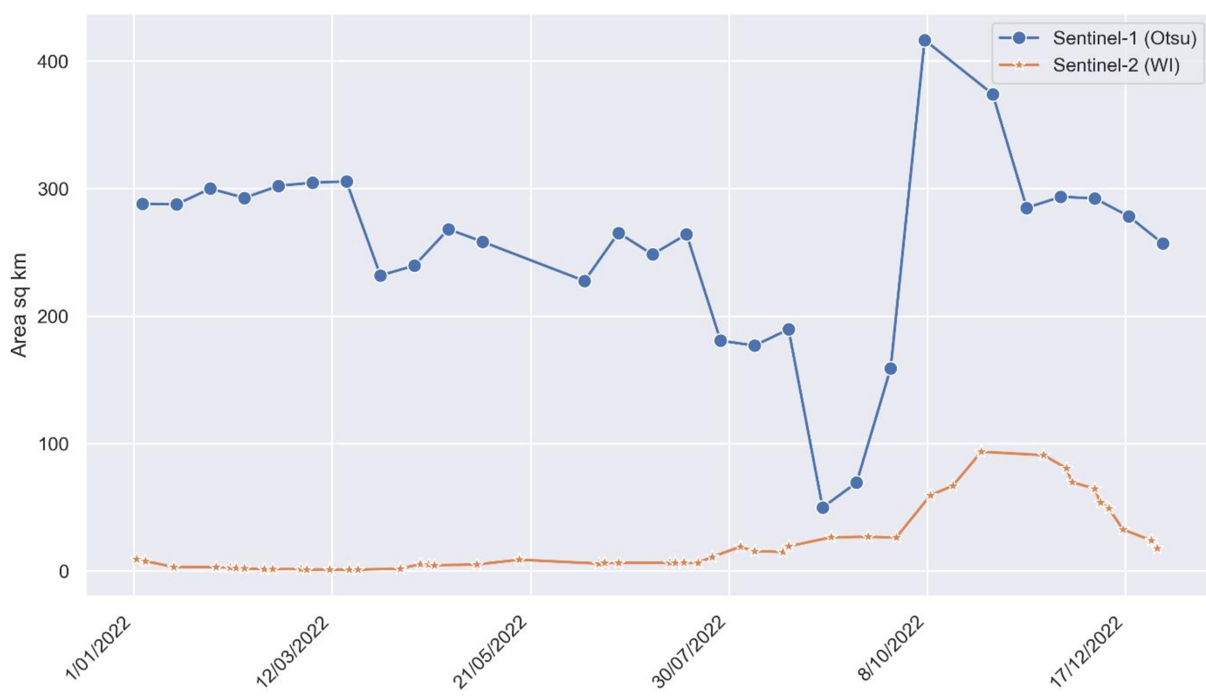

Figure 3.42: Figure showing discrepancy between area delineated using Sentinel-1and Sentinel-2 in sq km.

The Otsu thresholding algorithm has been applied to Sentinel-1 scenes to separate water from remaining land covers because it is regarded as the simplest yet efficient technique for surface water mapping (Tran et al., 2022). The analysis demonstrated that the Otsu threshold technique exhibit certain advantages in the surface water extraction of low-noise scenes (Yu et al., 2022), and despite the extraction of rough water range with the Otsu thresholding, the misclassification phenomena needs to be addressed.

The Otsu algorithm may not be the best choice for water delineation if the water and land regions have similar pixel intensities, or the presence of significant noise or other image artifacts causing it difficult to separate water and non-water areas. Extreme values in the data can influence the results' accuracy. The threshold determination can be disproportionately impacted by the outliers (extreme high or low values) in the image, potentially providing with inaccurate results. And in some case, a more manual approach of thresholding based on personal judgment or domain expertise may be more effective. In order, to evaluate the manual thresholding, all the Sentinel-1 scenes would have to be visually inspected (Di Baldassarre et al., 2011). As a result, the interpretation of Sentinel 1 images is qualitative rather than quantitative, and the incidence angle, polarisation and other environmental conditions can influence the visual appearance of water. And it is also important that manual thresholding cannot be used when dealing with a large number of images, because it would be tedious and time-consuming process, and this is not a practical solution for processing large volumes of images, when water occupies only a small fraction of the image and the distributions of water and background significantly overlap, and often do not exhibit a characteristic bimodal distribution (Cao et al., 2019).

The Otsu thresholding also did not explicitly consider spatial relationships within the image. It independently treats each pixel on the basis of their intensity value, disregarding the surrounding pixels, and in case of presence of noise or complex backgrounds like wetlands, potential errors can occur in accurate delineation of water. The SAR backscatter values for water bodies are typically lower than those for land, and Otsu is applied as image segmentation algorithm to delineate water. It is also essential to potentially consider ancillary data that may affect water detection accuracy, for example, the presence of vegetation, elevation/slope of the area and temporal variations in water levels. Considering this, the Otsu thresholding approach needs to be adjusted to account for vegetation. As Martone et al. (2014) observed the SAR backscatter inaccurately results in an overestimation of flood due to misclassification of sandy soil because of weak backscatter. However, in the case of emergent vegetation, the sandy soil had a drier multispectral signature (negative NDWI) as compared to water and was separated accurately using Sentinel-2 (Foroughnia et al., 2022). The misclassification of vegetation with water can be the reason for the overestimation of floods in non-water areas, especially when the SAR backscatter signal is weak. And in some regions, the misclassification of vegetation and sandy areas occur while using VV SAR backscatter data. This issue may be tackled with the application of supervised RF utilising different texture, intensity, phase, and temporal-based features, though even the RF encountered the overestimations of water class over sandy soils (Foroughnia et al., 2022).

Just as Otsu thresholding is typically used for mapping surface water, likewise spectral indices are regarded as a typical technique to map surface water because of their simplicity and efficiency.

MNDWI, AWEI and a relatively new index by Fisher- WI are some of the commonly used techniques to delineate surface water extent (Feyisa et al., 2014; Fisher et al., 2016; Xu, 2006). MNDWI, AWEI and WI use green, red, near infrared and shortwave infrared surface reflectance bands. Another significant highlight of this study is the experimentation with different thresholding values for the Water Indices. In general, the recommended thresholding value for MNDWI, AWEI and WI was 0 and the pixels with values greater than 0 are considered as water while the pixels with values less than 0 are considered as non-water. But in this study, instead of relying on the thresholds as recommended by the past research (Ticehurst et al., 2022) an optimal threshold was found for the respective indices. The thresholding values to delineate water bodies were found to be negative values, which was actually consistent with other studies as well (Kaplan & Avdan, 2017). The reason is that the threshold value depends on the particular environmental conditions of the study area, and in case of environmental noise, like shadow, forest, built-up areas, and clouds, it could be challenging to depend on a threshold that could have performed well in some other environmental conditions (Acharya et al., 2018). The subject selection of the thresholds can be done on the basis of the knowledge of the study area and ancillary data. The variation in the threshold value also depends on the subpixel water/non-water components' proportions, which is why they need an adjustment on the basis of the spectral signatures and non-water proportions (soil and vegetation) (Figure 3.43) (Ji et al., 2009). The negative values of the threshold in this study are consistent with the spectral response of the water (Pena-Regueiro et al., 2020), because Macquarie Marshes are complex episodic wetlands (Wilson et al., 2008).

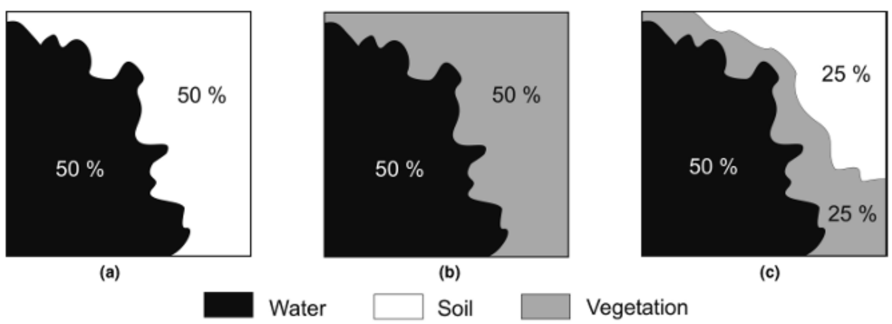

Figure 3.43: Hypothetical examples of mixed water pixels comprising 50 percent water and 50 percent non-water components. The square represents a single pixel in an image, and the water, soil, and vegetation are the subpixel components: (a) Water fraction 50%; soil fraction 50%, (b) Water fraction 50%; vegetation fraction 50%, and (c) Water fraction 50%; soil fraction 25%; vegetation fraction 25% (Ji et al., 2009)

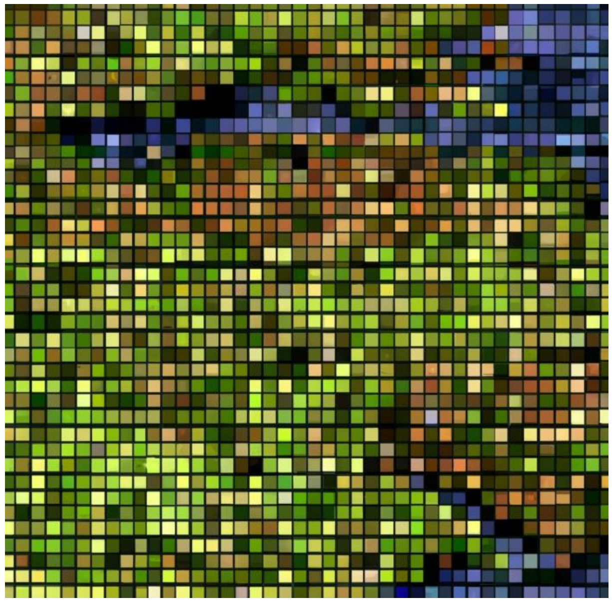

Figure 3.44: An example of mixed land pixels

To increase the accuracy of water delineation, high accuracy DEM and ancillary data from different sources can aid image segmentation and classification (Andrew et al., 2023). However, a drawback is that this data is not available for the Marshes and there are potential errors and biasness in manual intervention. This study also analysed the relationship between the patterns and associations observed between ancillary data, such as slope, NDVI, PDEP, and water presence with an aim to create better estimates for areas where water presence information is not available or where there are more chances of false negatives. In contrast the probability of depression and slope were not useful. However, congruous to other studies, negative values of NDVI correspond to water indirectly indicating the presence of water in the wetlands. Sims and Thoms (2002) used NDVI maps to study relationship between vegetation growth and flood frequency and found lesser flooding frequency in the areas with vigorous vegetation and high NDVI values (Albertini et al., 2022).

A disadvantage of using ancillary data is the time needed to produce near real time maps during the flooding events (Andrew et al., 2023), and machine learning techniques can be used to address this knowledge gap due to the increasingly availability of large volume of data (Sun & Scanlon, 2019). With the emergence of the deep learning techniques, there is a potential to improve the automation of the water delineation process (Bentivoglio et al., 2022). Training a predictive model using a dataset consisting of known water presence observations (single or a combination of Water Indices), radar datasets and corresponding NDVI and PDEP values can help establishing a relationship between these variables. Such a model can be used to identify areas with a higher likelihood of water presence, which is the approach taken for the WOfS product (Mueller et al., 2016). The inclusion of water indices, such as the Water Index (WI) or other relevant indices, in the predictive model allows for more accurate predictions of water presence. These indices serve as indicators of water bodies and can provide additional information to enhance the model's performance. In addition, as one of the challenges in Macquarie Marshes is visually detecting water beneath dense vegetation cover, the inclusion of NDVI enables capturing the relationship between water presence and vegetation dynamics.

Fused products might therefore exhibit spatially variable uncertainties in water extent mapping. The fusion of Sentinel-1 and Sentinel-2 images was explored as a method for accurately delineating the extent of water bodies (Saghafi et al., 2021). The combination of optical and radar sensors can complement each other, and both were used because they fix each other's defects, such as cloudy weather, low light conditions, and the distinction between textures. Initially Otsu thresholding technique was applied to the Sentinel-1 imagery. However, it was observed that this approach tended to overestimate the water body extent, resulting in less precise classifications. To overcome this limitation and improve the accuracy of the water body classification, a fusion technique was employed. The Sentinel-1 and Sentinel-2 images were combined at the pixel level. This fusion process enabled the utilization of complementary information present in both datasets, leading to a more robust and accurate classification of water bodies. By merging the two datasets, the RF classification could leverage the unique advantages offered by each satellite. Sentinel-1, a radar satellite, provides valuable information about backscattering properties and surface roughness, which can be indicative of water bodies. On the other hand, Sentinel-2, an optical satellite, captures information about spectral reflectance, enabling the identification of water based on its distinctive spectral characteristics. This fusion provides a valuable solution when cloud cover hampers the availability of information in Sentinel-2 images, and the radar data can effectively fill in the gaps caused by cloud cover.

3.4.2 Major limitations and Assumptions

A drawback/limitation of the proposed RF model is that the availability of close by optical data is necessary in conjunction with radar dataset. The RF model is based on pixel-based fusion of Sentinel-1 and Sentinel-2 based indices, but despite the increased revisit time of Sentinel-2, incomplete or missing satellite images due to cloud cover or other factors can lead to gaps in the dataset. If Sentinel-2 data is unavailable for certain time-period, solely relying on radar data for gap filling is not sufficient/possible. To address this limitation, the incorporation of optical data from other Earth Observation (EO) systems, such as Landsat-8 or Sentinel-3, can be done to fill the gaps in the Sentinel-2 time series (Caballero et al., 2023). This approach involves combining optical data from these systems with the available radar data to create a more complete and consistent time series dataset.

One of the limitations was potential inaccuracies of the surface water extent delineation while applying Otsu thresholding using Sentinel-1, which can possibly be due to the presence of speckle noise. Especially in the context of water delineation, speckle noise can introduce fluctuations in pixel intensities within Sentinel-1 image leading to variability in brightness and darkness, and bright speckle pixels can be misclassified as water. The granular texture created by speckle noise can also be misinterpreted as water. Though lee filter was applied to the Sentinel-1 images for more accurate results but there seems to be still some false positives.

Another limitation of the study was obtaining truly “accurate” observed data as it was quite challenging and was almost impossible, particularly when considering extended timeframes within wetlands like the Macquarie Marshes. The lack of a reliable reference data causes validation of the results challenging (Fichtner et al., 2023). As a validation dataset, there is Water Observations from Space (WOfS) dataset, but water estimation of WOfS also underestimates the water surface area. On the other hand, the NSW inundation map suggests potential overestimation, potentially arising from the merging of NDVI and the Water Index. A lack of definitive benchmarks prevents a strong conclusion whether the estimates lean towards underestimation or overestimation. Despite that data can be observed and analysed from diverse sources, integration of these observations and insights into effective decision-making poses a complex challenge. Defining an acceptable level of uncertainty also poses its own challenge, and even if defined, there is also a lack of consensus on what level of uncertainty is acceptable for specific contexts. Although satellite data offers more detail and fine-tuned data with every passing day, the discrepancies between satellite observations and ground truth data cannot be fully resolved. This will require further modelling and a refined quantification process (Vervoort et al., 2022).

3.4.3 Future Work

Future work can include developing a model that would incorporate additional indices from Sentinel-1, such as the Surface Water Index (SWI), the Gray Level Co-occurrence Matrix (GLCM) derived from radar datasets to capture textural information related to water bodies within wetland areas alongside the soil moisture index, Land Surface Temperature, and monthly lagged rainfall to capture the temporal variations. GLCM-mean matrix features have demonstrated to improve the accuracy of soil moisture retrieval along with other features (Attarzadeh et al., 2018), GLCM textural features can suppress speckle noise in SAR imagery (Yu et al., 2022). EVI and NDVI index differentiate the vegetation and the agricultural fields from other land cover (Billah et al., 2023) and though this study utilise NDVI but the inclusion of EVI may increase the result’s accuracy. The integration of these parameter will result in a more detailed and comprehensive analysis of wetland dynamics. Furthermore, the future aspiration is to propose a model that can be implemented beyond the specific wetland under study, i.e., a scalable and adaptable model that can be applied to other wetlands, enabling a broader understanding of wetland ecosystems and their response to environmental factors. The model will be applied for predicting and quantifying wetland function at large and extensive scales using remote sensing and other geospatial data. Future work could also include looking for backscatter differences through time as an increase in backscatter in flooded vegetation can be expected compared to dry vegetation, and a reduction in backscatter in open water compared to dry land.

3.4.4 Conclusions

The major findings of this study are summarised as follows:

- The Fisher's Water Index had a higher overall accuracy and lower omission error compared to MNDWI and AWEI for the water detection with accuracy.
- Macquarie Marshes are characterised by different vegetation types including swamps, and using a negative threshold value can help to distinguish water pixels from vegetation pixels.
- There are multiple water indices to derive surface water extent maps, but the key challenge in the utilisation of the spectral water index technique, especially in the context of wetlands, is identification of an optimal or suitable thresholding value that can differentiate non-water from water features adequately and can possibly identify the inundated vegetated cover.
- NDVI, being a vegetation index, is not specifically designed to detect water but it can differentiate between water and vegetation, as water has a low NDVI value close to zero or negative. And in case of time series analysis, monitoring NDVI over time enables the tracking of seasonal and long-term changes in wetland vegetation. During periods of vegetation growth, NDVI values typically increase, while they decrease when vegetation is stressed or dormant, or in case of flooding, the NDVI values also tend to be lowered because of a reduction in the NIR reflectance.
- As the literature suggests that rainfall is closely related to the potential for flooding but cannot always be a direct indicator of flooding only; this study also concludes that rainfall is not a significant predictor of water availability in the region.
- Macquarie Marshes has a relatively flat topography; therefore, slope did not prove to be a primary driver of the water availability in the region, which is an expected outcome in an allogenic system like the Macquarie Marshes.

4 Conclusion & Future Implications

Increasing water scarcity, climatic variability, and the interdependence of wetland ecosystems on flood patterns require better understanding of wetlands and floodplains and quantification of water in the wetlands (Schweizer et al., 2022). These ecosystems are often underappreciated but serve a crucial role in the world of ecology. Despite accounting for only 6% of the Earth's land surface, they host approximately 40% plant and animal species (*Why Healthy Wetlands Are Vital to Protecting Endangered Species*, 2023). The rich biodiversity and gradual flow characteristics of wetlands also work together harmoniously to facilitate highly effective natural filtration processes. However, many wetlands are currently under threat due to climatic changes and human intervention, as evidenced by the decline of important wetland ecosystems like the Macquarie Marshes. The mapping endeavour holds crucial importance in assessing ecological resilience, understanding the consequences of developmental activities, and exploring possibilities for restoration through the implementation of environmental flow strategies (Thomas et al., 2015). The Macquarie Marshes and its natural resources are also influenced by long-term climate variations, and slowly evolve over time due to past wet and dry periods, and hence underscore an insight into the availability, distribution, and changes in water resources within the region.

There are multiple indices and processes related to Sentinel-1 and Sentinel- 2 to delineate surface water. This thesis aimed to test different indices to accurately map surface water extent dynamics of Macquarie Marshes using a series of globally applicable algorithms based on Sentinel-1 and Sentinel-2 imagery across a whole year in a complex semi-arid wetland. Initially, this study compares the performance of multiple water indices, including Automated Water Extraction Index (AWEI), MNDWI, and Water Index, and found that Water Index and AWEI demonstrated better accuracy in detecting surface water under different environmental conditions as compared to MNDWI. One limitation that complicated the analysis was mixed pixels (Figure 3.44) or a combination of water, vegetation, and other land cover types, and the standard recommended thresholds for the water indices failed to accurately capture the spectral characteristics of these mixed pixels, leading to underestimation or misclassification of water. High spectral variability also made it challenging to define a single threshold that can effectively separate water from other land cover types, therefore, for future work, there is a need to the development of automated methods for threshold selection that can also reduce the need for manual threshold selection.

The proposed Random Forest (RF) model in this study relied on the training data based on a total of around 1200 points manually demarcated as water and non-water pixels using PlanetScope imagery. The use of a manual approach leads to a dataset that has its own biasedness. The evaluation results compared with the original PlanetScope image indicated that an inundation map can be generated with acceptable accuracy. The findings of this research have multiple downstream applications, including surface water mapping and analysis of water changes influenced by environmental dynamics, like vegetation cover and elevation profiles. As the

Macquarie Marshes is an inland wetland, therefore, local rainfall is not the main driver of flooding and that's why, any impact of rainfall on the surface water extent could not be found. The finding is that in general Sentinel-2 derived indices underestimate the area of inundation and Sentinel-1 overestimates the area of inundation, but a fusion of both sensors can provide with more accurate results.

The work emphasises the essential role of satellite remote sensing technology in wetlands and flood mapping, especially given the capability of RS techniques over in-situ measurements to monitor large geographical regions. With the reporting of temporal nature of surface water in the Macquarie Marshes over a year alongside other descriptors- water depth and water volume, this study provided an analysis of inundation dynamics at the wetlands. The main objectives of the research study have been predominantly achieved; however, the need for additional global case studies remains to substantiate the viability of the proposed RF model and to verify the accuracy of the results (Clement, 2020). In the future, the suggested model could be applied to other wetland areas globally to assess the scalability of the model and its limitations (Manakos et al., 2020). Alternative post-processing techniques could be assessed in future for the elimination of small objects mistakenly denoted as inundated. For future work, the misclassification, underestimation, and overestimation of water in areas with dense vegetation cover and turbidity may be improved by utilising higher spatial and spectral resolutions of MSI imagery, for instance, the PlanetScope with 3m resolution. The testing and verification of the model with further improvements (as proposed in the last chapter) at more areas globally could develop an operational tool and can support finer scale data-driven decisions and for validating hydrodynamic models. In future, the HEC-RAS 2D model could be used to determine the Macquarie River discharge, its route and flood extent and the depth of especially the river and neighbouring areas that might have been affected by a flood episode. The accuracy of the satellite derived flood volumes can be assessed by comparing results with HEC-RAS simulations. Though the satellite-driven prediction is an efficient solution for the continuous monitoring of watering events; the HEC-RAS simulations can provide with the hydrological parameters that can assist in estimating the accuracy of results. This is imperative, as it was challenging to accurately discern the actual water flow within the Macquarie Marshes, even during peak periods. Future research could also involve studying changes in backscatter over time, particularly in relation to different types of land cover, with the anticipation of observing specific backscatter patterns associated with flooded vegetation and open water.

5 References

2021-2022 inundation maps. (2023). https://datasets.seed.nsw.gov.au/dataset/219182a0-02a2-4916-b21c-2e330e65f8de/resource/aca9b0ba-4d4e-4b70-b917-83603abb0102/download/2021-2022_inundation_maps.zip

Abazaj, F. (2020). Sentinel-2 Imagery for mapping and monitoring flooding in Buna River area. *Journal of International Environmental Application and Science*, *15*(2), 48-53.

Acharya, T. D., Subedi, A., & Lee, D. H. (2018). Evaluation of water indices for surface water extraction in a Landsat 8 scene of Nepal. *Sensors*, *18*(8), 2580.

Acreman, M., & Holden, J. (2013). How wetlands affect floods. *Wetlands*, *33*, 773-786.

Adeli, S., Salehi, B., Mahdianpari, M., Quackenbush, L. J., & Chapman, B. (2021). Moving Toward L-Band NASA-ISRO SAR Mission (NISAR) Dense Time Series: Multipolarization Object-Based Classification of Wetlands Using Two Machine Learning Algorithms. *Earth and Space Science*, *8*(11), e2021EA001742.

Adhikari, S. (2019). A Comparison of Water Indices and Binary Thresholding Techniques for Water Surface Delineation for St. Croix Watershed Area. *Yearbook of the Association of Pacific Coast Geographers*, *81*, 182-204.

Al-Nasrawi, A. K., Fuentes, I., & Al-Shammari, D. (2021). Changes in Mesopotamian wetlands: investigations using diverse remote sensing datasets. *Wetlands*, *41*, 1-17.

Albertini, C., Gioia, A., Iacobellis, V., & Manfreda, S. (2022). Detection of surface water and floods with multispectral satellites. *Remote Sensing*, *14*(23), 6005.

Andrew, O., Apan, A., Paudyal, D. R., & Perera, K. (2023). Convolutional Neural Network-Based Deep Learning Approach for Automatic Flood Mapping Using NovaSAR-1 and Sentinel-1 Data. *ISPRS International Journal of Geo-Information*, *12*(5), 194.

Area, W. R. M. (2018). *Flood Inundation Mapping Science*. https://www.usgs.gov/mission-areas/water-resources/science/flood-inundation-mapping-science

Attarzadeh, R., Amini, J., Notarnicola, C., & Greifeneder, F. (2018). Synergetic use of Sentinel-1 and Sentinel-2 data for soil moisture mapping at plot scale. *Remote Sensing*, *10*(8), 1285.

Ayalew, L., & Yamagishi, H. (2005). The application of GIS-based logistic regression for landslide susceptibility mapping in the Kakuda-Yahiko Mountains, Central Japan. *Geomorphology*, *65*(1-2), 15-31.

Bayanudin, A. A., & Jatmiko, R. H. (2016). Orthorectification of Sentinel-1 SAR (synthetic aperture radar) data in Some parts of south-eastern Sulawesi using Sentinel-1 toolbox. IOP Conference Series: Earth and Environmental Science,

Bentivoglio, R., Isufi, E., Jonkman, S. N., & Taormina, R. (2022). Deep learning methods for flood mapping: a review of existing applications and future research directions. *Hydrology and Earth System Sciences*, *26*(16), 4345-4378.

Bijeesh, T., & Narasimhamurthy, K. (2020). Surface water detection and delineation using remote sensing images: A review of methods and algorithms. *Sustainable Water Resources Management*, *6*, 1-23.

Billah, M., Islam, A. S., Mamoon, W. B., & Rahman, M. R. (2023). Random forest classifications for landuse mapping to assess rapid flood damage using Sentinel-1 and Sentinel-2 data. *Remote Sensing Applications: Society and Environment*, *30*, 100947.

Bioresita, F., Puissant, A., Stumpf, A., & Malet, J.-P. (2019). Fusion of Sentinel-1 and Sentinel-2 image time series for permanent and temporary surface water mapping. *International Journal of Remote Sensing*, *40*(23), 9026-9049.

Bolanos, S., Stiff, D., Brisco, B., & Pietroniro, A. (2016). Operational surface water detection and monitoring using Radarsat 2. *Remote Sensing*, *8*(4), 285.

Bond, N. R., Lake, P. S., & Arthington, A. H. (2008). The impacts of drought on freshwater ecosystems: an Australian perspective. *Hydrobiologia*, *600*, 3-16.

Bowen, S. M. (2019). *Quantifying the water needs of flood-dependent plant communities in the Macquarie Marshes, south-eastern Australia*

Brinkhoff, J., Backhouse, G., Saunders, M. E., Bower, D. S., & Hunter, J. T. (2022). Remote sensing to characterize inundation and vegetation dynamics of upland lagoons. *Ecosphere*, *13*(1), e3906.

Brunner, M. I., Slater, L., Tallaksen, L. M., & Clark, M. (2021). Challenges in modeling and predicting floods and droughts: A review. *Wiley Interdisciplinary Reviews: Water*, *8*(3), e1520.

Buma, W. G., Lee, S.-I., & Seo, J. Y. (2018). Recent surface water extent of Lake Chad from multispectral sensors and GRACE. *Sensors*, *18*(7), 2082.

Caballero, G., Pezzola, A., Winschel, C., Sanchez Angonova, P., Casella, A., Orden, L., Salinero-Delgado, M., Reyes-Muñoz, P., Berger, K., & Delegido, J. (2023). Synergy of Sentinel-1 and Sentinel-2 Time Series for Cloud-Free Vegetation Water Content Mapping with Multi-Output Gaussian Processes. *Remote Sensing*, *15*(7), 1822.

Caballero, I., Ruiz, J., & Navarro, G. (2019). Sentinel-2 satellites provide near-real time evaluation of catastrophic floods in the west mediterranean. *Water*, *11*(12), 2499.

Cai, Y., Li, X., Zhang, M., & Lin, H. (2020). Mapping wetland using the object-based stacked generalization method based on multi-temporal optical and SAR data. *International Journal of Applied Earth Observation and Geoinformation*, *92*, 102164.

Cao, H., Zhang, H., Wang, C., & Zhang, B. (2019). Operational flood detection using Sentinel-1 SAR data over large areas. *Water*, *11*(4), 786.

Capon SJ, P. G., Turschwell M, Leigh C, Kennard M, Sheldon F (2018). *Technical review of the environmental outcomes associated with environmental watering of the Macquarie Marshes Ramsar Site 2009–2017*. Australian Rivers Institute, Griffith University,. http://www.environment.gov.au/water/topics/wetlands/database/pubs/technical-review-environmental-outcomes-macquarie-marshes-2009-2017.pdf

Casanova, M. T. (2007). The effect of grazing on freshwater wetlands in Australia. *A review of literature with particular emphasis on the Macquarie Marshes and Gwydir Wetlands. Charophyte Services, Lake Bolac, Victoria*.

CDP. (2022). *2022 Australian Flooding*. Retrieved 09/01/2023 from https://disasterphilanthropy.org/disasters/2022-australian-flooding/

Chen, J., Chen, S., Fu, R., Li, D., Jiang, H., Wang, C., Peng, Y., Jia, K., & Hicks, B. J. (2022). Remote sensing big data for water environment monitoring: current status, challenges, and future prospects. *Earth's Future*, *10*(2), e2021EF002289.

Chen, Y., Colloff, M. J., Lukasiewicz, A., & Pittock, J. (2020). A trickle, not a flood: environmental watering in the Murray–Darling Basin, Australia. *Marine and Freshwater Research*, *72*(5), 601-619.

Chen, Y., Wang, B., Pollino, C., & Merrin, L. (2012). Spatial modelling of potential soil water retention under floodplain inundation using remote sensing and GIS.

Chen, Z., & Zhao, S. (2022). Automatic monitoring of surface water dynamics using Sentinel-1 and Sentinel-2 data with Google Earth Engine. *International Journal of Applied Earth Observation and Geoinformation*, *113*, 103010.

Chuvieco, E., Mouillot, F., Van der Werf, G. R., San Miguel, J., Tanase, M., Koutsias, N., García, M., Yebra, M., Padilla, M., & Gitas, I. (2019). Historical background and current developments for mapping burned area from satellite Earth observation. *Remote Sensing of Environment*, *225*, 45-64.

Clement, M. A. (2020). *Flood Extent and Volume Estimation using Multi-Temporal Synthetic Aperture Radar* Newcastle University].

Comparison of Landsat 7 and 8 bands with Sentinel-2. (2015). Earth Resources Observation and Science (EROS) Center https://www.usgs.gov/media/images/comparison-landsat-7-and-8-bands-sentinel-2

Conradsen, K., Nielsen, A. A., & Skriver, H. (2016). Determining the points of change in time series of polarimetric SAR data. *IEEE transactions on geoscience and remote sensing*, *54*(5), 3007-3024.

Crist, E. P. (1985). A TM tasseled cap equivalent transformation for reflectance factor data. *Remote Sensing of Environment*, *17*(3), 301-306.

Daly, E., Calabrese, S., Yin, J., & Porporato, A. (2019). Hydrological spaces of long-term catchment water balance. *Water Resources Research*, *55*(12), 10747-10764.

Danaher, T., & Collett, L. (2006). Development, optimisation and multi-temporal application of a simple Landsat based water index. Proceeding of the 13th Australasian Remote Sensing and Photogrammetry Conference, Canberra, ACT, Australia,

De La Cruz, R., Olfindo Jr, N., Felicen, M., Borlongan, N., Difuntorum, J., & Marciano Jr, J. (2020). Near-realtime flood detection from multi-temporal sentinel radar images using artificial intelligence. *The International Archives of the Photogrammetry, Remote Sensing and Spatial Information Sciences*, *43*, 1663-1670.

De Lavenne, A., Andréassian, V., Thirel, G., Ramos, M. H., & Perrin, C. (2019). A regularization approach to improve the sequential calibration of a semidistributed hydrological model. *Water Resources Research*, *55*(11), 8821-8839.

de Liz, M. S. M., & Ribas, R. P. (2022). Flood extent delineation using Sentinel-1 data as information source: systematic review of processing methods. *Revista Brasileira de Geografia Física*, *15*(06), 3047-3076.

Di Baldassarre, G., Schumann, G., Brandimarte, L., & Bates, P. (2011). Timely low resolution SAR imagery to support floodplain modelling: a case study review. *Surveys in geophysics*, *32*, 255-269.

Doña, C., Morant, D., Picazo, A., Rochera, C., Sánchez, J. M., & Camacho, A. (2021). Estimation of Water Coverage in Permanent and Temporary Shallow Lakes and Wetlands by Combining Remote Sensing Techniques and Genetic Programming: Application to the Mediterranean Basin of the Iberian Peninsula. *Remote Sensing*, *13*(4), 652.

Dorji, P., & Fearns, P. (2017). Impact of the spatial resolution of satellite remote sensing sensors in the quantification of total suspended sediment concentration: A case study in turbid waters of Northern Western Australia. *PloS one*, *12*(4), e0175042.

Dronova, I. (2015). Object-based image analysis in wetland research: A review. *Remote Sensing*, *7*(5), 6380-6413.

Du, Y., Zhang, Y., Ling, F., Wang, Q., Li, W., & Li, X. (2016). Water bodies' mapping from Sentinel-2 imagery with modified normalized difference water index at 10-m spatial resolution produced by sharpening the SWIR band. *Remote Sensing*, *8*(4), 354.

Dutta, D., Vaze, J., Karim, F., Kim, S., Mateo, C., Ticehurst, C., Teng, J., Marvanek, S., Gallant, J., & Austin, J. (2016). Floodplain inundation mapping and modelling in the northern regions, the Murray Darling Basin. *Land and Water; CSIRO: Canberra, Australia*.

Ebaid, H. M., & Aziz, M. (2017). Integrating radar altimeters and optical imagery data for estimating water volume variations in lakes and reservoirs (case study: Lake Nasser). *Journal of Geographic Information System*, *9*(6), 648-662.

Elkhrachy, I., Pham, Q. B., Costache, R., Mohajane, M., Rahman, K. U., Shahabi, H., Linh, N. T. T., & Anh, D. T. (2021). Sentinel-1 remote sensing data and Hydrologic Engineering Centres River Analysis System two-dimensional integration for flash flood detection and modelling in New Cairo City, Egypt. *Journal of Flood Risk Management*, *14*(2), e12692.

Falconer, R. (2023). *Australian official: Climate change making historic flooding "less natural"*. https://www.axios.com/2023/01/09/australia-floods-climate-change-link

Feyisa, G. L., Meilby, H., Fensholt, R., & Proud, S. R. (2014). Automated Water Extraction Index: A new technique for surface water mapping using Landsat imagery. *Remote Sensing of Environment*, *140*, 23-35.

Fichtner, F., Mandery, N., Wieland, M., Groth, S., Martinis, S., & Riedlinger, T. (2023). Time-series analysis of Sentinel-1/2 data for flood detection using a discrete global grid system and seasonal decomposition. *International Journal of Applied Earth Observation and Geoinformation*, *119*, 103329.

Fisher, A., Flood, N., & Danaher, T. (2016). Comparing Landsat water index methods for automated water classification in eastern Australia. *Remote Sensing of Environment*, *175*, 167-182.

Flood, N. (2017). Comparing Sentinel-2A and Landsat 7 and 8 using surface reflectance over Australia. *Remote Sensing*, *9*(7), 659.

Foroughnia, F., Alfieri, S. M., Menenti, M., & Lindenbergh, R. (2022). Evaluation of SAR and Optical Data for Flood Delineation Using Supervised and Unsupervised Classification. *Remote Sensing*, *14*(15), 3718.

Fraccaro, P., Stoyanov, N., Gaffoor, Z., La Rosa, L. E. C., Singh, J., Ishikawa, T., Edwards, B., Jones, A., & Weldermariam, K. (2022). Deploying an Artificial Intelligence Application to Detect Flood from Sentinel 1 Data. Proceedings of the AAAI Conference on Artificial Intelligence,

Frappart, F., Minh, K. D., L'Hermitte, J., Cazenave, A., Ramillien, G., Le Toan, T., & Mognard-Campbell, N. (2006). Water volume change in the lower Mekong from satellite altimetry and imagery data. *Geophysical Journal International*, *167*(2), 570-584.

Fuentes, I., Padarian, J., Van Ogtrop, F., & Vervoort, R. W. (2019). Spatiotemporal evaluation of inundated areas using MODIS imagery at a catchment scale. *Journal of hydrology*, *573*, 952-963.

Gargiulo, M., Dell'Aglio, D. A., Iodice, A., Riccio, D., & Ruello, G. (2020). Integration of Sentinel-1 and Sentinel-2 data for land cover mapping using W-Net. *Sensors*, *20*(10), 2969.

Gašparović, M., & Klobučar, D. (2021). Mapping floods in lowland forest using sentinel-1 and sentinel-2 data and an object-based approach. *Forests*, *12*(5), 553.

Gemechu, G. F., Rui, X., & Lu, H. (2021). Wetland Change Mapping Using Machine Learning Algorithms, and Their Link with Climate Variation and Economic Growth: A Case Study of Guangling County, China. *Sustainability*, *14*(1), 439.

Giustarini, L., Hostache, R., Matgen, P., Schumann, G. J.-P., Bates, P. D., & Mason, D. C. (2012). A change detection approach to flood mapping in urban areas using TerraSAR-X. *IEEE transactions on geoscience and remote sensing*, *51*(4), 2417-2430.

Glenn, E. P., Huete, A. R., Nagler, P. L., & Nelson, S. G. (2008). Relationship between remotely-sensed vegetation indices, canopy attributes and plant physiological processes: What vegetation indices can and cannot tell us about the landscape. *Sensors*, *8*(4), 2136-2160.

Goffi, A., Stroppiana, D., Brivio, P. A., Bordogna, G., & Boschetti, M. (2020). Towards an automated approach to map flooded areas from Sentinel-2 MSI data and soft integration of water spectral features. *International Journal of Applied Earth Observation and Geoinformation*, *84*, 101951.

Grimaldi, S., Xu, J., Li, Y., Pauwels, V. R., & Walker, J. P. (2020). Flood mapping under vegetation using single SAR acquisitions. *Remote Sensing of Environment*, *237*, 111582.

Gu, H., Yu, Z., Yang, C., & Ju, Q. (2018). Projected changes in hydrological extremes in the Yangtze River Basin with an ensemble of regional climate simulations. *Water*, *10*(9), 1279.

Guerschman, J. P., Warren, G., Byrne, G., Lymburner, L., Mueller, N., & Van Dijk, A. (2011). MODIS-based standing water detection for flood and large reservoir mapping: algorithm development and applications for the Australian continent. *Water for a Healthy Country National Research Flagship Report, Canberra*.

Gulácsi, A., & Kovács, F. (2020). Sentinel-1-imagery-based high-resolution water cover detection on wetlands, Aided by Google Earth Engine. *Remote Sensing*, *12*(10), 1614.

Guo, J., Luan, Y., Li, Z., Liu, X., Li, C., & Chang, X. (2021). Mozambique flood (2019) caused by tropical cyclone idai monitored from sentinel-1 and sentinel-2 images. *IEEE Journal of Selected Topics in Applied Earth Observations and Remote Sensing*, *14*, 8761-8772.

Güvel, Ş. P., Akgül, M. A., & Aksu, H. (2022). Flood inundation maps using Sentinel-2: a case study in Berdan Plain. *Water Supply*, *22*(4), 4098-4108.

Guzder-Williams, B., & Alemohammad, H. (2021). Surface Water Detection from Sentinel-1. 2021 IEEE International Geoscience and Remote Sensing Symposium IGARSS,

Gxokwe, S., Dube, T., & Mazvimavi, D. (2020). Multispectral remote sensing of wetlands in semi-arid and arid areas: a review on applications, challenges and possible future research directions. *Remote Sensing*, *12*(24), 4190.

Halder, B., & Bandyopadhyay, J. (2022). Delineation of geospatial indices based water bodies' and vegetation change mapping using Sentinel-2 imagery in Canning blocks of south 24 parganas district, India. *Remote Sensing Applications: Society and Environment*, *25*, 100688.

Hardy, A., Ettritch, G., Cross, D. E., Bunting, P., Liywalii, F., Sakala, J., Silumesii, A., Singini, D., Smith, M., & Willis, T. (2019). Automatic detection of open and vegetated water bodies using Sentinel 1 to map African malaria vector mosquito breeding habitats. *Remote Sensing*, *11*(5), 593.

Helleis, M., Wieland, M., Krullikowski, C., Martinis, S., & Plank, S. (2022). Sentinel-1-based water and flood mapping: Benchmarking convolutional neural networks against an operational rule-based processing chain. *IEEE Journal of Selected Topics in Applied Earth Observations and Remote Sensing*, *15*, 2023-2036.

Herron, N., Davis, R., & Jones, R. (2002). The effects of large-scale afforestation and climate change on water allocation in the Macquarie River catchment, NSW, Australia. *Journal of Environmental Management*, *65*(4), 369-381.

Howarth, C. (2022). *State of the Climate 2022 – Australia continues to warm; heavy rainfall becomes more intense*. Retrieved 09/01/2023 from https://www.csiro.au/en/news/news-releases/2022/state-of-the-climate-report-2022

Huang, C., Chen, Y., & Wu, J. (2014). Mapping spatio-temporal flood inundation dynamics at large river basin scale using time-series flow data and MODIS imagery. *International Journal of Applied Earth Observation and Geoinformation*, *26*, 350-362.

Huang, C., Chen, Y., Zhang, S., & Wu, J. (2018). Detecting, extracting, and monitoring surface water from space using optical sensors: A review. *Reviews of Geophysics*, *56*(2), 333-360.

Huang Lin, C. (2021). Water Surfaces Detection from Sentinel-1 SAR Images using Deep Learning.

Huang, M., & Liang, X. (2006). On the assessment of the impact of reducing parameters and identification of parameter uncertainties for a hydrologic model with applications to ungauged basins. *Journal of hydrology*, *320*(1-2), 37-61.

Hunink, J., Simons, G., Suárez-Almiñana, S., Solera, A., Andreu, J., Giuliani, M., Zamberletti, P., Grillakis, M., Koutroulis, A., & Tsanis, I. (2019). A simplified water accounting procedure to assess climate change impact on water resources for agriculture across different European river basins. *Water*, *11*(10), 1976.

Islam, A., Bala, S., & Haque, M. (2010). Flood inundation map of Bangladesh using MODIS time-series images. *Journal of Flood Risk Management*, *3*(3), 210-222.

Jamali, A., Mahdianpari, M., Mohammadimanesh, F., Brisco, B., & Salehi, B. (2021). A synergic use of sentinel-1 and sentinel-2 imagery for complex wetland classification using generative adversarial network (GAN) scheme. *Water*, *13*(24), 3601.

Ji, L., Zhang, L., & Wylie, B. (2009). Analysis of dynamic thresholds for the normalized difference water index. *Photogrammetric Engineering & Remote Sensing*, *75*(11), 1307-1317.

Jiang, C., Zhang, H., Wang, C., Ge, J., & Wu, F. (2022). Water Surface Mapping from Sentinel-1 Imagery Based on Attention-UNet3+: A Case Study of Poyang Lake Region. *Remote Sensing*, *14*(19), 4708.

Jiang, W., Ni, Y., Pang, Z., Li, X., Ju, H., He, G., Lv, J., Yang, K., Fu, J., & Qin, X. (2021). An effective water body extraction method with new water index for sentinel-2 imagery. *Water*, *13*(12), 1647.

Jones, J. W. (2015). Efficient wetland surface water detection and monitoring via landsat: Comparison with in situ data from the everglades depth estimation network. *Remote Sensing*, *7*(9), 12503-12538.

Jose, H. (2022). *Macquarie Marshes flooded in 'wettest period in living memory' as farmers face mounting losses*. https://www.abc.net.au/news/2022-09-07/macquarie-marshes-floodplain-underwater-12-months-farming-losses/101409716

Kaplan, G., & Avdan, U. (2017). Mapping and monitoring wetlands using Sentinel-2 satellite imagery.

Kaplan, G., & Avdan, U. (2018). Sentinel-1 and Sentinel-2 data fusion for wetlands mapping: Balikdami, Turkey. *The International Archives of the Photogrammetry, Remote Sensing and Spatial Information Sciences*, *42*, 729-734.

Karim, F., Peña-Arancibia, J., Ticehurst, C., Marvanek, S., Gallant, J., Hughes, J., Dutta, D., Vaze, J., Petheram, C., & Seo, L. (2018). Floodplain inundation mapping and modelling for the Fitzroy, Darwin and Mitchell catchments. *Australia: CSIRO*.

Kavats, O., Khramov, D., & Sergieieva, K. (2022). Surface Water Mapping from SAR Images Using Optimal Threshold Selection Method and Reference Water Mask. *Water*, *14*(24), 4030.

Kennard, M. J., Pusey, B. J., Olden, J. D., Mackay, S. J., Stein, J. L., & Marsh, N. (2010). Classification of natural flow regimes in Australia to support environmental flow management. *Freshwater biology*, *55*(1), 171-193.

Kent, D. M. (2000). Evaluating wetland functions and values. *KENT D M. Applied Wetland Science and Technology. 2nd ed. New York: Lewis Publishers*, 55-80.

Khurshed, S. (2021). *Defining events: the 2010-11 Australia and New Zealand disasters, 10 years on*. https://www.swissre.com/australia_newzealand/insights/australia-and-new-zealand-disasters-10-years-on.html

Kingsford, R. T., & Thomas, R. F. (1995). The Macquarie Marshes in arid Australia and their waterbirds: a 50-year history of decline. *Environmental management*, *19*, 867-878.

Konapala, G., Kumar, S. V., & Ahmad, S. K. (2021). Exploring Sentinel-1 and Sentinel-2 diversity for flood inundation mapping using deep learning. *ISPRS journal of photogrammetry and remote sensing*, *180*, 163-173.

Kordelas, G. A., Manakos, I., Aragonés, D., Díaz-Delgado, R., & Bustamante, J. (2018). Fast and automatic data-driven thresholding for inundation mapping with Sentinel-2 data. *Remote Sensing*, *10*(6), 910.

Krause, C. E., Newey, V., Alger, M. J., & Lymburner, L. (2021). Mapping and monitoring the multi-decadal dynamics of Australia's open waterbodies using Landsat. *Remote Sensing*, *13*(8), 1437.

Krzysztofowicz, R. (2001). The case for probabilistic forecasting in hydrology. *Journal of hydrology*, *249*(1-4), 2-9.

Kuchment, L., & Gelfan, A. (2011). Assessment of extreme flood characteristics based on a dynamic-stochastic model of runoff generation and the probable maximum discharge. *Journal of Flood Risk Management*, *4*(2), 115-127.

Landuyt, L., Verhoest, N. E., & Van Coillie, F. M. (2020). Flood mapping in vegetated areas using an unsupervised clustering approach on sentinel-1 and-2 imagery. *Remote Sensing*, *12*(21), 3611.

Laonamsai, J., Julphunthong, P., Saprathet, T., Kimmany, B., Ganchanasuragit, T., Chomcheawchan, P., & Tomun, N. (2023). Utilizing NDWI, MNDWI, SAVI, WRI, and AWEI for Estimating Erosion and Deposition in Ping River in Thailand. *Hydrology*, *10*(3), 70.

Law, W. B., Hiscock, P., Ostendorf, B., & Lewis, M. (2021). Using satellite imagery to evaluate precontact Aboriginal foraging habitats in the Australian Western Desert. *Scientific reports*, *11*(1), 1-14.

Lefebvre, G., Davranche, A., Willm, L., Campagna, J., Redmond, L., Merle, C., Guelmami, A., & Poulin, B. (2019). Introducing WIW for detecting the presence of water in wetlands with landsat and sentinel satellites. *Remote Sensing*, *11*(19), 2210.

Lekhak, K., Pawan, R., & Budha, P. B. (2023). Extraction of Water Bodies from Sentinel-2 Images in the Foothills of Nepal Himalaya. *International Journal of Environment and Geoinformatics*, *10*(2), 70-81.

Li, H., Zech, J., Ludwig, C., Fendrich, S., Shapiro, A., Schultz, M., & Zipf, A. (2021). Automatic mapping of national surface water with OpenStreetMap and Sentinel-2 MSI data using deep learning. *International Journal of Applied Earth Observation and Geoinformation*, *104*, 102571.

Li, L., Su, H., Du, Q., & Wu, T. (2021). A novel surface water index using local background information for long term and large-scale Landsat images. *ISPRS journal of photogrammetry and remote sensing*, *172*, 59-78.

Li, L., Yan, Z., Shen, Q., Cheng, G., Gao, L., & Zhang, B. (2019). Water body extraction from very high spatial resolution remote sensing data based on fully convolutional networks. *Remote Sensing*, *11*(10), 1162.

Li, Y., Martinis, S., Plank, S., & Ludwig, R. (2018). An automatic change detection approach for rapid flood mapping in Sentinel-1 SAR data. *International Journal of Applied Earth Observation and Geoinformation*, *73*, 123-135.

Li, Z., & Demir, I. (2023). U-net-based semantic classification for flood extent extraction using SAR imagery and GEE platform: A case study for 2019 central US flooding. *Science of The Total Environment*, 161757.

Liang, J., & Liu, D. (2020). A local thresholding approach to flood water delineation using Sentinel-1 SAR imagery. *ISPRS journal of photogrammetry and remote sensing*, *159*, 53-62.

Liew, S. C. (2001). *SAR Images*. https://crisp.nus.edu.sg/~research/tutorial/sar_int.htm

Lindsay, J. B., & Creed, I. F. (2005). Sensitivity of digital landscapes to artifact depressions in remotely-sensed DEMs. *Photogrammetric Engineering & Remote Sensing*, *71*(9), 1029-1036.

Liu, Q., Qin, Y., Zhang, Y., & Li, Z. (2015). A coupled 1D–2D hydrodynamic model for flood simulation in flood detention basin. *Natural Hazards*, *75*, 1303-1325.

Luo, X., Hu, Z., & Liu, L. (2023). Investigating the seasonal dynamics of surface water over the Qinghai–Tibet Plateau using Sentinel-1 imagery and a novel gated multiscale ConvNet. *International Journal of Digital Earth*, *16*(1), 1372-1394.

Manakos, I., Kordelas, G. A., & Marini, K. (2020). Fusion of Sentinel-1 data with Sentinel-2 products to overcome non-favourable atmospheric conditions for the delineation of inundation maps. *European Journal of Remote Sensing*, *53*(sup2), 53-66.

Markert, K. N., Markert, A. M., Mayer, T., Nauman, C., Haag, A., Poortinga, A., Bhandari, B., Thwal, N. S., Kunlamai, T., & Chishtie, F. (2020). Comparing sentinel-1 surface water mapping algorithms and radiometric terrain correction processing in southeast asia utilizing google earth engine. *Remote Sensing*, *12*(15), 2469.

Martone, M., Bräutigam, B., Rizzoli, P., & Krieger, G. (2014). TanDEM-X performance over sandy areas. EUSAR 2014; 10th European Conference on Synthetic Aperture Radar,

Mason, T. J., Honeysett, J., Thomas, R. F., Popovic, G. C., Hosking, T., Shelly, D. J., & Bowen, S. (2022). Monitoring vital signs: wetland vegetation responses to hydrological resources in the Macquarie Marshes NSW, Australia. *Austral Ecology*, *47*(6), 1296-1314.

Mayer, T., Poortinga, A., Bhandari, B., Nicolau, A. P., Markert, K., Thwal, N. S., Markert, A., Haag, A., Kilbride, J., & Chishtie, F. (2021). Deep learning approach for Sentinel-1 surface water mapping leveraging Google Earth Engine. *ISPRS Open Journal of Photogrammetry and Remote Sensing*, *2*, 100005.

McFeeters, S. K. (1996). The use of the Normalized Difference Water Index (NDWI) in the delineation of open water features. *International Journal of Remote Sensing*, *17*(7), 1425-1432.

Melkamu, T., Bagyaraj, M., Adimaw, M., Ngusie, A., & Karuppannan, S. (2022). Detecting and mapping flood inundation areas in Fogera-Dera Floodplain, Ethiopia during an extreme wet season using Sentinel-1 data. *Physics and Chemistry of the Earth, Parts A/B/C*, *127*, 103189.

Meyer, R. P., Søgaard, M. G., Schødt, M. P., Horion, S., & Prishchepov, A. V. (2022). Emergency flood mapping in Australia with Sentinel-1 and Sentinel-2 satellite imagery. *Bulletin de la Société Géographique de Liège*.

Mialhe, F., Gunnell, Y., & Mering, C. (2008). Synoptic assessment of water resource variability in reservoirs by remote sensing: General approach and application to the runoff harvesting systems of south India. *Water Resources Research*, *44*(5).

Milczarek, M., Robak, A., & Gadawska, A. (2017). Sentinel Water Mask (SWM)-new index for water detection on Sentinel-2 images. *Proceedings of the 7th Advanced Training Course on Land Remote Sensing, Gödöllo, Hungary*, 4-9.

Milne, A. K., & Tapley, I. J. (2010). Wetland monitoring of flood-extent, inundation patterns and vegetation, Mekong River Basin, Southeast Asia, and Murray-Darling Basin, Australia. *ALOS Kyoto & Carbon Initiative, Science Team Reports, Phase*, *1*, 2006-2008.

Mission ends for Copernicus Sentinel-1B satellite. (2022). https://www.esa.int/Applications/Observing_the_Earth/Copernicus/Sentinel-1/Mission_ends_for_Copernicus_Sentinel-1B_satellite

Moharrami, M., Javanbakht, M., & Attarchi, S. (2021). Automatic flood detection using sentinel-1 images on the google earth engine. *Environmental Monitoring and Assessment*, *193*(5), 1-17.

Morelli, S., Del Soldato, M., Bianchini, S., Pazzi, V., Krymbi, E., Shpori, E., & Casagli, N. (2019). Detection of seasonal inundations by satellite data at Shkoder Urban Area, North Albania for sustainable management. *Sustainability*, *11*(16), 4454.

Mueller, N., Lewis, A., Roberts, D., Ring, S., Melrose, R., Sixsmith, J., Lymburner, L., McIntyre, A., Tan, P., & Curnow, S. (2016). Water observations from space: Mapping surface water from 25 years of Landsat imagery across Australia. *Remote Sensing of Environment*, *174*, 341-352.

Mullen, A. L., Watts, J. D., Rogers, B. M., Carroll, M. L., Elder, C. D., Noomah, J., Williams, Z., Caraballo-Vega, J. A., Bredder, A., & Rickenbaugh, E. (2023). Using High-Resolution Satellite Imagery and Deep Learning to Track Dynamic Seasonality in Small Water Bodies. *Geophysical Research Letters*, *50*(7), e2022GL102327.

Muro, J., Canty, M., Conradsen, K., Hüttich, C., Nielsen, A. A., Skriver, H., Remy, F., Strauch, A., Thonfeld, F., & Menz, G. (2016). Short-term change detection in wetlands using Sentinel-1 time series. *Remote Sensing*, *8*(10), 795.

Muro, J., Varea, A., Strauch, A., Guelmami, A., Fitoka, E., Thonfeld, F., Diekkrüger, B., & Waske, B. (2020). Multitemporal optical and radar metrics for wetland mapping at national level in Albania. *Heliyon*, *6*(8), e04496.

Muszynski, M., Hölzer, T., Weiss, J., Fraccaro, P., Zortea, M., & Brunschwiler, T. (2022). Flood Event Detection from Sentinel 1 and Sentinel 2 Data: Does Land Use Matter for Performance of U-Net based Flood Segmenters? 2022 IEEE International Conference on Big Data (Big Data),

Nallapareddy, A., & Balakrishnan, B. (2020). Automatic Flood Detection in Multi-Temporal Sentinel-1 Synthetic Aperture Radar Imagery Using ANN Algorithms. *INTERNATIONAL JOURNAL OF COMPUTERS COMMUNICATIONS & CONTROL*, *15*(3).

Nasirzadehdizaji, R., Akyuz, D., & Cakir, Z. (2019). Flood mapping and permanent water bodies change detection using Sentinel SAR data. *The International Archives of the Photogrammetry, Remote Sensing and Spatial Information Sciences*, *42*, 797-801.

Ndehedehe, C. E., Onojeghuo, A. O., Stewart-Koster, B., Bunn, S. E., & Ferreira, V. G. (2021). Upstream flows drive the productivity of floodplain ecosystems in tropical Queensland. *Ecological Indicators*, *125*, 107546.

Nemni, E., Bullock, J., Belabbes, S., & Bromley, L. (2020). Fully convolutional neural network for rapid flood segmentation in synthetic aperture radar imagery. *Remote Sensing*, *12*(16), 2532.

Nigro, J., Slayback, D., Policelli, F., & Brakenridge, G. R. (2014). NASA/DFO MODIS near real-time (NRT) global flood mapping product evaluation of flood and permanent water detection. *Evaluation, Greenbelt, MD*, *27*.

Nilsson, C., Reidy, C. A., Dynesius, M., & Revenga, C. (2005). Fragmentation and flow regulation of the world's large river systems. *Science*, *308*(5720), 405-408.

Notti, D., Giordan, D., Caló, F., Pepe, A., Zucca, F., & Galve, J. P. (2018). Potential and limitations of open satellite data for flood mapping. *Remote Sensing*, *10*(11), 1673.

Observatory, N. E. (2000). *Measuring Vegetation*. https://earthobservatory.nasa.gov/features/MeasuringVegetation/measuring_vegetation_2.php

Okoli, K., Mazzoleni, M., Breinl, K., & Di Baldassarre, G. (2019). A systematic comparison of statistical and hydrological methods for design flood estimation. *Hydrology Research*, *50*(6), 1665-1678.

Otsu, N. (1979). A threshold selection method from gray-level histograms. *IEEE transactions on systems, man, and cybernetics*, *9*(1), 62-66.

Ottinger, M., Clauss, K., & Kuenzer, C. (2017). Large-scale assessment of coastal aquaculture ponds with Sentinel-1 time series data. *Remote Sensing*, *9*(5), 440.

PBC, P. L. (2022). *Planet Application Program Interface: In Space for Life on Earth* https://api.planet.com

Pedzisai, E., Mutanga, O., Odindi, J., & Bangira, T. (2023). A novel change detection and threshold-based ensemble of scenarios pyramid for flood extent mapping using Sentinel-1 data. *Heliyon*, *9*(3).

Pekel, J.-F., Cottam, A., Gorelick, N., & Belward, A. S. (2016). High-resolution mapping of global surface water and its long-term changes. *Nature*, *540*(7633), 418-422.

Pena-Regueiro, J., Sebastia-Frasquet, M.-T., Estornell, J., & Aguilar-Maldonado, J. A. (2020). Sentinel-2 application to the surface characterization of small water bodies in Wetlands. *Water*, *12*(5), 1487.

Phiri, D., Simwanda, M., Salekin, S., Nyirenda, V. R., Murayama, Y., & Ranagalage, M. (2020). Sentinel-2 data for land cover/use mapping: A review. *Remote Sensing*, *12*(14), 2291.

Pittock, J. (2019). Are we there yet? The Murray-Darling Basin and sustainable water management. *Thesis Eleven*, *150*(1), 119-130.

Puszka, S. (2021). The Royal Commission into National Natural Disaster Arrangements Report. *Interaction*, *49*(1), 23-28.

Rakwatin, P., Sansena, T., Marjang, N., & Rungsipanich, A. (2013). Using multi-temporal remote-sensing data to estimate 2011 flood area and volume over Chao Phraya River basin, Thailand. *Remote sensing letters*, *4*(3), 243-250.

Ralph, T. J., Hesse, P. P., & Kobayashi, T. (2015). Wandering wetlands: spatial patterns of historical channel and floodplain change in the Ramsar-listed Macquarie Marshes, Australia. *Marine and Freshwater Research*, *67*(6), 782-802.

Rana, V. K., & Suryanarayana, T. (2019). Evaluation of SAR speckle filter technique for inundation mapping. *Remote Sensing Applications: Society and Environment*, *16*, 100271.

Regulator, N. R. A. (2022). *Why we are at risk of flood-induced drought amnesia*. https://www.nrar.nsw.gov.au/news/why-we-are-at-risk-of-flood-induced-drought-amnesia

Restoring and protecting the Macquarie River Valley 2017–18 Snapshot. https://www.dcceew.gov.au/sites/default/files/documents/restoring-protecting-macquarie-2017-18.pdf

Revilla-Romero, B., Hirpa, F. A., Pozo, J. T.-d., Salamon, P., Brakenridge, R., Pappenberger, F., & De Groeve, T. (2015). On the use of global flood forecasts and satellite-derived inundation maps for flood monitoring in data-sparse regions. *Remote Sensing*, *7*(11), 15702-15728.

Robinove, C. J. (1978). Interpretation of a Landsat image of an unusual flood phenomenon in Australia. *Remote Sensing of Environment*, *7*(3), 219-225.

Rogers, K., Ralph, T., & Imgraben, S. (2010). Water requirements of biota, geomorphology and climate change in the Macquarie Marshes. *Ecosystem Response Modelling in the Murray-Darling Basin. CSIRO Publishing, Melbourne*, 151-170.

Rosenberg, D. M., McCully, P., & Pringle, C. M. (2000). Global-scale environmental effects of hydrological alterations: introduction. *BioScience*, *50*(9), 746-751.

Rosenthal, N., Anderson, T., Glinskis, E., & Tellman, B. (2020). Communicating Flood Risk in Near Real-Time-Turning Pixel Flood Maps Into Three Word Warnings. AGU Fall Meeting Abstracts,

Rossi, M., & Vervoort, R. W. (2022). Geomorphic approach to fill existing gaps in remote sensing surface water extent mapping.

Ryan, A., Colloff, M. J., & Pittock, J. (2021). Flow to nowhere: the disconnect between environmental watering and the conservation of threatened species in the Murray–Darling Basin, Australia. *Marine and Freshwater Research*.

Saghafi, M., Ahmadi, A., & Bigdeli, B. (2021). Sentinel-1 and Sentinel-2 data fusion system for surface water extraction. *Journal of Applied Remote Sensing*, *15*(1), 014521-014521.

Sandi, S. G., Saco, P. M., Kuczera, G., Wen, L., Saintilan, N., & Rodriguez, J. F. (2018). Predicting floodplain inundation and vegetation dynamics in arid wetlands. E3S Web of Conferences,

Sarp, G., & Ozcelik, M. (2017). Water body extraction and change detection using time series: A case study of Lake Burdur, Turkey. *Journal of Taibah University for Science*, *11*(3), 381-391.

School, W. S. (2018). *Rivers Contain Groundwater* https://www.usgs.gov/special-topics/water-science-school/science/rivers-contain-groundwater

Schumann, G., Matgen, P., Hoffmann, L., Hostache, R., Pappenberger, F., & Pfister, L. (2007). Deriving distributed roughness values from satellite radar data for flood inundation modelling. *Journal of hydrology*, *344*(1-2), 96-111.

Schweizer, V., Colloff, M. J., & Pittock, J. (2022). The Dammed and the Saved: a Conservation Triage Framework for Wetlands under Climate Change in the Murray–Darling Basin, Australia. *Environmental management*, *70*(4), 549-564.

Science Toolbox Exploitation Platform. European Space Agency. https://step.esa.int/main/toolboxes/snap/

Sekertekin, A., Cicekli, S. Y., & Arslan, N. (2018). Index-based identification of surface water resources using Sentinel-2 satellite imagery. 2018 2nd International Symposium on Multidisciplinary Studies and Innovative Technologies (ISMSIT),

Senanayake, I. P., Yeo, I.-Y., & Kuczera, G. A. (2023). A Random Forest-Based Multi-Index Classification (RaFMIC) Approach to Mapping Three-Decadal Inundation Dynamics in Dryland Wetlands Using Google Earth Engine. *Remote Sensing*, *15*(5), 1263.

Sentinel-1. (2022). www.asf.alaska.edu/data-sets/sar-data-sets/sentinel-1/

Service, N. N. P. a. W. (1993). *Macquarie Marshes Nature Reserve Plan of Engagement*. https://www.environment.nsw.gov.au/-/media/OEH/Corporate-Site/Documents/Parks-reserves-and-protected-areas/Parks-plans-of-management/macquarie-marshes-nature-reserve-plan-of-management-930002.pdf

Shahabi, H., Shirzadi, A., Ghaderi, K., Omidvar, E., Al-Ansari, N., Clague, J. J., Geertsema, M., Khosravi, K., Amini, A., & Bahrami, S. (2020). Flood detection and susceptibility mapping using sentinel-1 remote sensing data and a machine learning approach: Hybrid intelligence of bagging ensemble based on k-nearest neighbor classifier. *Remote Sensing*, *12*(2), 266.

Sharifi, A. (2021). Development of a method for flood detection based on Sentinel-1 images and classifier algorithms. *Water and Environment Journal*, *35*(3), 924-929.

Shen, X., Wang, D., Mao, K., Anagnostou, E., & Hong, Y. (2019). Inundation extent mapping by synthetic aperture radar: A review. *Remote Sensing*, *11*(7), 879.

Sherjah, P., & Sajikumar, N. (2021). Delineation of water body from Sentinel 2 MSI imagery–A comparative study. IOP Conference Series: Materials Science and Engineering,

Shi, Z., Chen, Y., Liu, Q., & Huang, C. (2020). Discharge estimation using harmonized landsat and sentinel-2 product: Case studies in the murray darling basin. *Remote Sensing*, *12*(17), 2810.

Shilengwe, C., Nyimbili, P. H., Msendo, R., Banda, F., Mukupa, W., & Erden, T. (2023). Synthetic Aperture Radar and Optical Sensor Techniques Using Google Earth Engine For Flood Monitoring and Damage Assessment–A Case Study of Mumbwa District, Zambia. *Zambia ICT Journal*, *7*(1), 7-15.

Sims, N., Anstee, J., Barron, O., Botha, E., Lehmann, E., Li, L., McVicar, T., Paget, M., Ticehurst, C., & Van Niel, T. (2016). Earth observation remote sensing. *A Technical Report to the Australian Government from the CSIRO Northern Australia Water Resource Assessment, Part of the National Water Infrastructure Development Fund: Water Resource Assessments*.

Sims, N., Warren, G., Overton, I., Austin, J., Gallant, J., King, D., Merrin, L., Donohue, R., McVicar, T., & Hodgen, M. (2014). RiM-FIM Floodplain Inundation Modelling for the Edward-Wakool, Lower Murrumbidgee and Lower Darling River Systems. Report prepared for the Murray-Darling Basin Authority. *Water for a Healthy Country Flagship; CSIRO: Canberra, Australia*.

Sims, N. C., & Thoms, M. C. (2002). What happens when flood plains wet themselves: vegetation response to inundation on the lower Balonne flood plain. *International Association of Hydrological Sciences, Publication*, *276*, 195-202.

Slagter, B., Tsendbazar, N.-E., Vollrath, A., & Reiche, J. (2020). Mapping wetland characteristics using temporally dense Sentinel-1 and Sentinel-2 data: A case study in the St. Lucia wetlands, South Africa. *International Journal of Applied Earth Observation and Geoinformation*, *86*, 102009.

Slinski, K. M., Hogue, T. S., & McCray, J. E. (2019). Active-passive surface water classification: a new method for high-resolution monitoring of surface water dynamics. *Geophysical Research Letters*, *46*(9), 4694-4704.

Storey, J., Roy, D. P., Masek, J., Gascon, F., Dwyer, J., & Choate, M. (2016). A note on the temporary misregistration of Landsat-8 Operational Land Imager (OLI) and Sentinel-2 Multi Spectral Instrument (MSI) imagery. *Remote Sensing of Environment*, *186*, 121-122.

Sturman, J., Ho, G., & Mathew, K. (2004). *Water auditing and water conservation*. IWA Publishing.

Sun, A. Y., & Scanlon, B. R. (2019). How can Big Data and machine learning benefit environment and water management: a survey of methods, applications, and future directions. *Environmental Research Letters*, *14*(7), 073001.

Talbot, C. J., Bennett, E. M., Cassell, K., Hanes, D. M., Minor, E. C., Paerl, H., Raymond, P. A., Vargas, R., Vidon, P. G., & Wollheim, W. (2018). The impact of flooding on aquatic ecosystem services. *Biogeochemistry*, *141*, 439-461.

Tarpanelli, A., Mondini, A. C., & Camici, S. (2022). Effectiveness of Sentinel-1 and Sentinel-2 for flood detection assessment in Europe. *Natural Hazards and Earth System Sciences*, *22*(8), 2473-2489.

Tavus, B., Can, R., & Kocaman, S. (2022). A CNN-based flood mapping approach using sentinel-1 data. *ISPRS Annals of the Photogrammetry, Remote Sensing and Spatial Information Sciences*, *3*, 549-556.

Tayer, T. C., Douglas, M. M., Cordeiro, M. C., Tayer, A. D., Callow, J. N., Beesley, L., & McFarlane, D. (2023). Improving the accuracy of the Water Detect algorithm using Sentinel-2, Planetscope and sharpened imagery: a case study in an intermittent river. *GIScience & Remote Sensing*, *60*(1), 2168676.

Tehrany, M. S., Pradhan, B., & Jebur, M. N. (2014). Flood susceptibility mapping using a novel ensemble weights-of-evidence and support vector machine models in GIS. *Journal of hydrology*, *512*, 332-343.

Thomas, R. F., Kingsford, R. T., Lu, Y., Cox, S. J., Sims, N. C., & Hunter, S. J. (2015). Mapping inundation in the heterogeneous floodplain wetlands of the Macquarie Marshes, using Landsat Thematic Mapper. *Journal of hydrology*, *524*, 194-213.

Thomas, R. F., Kingsford, R. T., Lu, Y., & Hunter, S. J. (2011). Landsat mapping of annual inundation (1979–2006) of the Macquarie Marshes in semi-arid Australia. *International Journal of Remote Sensing*, *32*(16), 4545-4569.

Ticehurst, C., Chen, Y., Karim, F., Dutta, D., & Gouweleeuw, B. (2013). Using MODIS for mapping flood events for use in hydrological and hydrodynamic models: Experiences so far. 20th international congress on modelling and simulation, Adelaide, Australia,

Ticehurst, C., Teng, J., & Sengupta, A. (2022). Development of a Multi-Index Method Based on Landsat Reflectance Data to Map Open Water in a Complex Environment. *Remote Sensing*, *14*(5), 1158.

Toh, M. (2022, 23/11/2022). *Australia will see more extreme weather events, putting strain on economy, report shows*. Retrieved 09/01/2023 from https://edition.cnn.com/2022/11/23/business/australia-extreme-weather-economy-strain-climate-intl-hnk/index.html

Tomkins, K. M. (2014). Uncertainty in streamflow rating curves: methods, controls and consequences. *Hydrological processes*, *28*(3), 464-481.

Tran, K. H., Menenti, M., & Jia, L. (2022). Surface Water Mapping and Flood Monitoring in the Mekong Delta Using Sentinel-1 SAR Time Series and Otsu Threshold. *Remote Sensing*, *14*(22), 5721.

Tsyganskaya, V., Martinis, S., Marzahn, P., & Ludwig, R. (2018). SAR-based detection of flooded vegetation–a review of characteristics and approaches. *International Journal of Remote Sensing*, *39*(8), 2255-2293.

Tulbure, M. G., & Broich, M. (2013). Spatiotemporal dynamic of surface water bodies using Landsat time-series data from 1999 to 2011. *ISPRS journal of photogrammetry and remote sensing*, *79*, 44-52.

Tulbure, M. G., Broich, M., Perin, V., Gaines, M., Ju, J., Stehman, S. V., Pavelsky, T., Masek, J. G., Yin, S., & Mai, J. (2022). Can we detect more ephemeral floods with higher density harmonized Landsat Sentinel 2 data compared to Landsat 8 alone? *ISPRS journal of photogrammetry and remote sensing*, *185*, 232-246.

Tupas, M. E., Roth, F., Bauer-Marschallinger, B., & Wagner, W. (2023). An Intercomparison of Sentinel-1 Based Change Detection Algorithms for Flood Mapping. *Remote Sensing*, *15*(5), 1200.

Van der Kamp, G., & Hayashi, M. (1998). The groundwater recharge function of small wetlands in the semi-arid northern prairies. *Great Plains Research*, 39-56.

Van Deventer, H., Linström, A., Durand, J., Naidoo, L., & Cho, M. (2022). Deriving the maximum extent and hydroperiod of open water from Sentinel-2 imagery for global sustainability and biodiversity reporting for wetlands. *Water SA*, *48*(1), 75–89-75–89.

Van Dijk, A., & Renzullo, L. J. (2011). Water resource monitoring systems and the role of satellite observations. *Hydrology and Earth System Sciences*, *15*(1), 39-55.

Van Dijk, A. I., Beck, H. E., Crosbie, R. S., De Jeu, R. A., Liu, Y. Y., Podger, G. M., Timbal, B., & Viney, N. R. (2013). The Millennium Drought in southeast Australia (2001–2009): Natural and human causes and implications for water resources, ecosystems, economy, and society. *Water Resources Research*, *49*(2), 1040-1057.

Vanderhoof, M. K., Alexander, L., Christensen, J., Solvik, K., Nieuwlandt, P., & Sagehorn, M. (2023). High-frequency time series comparison of Sentinel-1 and Sentinel-2 satellites for mapping open and vegetated water across the United States (2017–2021). *Remote Sensing of Environment*, *288*, 113498.

Vervoort, R. W., Fuentes, I., Brombacher, J., Degen, J., Chambel-Leitão, P., & Santos, F. (2022). Progress in Developing Scale-Able Approaches to Field-Scale Water Accounting Based on Remote Sensing. *Sustainability*, *14*(5), 2732.

Vervoort, R. W., Miechels, S. F., van Ogtrop, F. F., & Guillaume, J. H. (2014). Remotely sensed evapotranspiration to calibrate a lumped conceptual model: Pitfalls and opportunities. *Journal of hydrology*, *519*, 3223-3236.

Villarroya-Carpio, A., Lopez-Sanchez, J. M., & Engdahl, M. E. (2022). Sentinel-1 interferometric coherence as a vegetation index for agriculture. *Remote Sensing of Environment*, *280*, 113208.

Vinayaraj, P., Imamoglu, N., Nakamura, R., & Oda, A. (2018). Investigation on perceptron learning for water region estimation using large-scale multispectral images. *Sensors*, *18*(12), 4333.

Vorosmarty, C. J., Green, P., Salisbury, J., & Lammers, R. B. (2000). Global water resources: vulnerability from climate change and population growth. *Science*, *289*(5477), 284-288.

Wan, L., Liu, M., Wang, F., Zhang, T., & You, H. (2019). Automatic extraction of flood inundation areas from SAR images: A case study of Jilin, China during the 2017 flood disaster. *International Journal of Remote Sensing*, *40*(13), 5050-5077.

Wang, Y., & Xu, H. (2020). Comparison of remote sensing water indices based on objective threshold value and the random forest gini coefficient. *Remote Sensing Technology and Application*, *35*(5), 1089-1098.

Wangchuk, S., & Bolch, T. (2020). Mapping of glacial lakes using Sentinel-1 and Sentinel-2 data and a random forest classifier: Strengths and challenges. *Science of Remote Sensing*, *2*, 100008.

Wasko, C., Guo, D., Ho, M., Nathan, R., & Vogel, E. (2023). Diverging projections for flood and rainfall frequency curves. *Journal of hydrology*, 129403.

Wen, L., Macdonald, R., Morrison, T., Hameed, T., Saintilan, N., & Ling, J. (2013). From hydrodynamic to hydrological modelling: Investigating long-term hydrological regimes of key wetlands in the Macquarie Marshes, a semi-arid lowland floodplain in Australia. *Journal of hydrology*, *500*, 45-61.

Why Healthy Wetlands Are Vital to Protecting Endangered Species. (2023). U.S. Fish & Wildlife Service. https://www.fws.gov/story/2023-04/why-healthy-wetlands-are-vital-protecting-endangered-species

Whyte, A., Ferentinos, K. P., & Petropoulos, G. P. (2018). A new synergistic approach for monitoring wetlands using Sentinels-1 and 2 data with object-based machine learning algorithms. *Environmental Modelling & Software*, *104*, 40-54.

Wilson, G., Berney, P., Ryder, D., & Price, J. N. (2008). Stage 2: Grazing/Landuse in the Macquarie Marshes and Gwydir Wetlands: Final Report to the New South Wales Department of Environment and Climate Change.

WMO. (2021). *Weather-related disasters increase over past 50 years, causing more damage but fewer deaths*. https://public.wmo.int/en/media/press-release/weather-related-disasters-increase-over-past-50-years-causing-more-damage-fewer

Xing, L., Tang, X., Wang, H., Fan, W., & Wang, G. (2018). Monitoring monthly surface water dynamics of Dongting Lake using Sentinel-1 data at 10 m. *PeerJ*, *6*, e4992.

Xu, H. (2006). Modification of normalised difference water index (NDWI) to enhance open water features in remotely sensed imagery. *International Journal of Remote Sensing*, *27*(14), 3025-3033.

Yamaguchi, Y. (2020). *Polarimetric SAR imaging: theory and applications*. CRC Press.

Yang, F., Feng, T., Xu, G., & Chen, Y. (2020). Applied method for water-body segmentation based on mask R-CNN. *Journal of Applied Remote Sensing*, *14*(1), 014502-014502.

Yang, L., Driscol, J., Sarigai, S., Wu, Q., Lippitt, C. D., & Morgan, M. (2022). Towards synoptic water monitoring systems: a review of AI methods for automating water body detection and water quality monitoring using remote sensing. *Sensors*, *22*(6), 2416.

Yang, X., & Chen, L. (2017). Evaluation of automated urban surface water extraction from Sentinel-2A imagery using different water indices. *Journal of Applied Remote Sensing*, *11*(2), 026016-026016.

Yang, X., Zhao, S., Qin, X., Zhao, N., & Liang, L. (2017). Mapping of urban surface water bodies from Sentinel-2 MSI imagery at 10 m resolution via NDWI-based image sharpening. *Remote Sensing*, *9*(6), 596.

Yousefi, N., Ralph, T. J., Farebrother, W., Chang, H.-C., & Hesse, P. P. (2018). Assessment of channel expansion and contraction using cross-section data from repeated LiDAR acquisitions in the Macquarie Marshes, NSW. Proceedings of the 9th Australian Stream Management Conference,

Yu, J., Qin, X., & Larsen, O. (2013). Joint Monte Carlo and possibilistic simulation for flood damage assessment. *Stochastic environmental research and risk assessment*, *27*, 725-735.

Yu, Z., An, Q., Liu, W., & Wang, Y. (2022). Analysis and evaluation of surface water changes in the lower reaches of the Yangtze River using Sentinel-1 imagery. *Journal of Hydrology: Regional Studies*, *41*, 101074.

Zhai, K., Wu, X., Qin, Y., & Du, P. (2015). Comparison of surface water extraction performances of different classic water indices using OLI and TM imageries in different situations. *Geo-spatial Information Science*, *18*(1), 32-42.

Zhang, J., Xu, K., Yang, Y., Qi, L., Hayashi, S., & Watanabe, M. (2006). Measuring water storage fluctuations in Lake Dongting, China, by Topex/Poseidon satellite altimetry. *Environmental Monitoring and Assessment*, *115*, 23-37.

Zhang, M., Chen, F., Liang, D., Tian, B., & Yang, A. (2020). Use of Sentinel-1 GRD SAR images to delineate flood extent in Pakistan. *Sustainability*, *12*(14), 5784.

Zhang, Q., & Werner, A. D. (2015). Hysteretic relationships in inundation dynamics for a large lake–floodplain system. *Journal of hydrology*, *527*, 160-171.

Zhang, X., Chan, N. W., Pan, B., Ge, X., & Yang, H. (2021). Mapping flood by the object-based method using backscattering coefficient and interference coherence of Sentinel-1 time series. *Science of The Total Environment*, *794*, 148388.

Zhao, J., Chini, M., Pelich, R., Matgen, P., Hostache, R., Cao, S., & Wagner, W. (2020). Deriving exclusion maps from C-band SAR time-series: an additional information layer for SAR-based flood extent mapping. *ISPRS Annals of the Photogrammetry, Remote Sensing and Spatial Information Sciences*, *1*, 395-400.

Zhou, R., Wang, G., Xu, H., & Zhang, Z. (2023). A Sub-Second Method for SAR Image Registration Based on Hierarchical Episodic Control. *Remote Sensing*, *15*(20), 4941.

Zortea, M., Fraccaro, P., Brunschwiler, T., Muszynski, M., & Weiss, J. (2022). Surface Water Mapping in Sentinel-1 Images: A Probabilistic Approach Combining Classic Detection Methods. IGARSS 2022-2022 IEEE International Geoscience and Remote Sensing Symposium,

6 Supplementary Materials

Table 6.1: Statistical Significance of Correlations Between Rainfall, Water Discharge, and Water Indices

	Rainfall (mm)	**421147 (Upstream)**	**421135 (Downstream)**	**WI**	**MNDWI**	**AWEInsh**	**AWEIsh**
Rainfall (mm)	**0**	**0.0336**	**0.029**	0.2241	0.3508	0.0845	0.2703
421147 (Upstream)	**0.0336**	**0**	**< 0.001**	**< 0.001**	**< 0.001**	**< 0.001**	**< 0.001**
421135 (Downstream)	**0.029**	**< 0.001**	**0**	**< 0.001**	**< 0.001**	**< 0.001**	**< 0.001**
WI	0.2241	**< 0.001**	**< 0.001**	**0**	**< 0.001**	**< 0.001**	**< 0.001**
MNDWI	0.3508	**< 0.001**	**< 0.001**	**< 0.001**	**0**	**< 0.001**	**< 0.001**
AWEInsh	0.0845	**< 0.001**	**< 0.001**	**< 0.001**	**< 0.001**	**0**	**< 0.001**
AWEIsh	0.2703	**< 0.001**	**< 0.001**	**< 0.001**	**< 0.001**	**< 0.001**	**0**

p values < 0.05

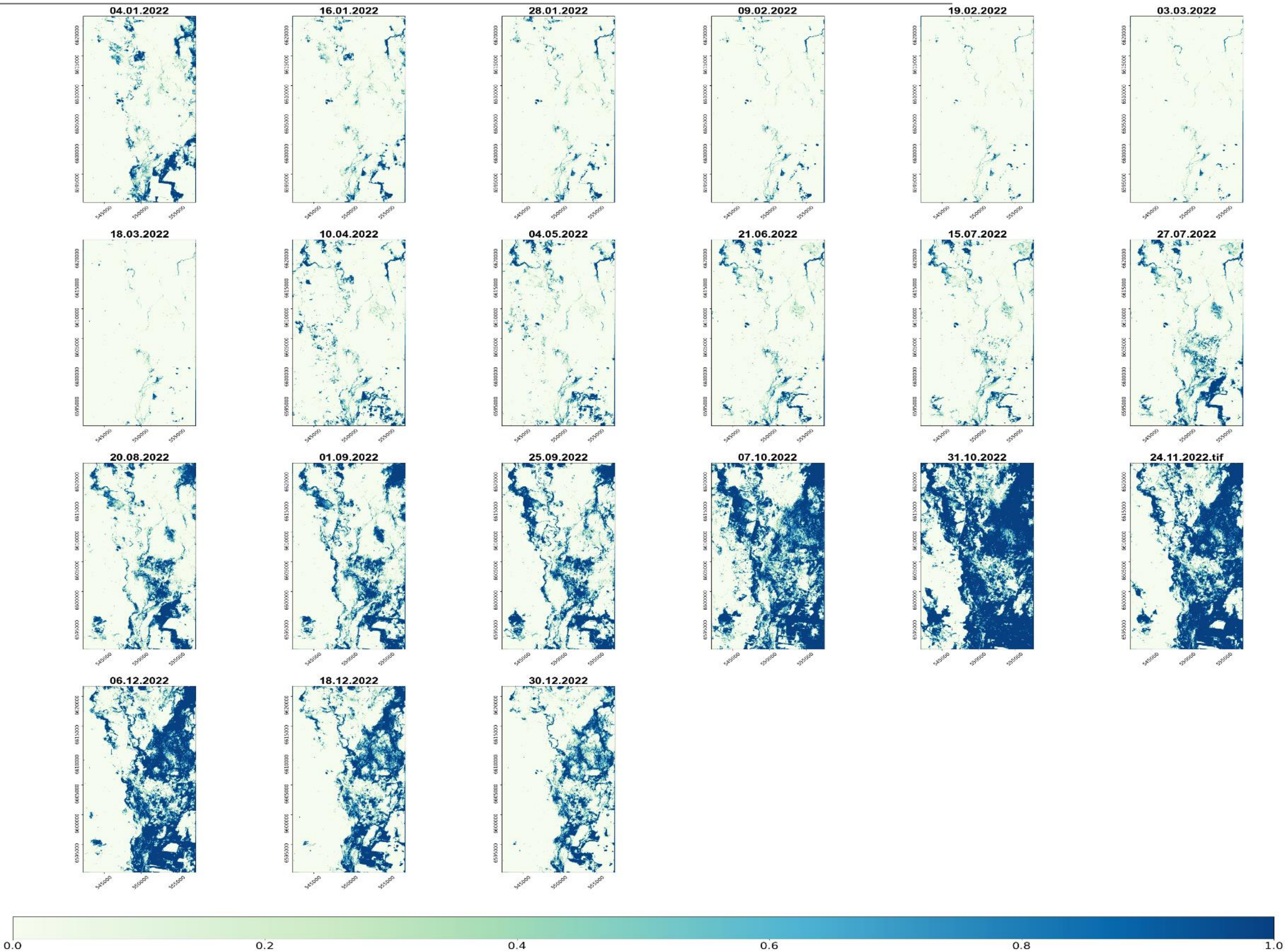

Figure 6.1: Probability of Water Occurrence in the Macquarie Marshes for the Year 2022